University of Alberta

Molecular mechanisms of ICAM-1-induced MUC1 signaling: A study using MUC1/Y

by

Jeffrey Wai-man Chow 

A thesis submitted to the Faculty of Graduate Studies and Research
in partial fulfillment of the requirements for the degree of

Master of Science

Medical Sciences – Laboratory Medicine and Pathology

Edmonton, Alberta
Fall 2006

Your file Votre référence
ISBN: 978-0-494-22243-0
Our file Notre référence
ISBN: 978-0-494-22243-0

Abstract:

The MUC1 glycoprotein is aberrantly expressed in many human breast cancers. Previous studies indicate that MUC1 adheres to ICAM-1, an adhesion molecule involved in arrest and transendothelial migration of leukocytes from the blood into tissues during inflammation and immune responses. The MUC1/ICAM-1 interaction has been demonstrated to participate in both arrest and transendothelial migration of tumor cells *in vitro*. Migration of tumor cells into and out of the circulatory system are necessary steps in metastasis, and the formation of metastases at distant sites is the cause of mortality for individuals with breast cancer. Although it is known that MUC1 homodimerizes and MUC1-mediated migration requires lipid rafts, the molecular mechanism of ICAM-1-induced MUC1 signaling remains unclear. This study investigated the role of the MUC1 extracellular tandem repeats in these events, and found that the tandem repeats were not needed for homodimerization, but were crucial for translocation of the dimers into rafts.

Table of Contents

Page

List of Figures

Abbreviations and Terms

ADAM	A disintegrin and metalloprotease
ADF	Actin depolymerizing factor
ATCC	American type culture collection
ATM	Ataxia-telangiectasia mutated, a serine/threonine protein kinase
ATP	Adenosine triphosphate
BRCA1/2	Breast cancer 1/2, tumor suppressor genes
BSA	Bovine serum albumin
CaM	Calmodulin
CAM	Cellular adhesion molecule
CCR	Cytokine receptor containing a double cysteine motif
CD	Cluster of differentiation
CFP	Cyan fluorescent protein
CHEK	Checkpoint homolog, a tumor suppressor gene
CICR	Calcium-induced calcium release
CMV	Cytomegalovirus
CTB	Cholera toxin B
CXCR	Cytokine receptor containing a specific motif: Cysteine-any amino acid-cysteine
ddH_2O	Distilled deionized water
DIC	Differential interference contrast
DMEM	Dulbecco's modified Eagle's medium
DMSO	Dimethyl sulfoxide
DNA	Deoxyribonucleic acid
dNTP	Deoxyribose nucleotide phosphate
DRM	Detergent-resistant membrane
DSS	Disccinimidyl suberate
ECL	Enhanced chemiluminescence
EDTA	Ethylenediaminetetraacetic acid

EGF	Epidermal growth factor
EGFR	Epidermal growth factor receptor
ERK	Extracellular signal-regulated kinase
FAK	Focal adhesion kinase
FBS	Fetal bovine serum
FGF	Fibroblast growth factor
FITC	Fluorescein isothiacyanate
FLAG	Octapeptide used for affinity purification
GAP	GTPase-activating protein
GDNF	Glial cell line-derived neurotrophic factor
GDP	Guanosine diphosphate
GEF	Guanine nucleotide exchange factor
GFP	Green fluorescent protein
GM1	Monosialotetrahexosylganglioside
GPCR	G protein-coupled receptor
GPI	Glycosylphosphatidylinositol
Grb2	Growth receptor binding protein 2
GSK3β	Glycogen synthase kinase 3 β
GTP	Guanosine triphosphate
GTPase	Enzyme that binds to and hydrolyzes GTP
HEPES	4-(2-hydroxyethyl)-1-piperazineethanesulfonic acid, an organic chemical buffer
HRP	Horseradish peroxidase
HSP	Heat shock protein
HUVEC	Human umbilical vein endothelial cell
ICAM	Intercellular adhesion molecule
IFN	Interferon
IL	Interleukin
IP_3	Inositol (1, 4, 5) triphosphate
IQGAP	IQ motif containing a GTPase activating protein
JAK	Janus kinase

JAM	Junctional adhesion molecule
LB	Luria broth
lck	leukocyte-specific protein tyrosine kinase
LFA	Lymphocyte function-associated antigen
LMP	Low melting point
MBCD	Methyl-β-cyclodextrin
MLCK	Myosin light-chain kinase
MMP	Matrix metalloproteinase
MT1-MMP	MMP-14, a matrix metalloproteinase
MUC1-CFP	A pECFP plasmid containing the full-length MUC1 gene N-terminal to the CFP gene
MUC1/Y	A MUC1 isoform generated from differential splicing of the MUC1 gene
MUC1/Y-YFP	MUC1/Y mucin with a C-terminal YFP tag
MUCY-YFP	A pEYFP plasmid containing the MUC1/Y gene N-terminal to the YFP gene
NIH	National Institute of Health
NIH ICAM	NIH 3T3 mouse cells expressing human ICAM-1
NIH mock	NIH 3T3 mouse cells mock transfected and not expressing human ICAM-1
NRTK	Non-receptor tyrosine kinase
NSAID	Non-steroidal anti-inflammatory drug
P53	Tumor protein 53, a tumor suppressor
PBS	Phosphate-buffered saline
PCR	Polymerase chain reaction
PDGF	Platelet-derived growth factor
PDGFR	Platelet-derived growth factor receptor
pECFP	A plasmid containing a gene for enhanced cyan fluorescent protein
pEYFP	A plasmid containing a gene for enhanced yellow fluorescent protein

PH	Pleckstrin homology domain
PI3K	Phosphoinositide 3-kinase
PIP2	Phosphatidylinositol (4, 5) disphosphate
PKA	Protein kinase A
PKC	Protein kinase C
PLC	Phospholipase C
PMCA	Plasma membrane calcium ATPase
PTB	Phosphotyrosine-binding domain
PTEN	Phosphatase and tensin homolog, a tumor suppressor gene
RIPA	Radioimmunoprecipitation assay
RTK	Receptor tyrosine kinase
SDS	Sodium dodecyl sulfate
SDS-PAGE	Sodium dodecyl sulfate polyacrylamide gel electrophoresis
SEA	Sea urchin sperm protein, enterokinase and agrin
SEC	Secreted
SERCA	Sarco(endo)plasmic reticulum calcium ATPase
SH	Src homology
Sos	Son of Sevenless
STAT	Signal Transducers and activators of transcription
Syk	Spleen tyrosine kinase
SYM	A pEYFP plasmid containing the full-length MUC1 gene C-terminal to the YFP gene
SYM25	Human embryonic kidney 293T cells expressing genes on the SYM plasmid
TACE	Tumor necrosis factor-alpha converting enzyme, a MMP
TBS	Tris-buffered saline
T-TBS	Tris-buffered saline with Tween 20
Tcf	T cell factor (T cell specific transcription factor)
TGF	Transforming growth factor
TMD	Transmembrane domain
TR	Tranferrin receptor

TSR	Template suppression reagent
UV	Ultraviolet
VCAM	Vascular cell adhesion molecule
VNTR	Variable number of tandem repeats
WASP	Wiskott-Aldrich syndrome protein
WAVE	WASP family Verprolin-homologous protein
YFP	Yellow fluorescent protein
ZAP	Zeta-chain-associated protein kinase

Chapter 1: Introduction

1.0 Introduction

1.1 Background

The MUC1 mucin has long been used as a tumor cell marker in breast cancer. Recent work on the protein has implicated a role in signal transduction and cell migration. The following subsections will expand on concepts associated with these topics as background to the subject of this thesis - the role of MUC1 in the initiation of breast cancer cell migration-related signaling.

1.1.1 Breast Cancer and Metastasis

Breast cancer is the most frequently diagnosed cancer in women, and the second leading cause of cancer deaths in women [1]. One in nine Canadian women will develop breast cancer in her lifetime, and 1/27 will die from it [1]. Ninety-nine percent of these cases arise in women over 30 years of age, with a positive correlation between death rate and increasing age [1]. In the majority of cases, mortality is not caused by the primary tumor, but by the growth of metastases at secondary sites. Distant metastases usually present within 3 years after detection of the primary tumor, but it may occur over 10 years after the initial diagnosis, so the patient is at risk for her entire life [2]. Fortunately, advances in treatment and diagnosis have decreased the rates of metastasis and mortality in recent years. Survival of an individual breast cancer patient ranges from normal life expectancy to as low as 13% survival at 5 years [3]. Several forms of treatment are utilized for breast cancer: partial or total mastectomy to remove the primary tumor, radiation therapy to target specific areas, and systemic adjuvant therapy with chemotherapy and hormone therapy for distant metastatic disease. But even though adjuvant therapy may succeed in eradicating micrometastatic breast tumor cells in some patients, in many others it is ineffective and causes significant negative side effects. In addition, approximately 40% of the patients who undergo adjuvant therapy

relapse and die from secondary metastases [2] – this illustrates the urgent need to develop better treatments to prevent and eradicate metastatic breast cancer.

Breast cancers can be classified into carcinoma *in situ* and invasive carcinoma. A carcinoma *in situ* is limited to the ducts and lobules of the breast, as it has not penetrated the basement membrane. In contrast, an invasive carcinoma has infiltrated through the basement membrane into the surrounding stroma, and is capable of spreading to distant sites. These two categories can be further classified by architecture. Carcinoma *in situ* is divided into ductal and lobular, which represent 15 – 30% and 1 – 6% of all breast cancers, respectively [3]. Invasive carcinomas are divided into ductal (70 – 80% of all breast cancers), lobular (5 – 10%), medullary (2%), mucinous/colloid (1- 6%), tubular (2%), papillary ($\leq$ 1%), and invasive metaplastic carcinomas (< 1%) [3]. Lobular carcinomas, *in situ* and invasive, arise against the background of a loss of the intercellular adhesion molecule, E-Cadherin. However, the majority of carcinomas, which are classified as "ductal", have no known common genetic abnormality.

Certain risk factors increase the chance of carcinogenesis in the breast. These factors can be divided into genetic and hormonal aberrations. The major genetic risk is vertical transmission or germ-line mutation of the autosomally dominant BRCA1 and BRCA2 tumor suppressor genes, where alterations to these genes leads to a 60 – 80% lifetime risk of developing breast cancer [3]. In addition, mutations in 5 other genes are known to increase the risk of breast cancer. These are: the CHEK2 gene, which is involved in DNA repair and activation of BRCA1, the p53 tumor suppressor, the PTEN tumor suppressor, the serine/threonine kinase LKBI, and certain mutations of the ATM gene that is involved in the ataxia telangiectasia disorder [3]. The hormonal factors linked to increased breast cancer risk relate to increasing amounts of hormone exposure. These include: female gender, early age at menarche, late menopause, late first full-term pregnancy or no full-term pregnancies, low time spent breast feeding, and exogenous estrogens [3]. These factors increase the lifetime exposure to estrogen, which drives cellular proliferation, causing pre-malignant lesions and cancers to grow [3]. Furthermore, the estrogen metabolites can depurinate nucleotide bases and generate free radicals

that can damage DNA, potentially resulting in transformation and carcinogenesis [4].

Over 95% of breast cancers are adenocarcinomas, which originate from the glandular tissues of the breast [3]. The initial cellular transformation leads to a number of changes, resulting in an increase in the proliferation rate of epithelial cells. Initially, the neoplastic cells acquire nutrients through simple diffusion [5]. However, as the tumor grows beyond a diameter of 1-2 mm, it must secrete angiogenic factors to generate new blood vessels within itself to support its metabolic needs [5]. At this point, the primary tumor is well established. Several features of the primary breast tumor are predictive of an increased risk of metastasis. These include tumor size, the presence of vascular invasion and a poor histologic grade. For tumor size, tumors that remain under 2 cm are considered to be low risk, tumors between 2 – 5 cm are considered high risk, and tumors over 5 cm have a very high risk of metastasis [2]. Histological grade is a subjective microscopic assessment of deviation from normal epithelial morphology. Grade serves as a surrogate marker for underlying genetic mutations. Increasing grade positively correlates with aggressive cancerous features and risk of metastasis [2].

Cells that metastasize must be able to adhere to the extracellular matrix and the constituent stromal cells, degrade matrix components, and move through the basement membrane and interstitial stroma into the lymphatic or circulatory system through a process known as intravasation [6, 7]. Consequently, an important prognostic marker for an increased risk of developing distant metastases is the presence of tumor emboli in blood or lymphatic vessels [2]. Tumor cells may disseminate through the lymphatic system or systemic blood circulatory system. These micrometastases give rise to lymph node or solid organ metastases respectively. The most important prognostic marker for systemic metastasis is the number of lymph node metastases, with the presence of 4 or more lymph node metastases correlating with a very high risk [2]. In one study of 24,740 cases, the five-year survival for patients with a primary tumor under 2 cm was 96.3% for the node negative group, 87.4% when 1 – 3 nodes were positive, and 66.0% when more than 3 nodes were positive [8].

Metastatic tumor cells that enter the circulatory system eventually become lodged in the capillary beds of secondary organs. The metastatic process in breast cancer is most likely a targeted process. This is supported by the predilection of metastases for certain organs (eg. the bones, liver, and lungs) [9] (Figure 1.1). One explanation for this intriguing finding is that these organs exhibit high levels of the ligands for the CXCR4 and CCR7 chemokine receptors upregulated in breast cancer cells, which would result in chemotactic and invasive responses [10]. Following arrest, the cells extravasate from the circulatory system by invading the surrounding tissue using mechanisms that are probably similar to intravasation [5]. Proliferation of the metastatic cells in the parenchyma of the organ results in the development of pre-angiogenic micrometasases [9]. Continued growth of the secondary metastases is supported by vascularization of the tumors through angiogenesis, enabling survival and engraftment of micrometastases and eventual development of macroscopic tumors, which subsequently impair organ functions, leading to patient mortality (Figure 1.2).

Although the steps of metastasis are known, the molecular events driving them are still poorly understood. Many factors that participate have been identified, but the mechanisms of their contribution are still largely unclear. Our lab has focused on the MUC1 molecule, a glycoprotein that participates in cellular migration. The rationale will be discussed in section 1.2.

1.1.2 Cell Locomotion

Cellular movement consists of cycles of: 1) Extension of membrane protrusions called lamellipodia at the leading edge, which form new attachments to the substratum; 2) Movement of the cell body; and 3) Detachment of adhesions from the rear of the cell (Figure 1.3 and 1.4). In order for lamellipodia to form, cells must grow actin filaments in the direction of movement. The stimulus to rearrange the cytoskeleton begins in the extracellular environment, which leads to preferential localization of adhesion molecules, chiefly integrins, to the leading edge of the cell [11]. Integrins are heterodimeric receptors made up of an α and a β chain. They

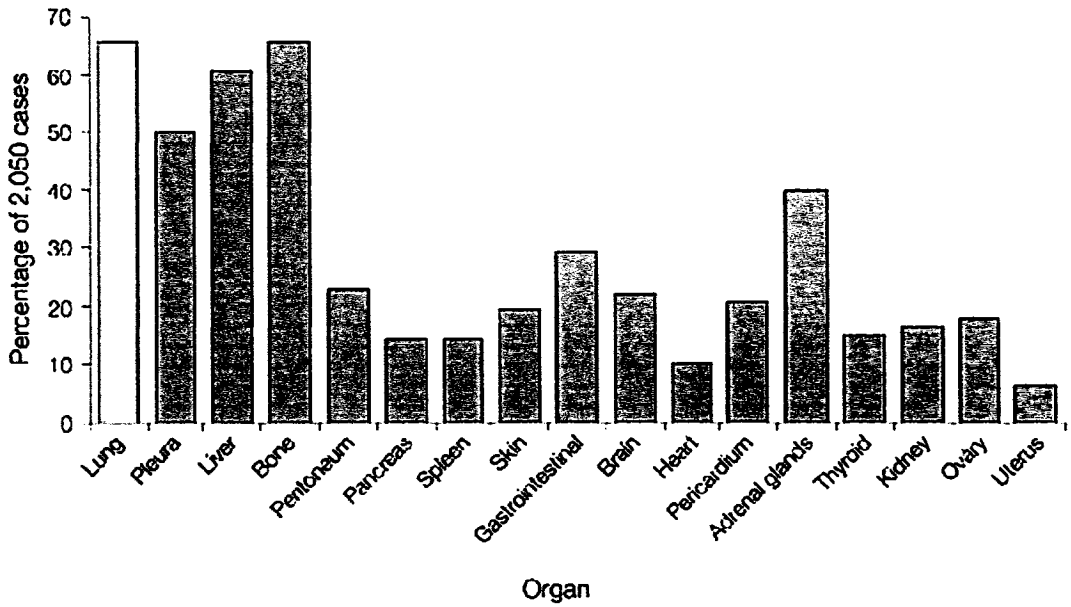

Figure 1.1 Common sites of breast cancer metastasis. Breast cancer cells metastasize through the circulatory system to a number of organs, and preferentially metastasize to the bones, liver, and lungs. (Adapted from [2])

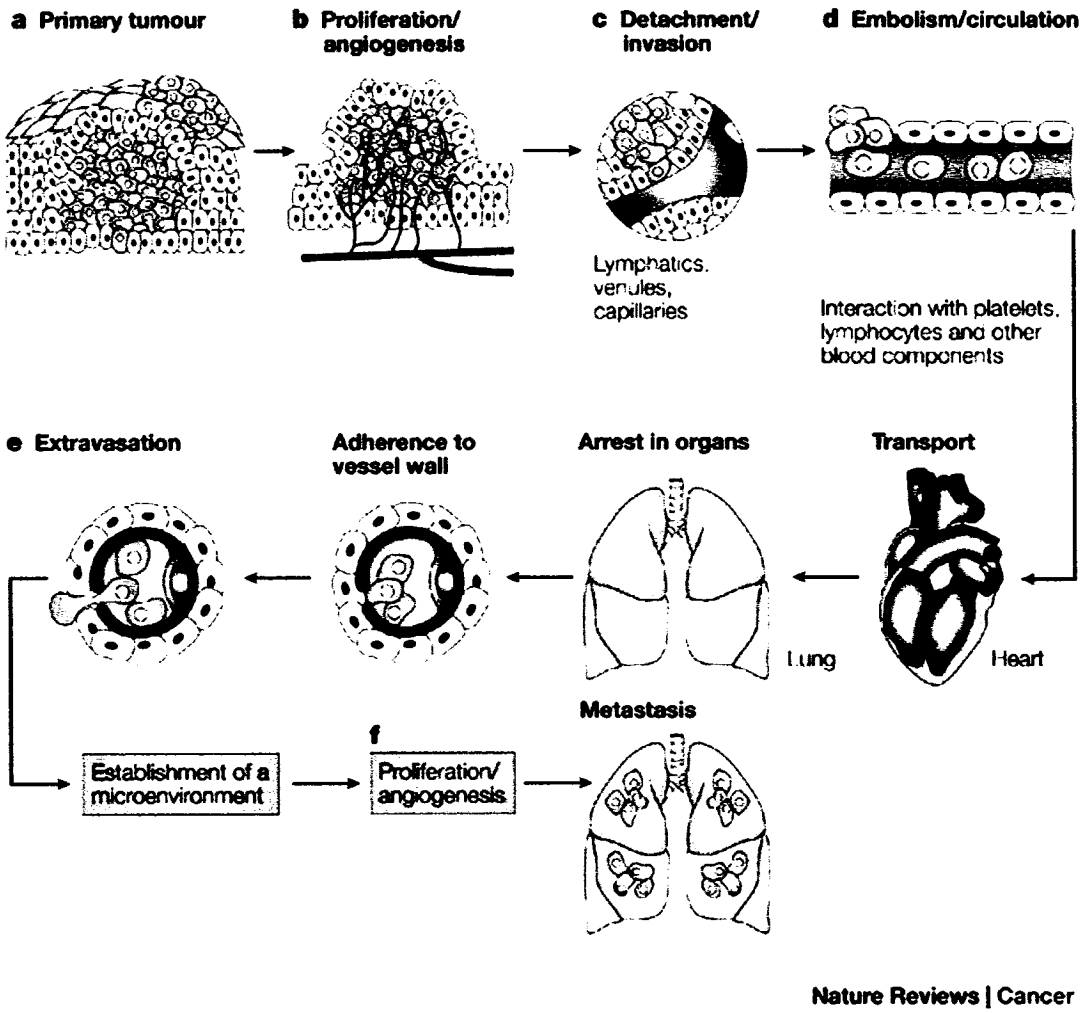

Figure 1.2 The main steps in cancer metastasis. **a)** Cellular transformation and tumour growth. **b)** As the tumor enlarges, vascularization is necessary to maintain growth. **c)** Some tumor cells invade the host stroma into the lymphatic or circulatory system. **d)** The embolus of tumour cells travel through the circulatory system, and eventually become trapped in the capillary beds of distant organs by adhering to the local endothelium. **e)** The tumor cells extravasate from the vessel lumen into surrounding tissues. **f)** The cells begin to proliferate. Micrometastases must develop a vascular network and evade destruction by host defences in order to continue growing. The cells can then invade blood vessels, enter the circulation and produce additional metastases. (Adapted from [5])

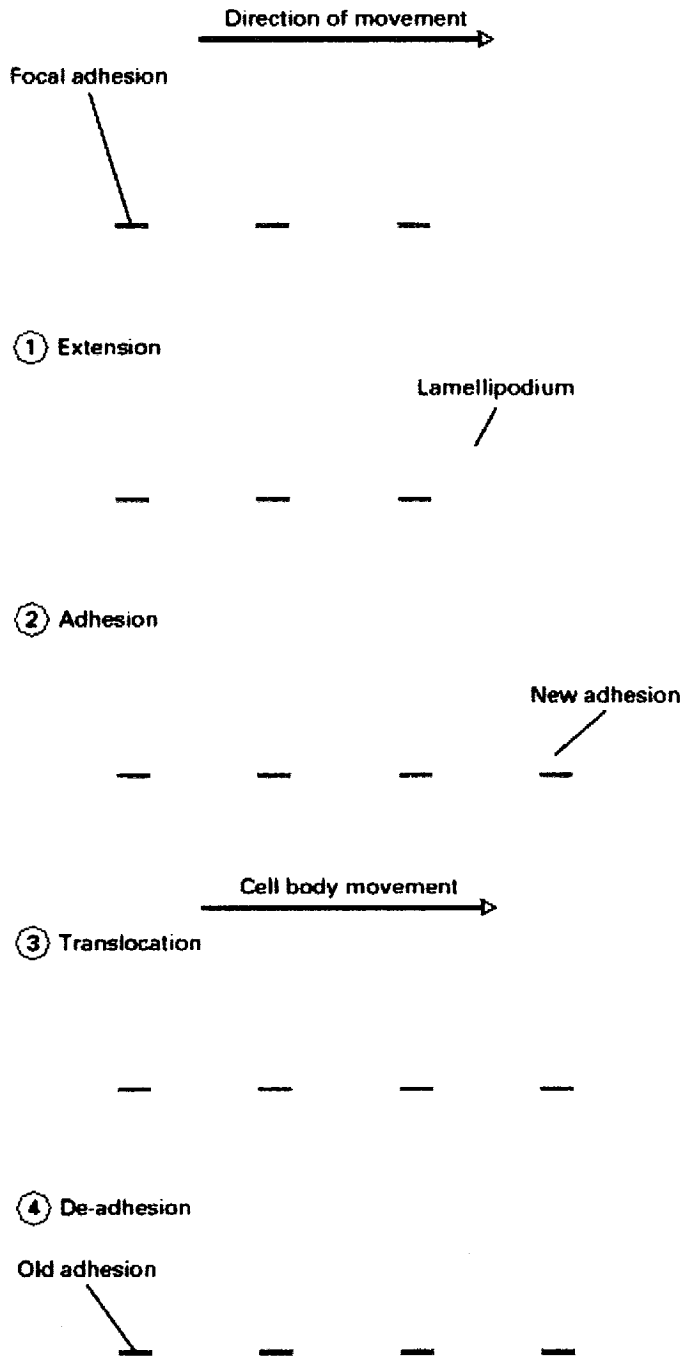

Figure 1.3 Steps in cell locomotion. **1.** The cell extends one or more membrane protrusions called lamellipodia from the leading edge of the cell. **2.** Lamellipodia are stabilized by the formation of new adhesions to the substratum. **3.** The cell body moves forward. **4.** The tail of the cell detaches and retracts into the cell body, allowing the cycle to repeat so the cell can continue directional movement. (Adapted from [12])

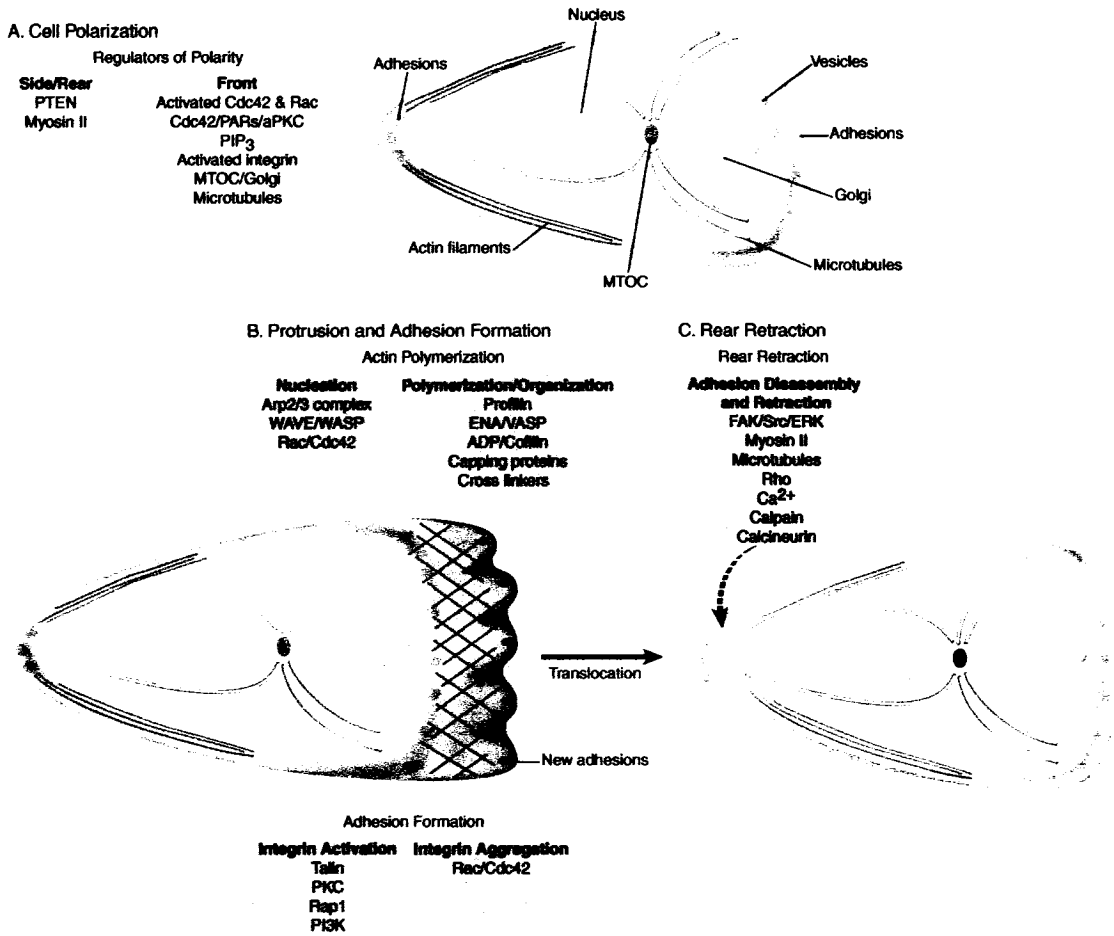

Figure 1.4 Regulation of cellular migration. Important events and the molecules involved in the regulation of these steps are listed in the figure. **A.** For directional movement to occur, the front of the cell behaves differently than the rear of the cell (polarity). Proteins such as Cdc42 are involved in generating polarity, which results in the concentration of molecules and organelles necessary for the formation of forward protrusions towards the front of the cells, and exclusion of these molecules at the rear of the cell. **B.** Formation of actin branches on existing actin filaments pushes the membrane at the front of the cell forward. Integrin activation and clustering, along with the recruitment of a number of structural and signal components, leads to the formation of adhesions, which stabilize the membrane protrusions. **C.** Rear adhesions disassemble through a number of possible mechanisms, allowing the cell to move forward. (Adapted from [11])

have a large extracellular domain that binds to ligands, and a short cytoplasmic domain that initiates many signaling cascades and is linked to the actin cytoskeleton through adaptor proteins [11]. Ligand-binding to the extracellular domain causes integrins to cluster and also induces a conformational change in the cytoplasmic domain [13]. This leads to changes in protein tyrosine phosphorylation, phospholipid biosynthesis, and activation of small GTPases, enzymes that bind to and hydrolyze GTP [14].

Activation of Rac, a Rho family GTPase, activates phosphoinositide 3-kinases (PI3Ks) at the leading edge of the cell through PI3K-sensitive Rac guanosine nucleotide exchange factors (Rac-GEFs) [11]. The PI3Ks produce phosphorylated phosphoinositides, which localize Cdc42, another Rho GTPase, to the front of the cell [11]. Subsequently, Cdc42 activity orients the microtubule-organizing center (MTOC) and Golgi apparatus to the front of the nucleus and faces them towards the leading edge [15, 16]. This promotes microtubule growth and delivery of proteins needed for forward protrusion into the lamella. Cdc42, in addition, activates WASP proteins, which belong to the WASP/WAVE family of Arp2/3 complex activators [11]. The WAVE members, in contrast, are activated by Rac [17]. WASP/WAVE proteins localize Arp2/3 complexes, which bind to the tips and sides of actin filaments at the front of the cell, inducing the growth of new daughter actin filaments [18, 19]. New actin monomers needed for actin polymerization may be released from old actin filaments. Proteins implicated in cleaving and depolymerizing actin include ADF/cofilin proteins and gelsolin [11, 20].

Following forward protrusion of the membrane, new adhesions to the substratum are formed through clustered integrins that associate with large complexes of proteins, providing traction for forward movement. The necessary force for movement is provided by myosin II, a motor protein that moves along actin filaments through conformational changes mediated by hydrolysis of ATP [11]. Myosins are composed of a head, neck, and tail region. Myosin II is composed of 2 heavy chains which make up the head and neck of the structure. The head is able to bind to ATP and actin, and therefore is responsible for the generation of force [12].

The neck, made up of α-helical sequences, regulates head domain activity and causes the myosin to form a rod-like coiled-coil dimer. The tail, made up of myosin light chains, contains binding sites for calcium-binding proteins and can associate with other myosin II chains to form a bipolar complex [12]. Hydrolysis of ATP, consequently, enables movement of the myosin heads along actin filaments anchored at the leading edge of the cell, which produces contractile force to allow the cell body to move forward [11].

As the cell moves, adhesions at the tail must be disassembled to maintain forward motion. Although the details are still not clearly understood, several mechanisms have been implicated to contribute to rear detachment. Tension could disconnect the linkages between the integrins and the actin cytoskeleton, leaving the integrins behind on the substratum [21]. Changes in affinity between integrins and the substratum could potentially detach adhesions. This could be mediated through alterations in the cytoplasmic domain of the integrins, which translates into changes in the extracellular domain [11, 21]. Similarly, detachment could occur through changes in affinity between integrins and its cytoplasmic adaptors [21]. Another possibility is the proteolysis of adhesion components, which could be mediated by enzymes such as the calcium-dependent calpain proteases, resulting in the dissociation of interactions between integrins and the actin cytoskeleton [21]. Finally, pericellular proteolysis could occur, where recruitment of cell surface proteases could digest contact sites on the substratum [21].

1.1.3 Intracellular calcium and regulation of cellular movement

Intracellular calcium is normally maintained at a 100 nM concentration. Following stimulation, however, influx of calcium from external and internal sources can raise this concentration to above 1 μM. External calcium enters the cell down a concentration gradient through various channels, including receptor-operated channels regulated by ligand-binding, voltage-operated channels, and store operated channels regulated by the levels of intracellular calcium [22]. Intracellular calcium is stored in the endoplasmic reticulum (and sarcoplasmic reticulum in muscle cells),

where release is mediated by channels on the endoplasmic reticulum, such as the inositol 1,4,5-triphosphate receptor (IP_3 receptor) and the ryanodine receptors [22]. Coordinated regulation of intracellular calcium results in patterns of calcium concentrations that vary in frequency, amplitude, duration, and subcellular localization [22]. Coupling of this complex pattern of calcium to calcium-sensitive molecules in signal transduction pathways, which are themselves controlled spatially and temporally, leads to changes in cell behavior.

Mechanistically, it has been proposed that calcium initially enters a cell following stimuli such as membrane depolarization, noxious stimuli, extracellular agonists, stretch, depletion of intracellular stores, or intracellular messengers [23]. External calcium is the principle source of calcium for calcium oscillations in this initial phase, and initial entry of calcium is promoted by the large electrochemical gradient across the cell membrane [23]. The calcium is used to activate diverse entry channels with different properties, and other calcium-entry channels, such as voltage operated channels, receptor-operated channels, second-messenger-operated channels, and stretch-operated channels can open in response to different external signals [23]. The subsequent release of calcium from internal stores is modulated by calcium or second messengers, which include IP_3, nicotinic acid adenine dinucleotide phosphate, cyclic ADP ribose, and sphingosine-1-phosphate [23].

Focusing on the IP_3 pathway, PLC-γ must be activated to produce IP_3, but the dynamics of IP_3 production varies depending on the receptor used in its activation – some of this variability might be attributed to the cell-type specific response of various receptors interacting with different transducing elements and PLC isoforms [23]. Synthesis of IP_3 leads to binding of the second messenger to the IP_3 receptor on the endoplasmic reticulum, thereby triggering calcium release from intracellular ER stores into the cytosol [24]. The IP_3 receptor, primarily regulated by IP_3 and calcium, generates local signals called "calcium puffs", which increase the surrounding (~2 – 6 μm) cytosolic calcium concentration to ~50 – 600 nM in durations of less than one second, reflecting the transient opening of the channels [23]. Calcium released in this manner can diffuse to and activate neighbouring IP_3

receptors in a process known as saltatoric propagation, enabling the initial local signal to induce global calcium oscillations and waves [23].

There is some controversy over the mechanism of generating calcium waves and spikes, but one view is centered around calcium-induced calcium release (CICR), and this self-activating process is thought to represent a key element in generating instability to produce repetitive calcium spikes [24]. Calcium has a biphasic effect on the IP_3 receptor, where low levels of calcium sensitizes the receptor to IP_3 to allow for its activation, and high levels of calcium inhibits the receptor by decreasing its sensitivity to IP_3 [23, 24]. As a result, once the IP_3 receptor is activated, calcium is released into the cytosol when the previous calcium puff has dissipated below a certain threshold concentration, thereby generating repetitive calcium waves. The amplitude of the calcium spikes eventually decreases as the internal calcium stores are depleted [24]. An alternate view for generating calcium waves is centered around IP_3 levels, where the periodic variation of IP_3 acts to induce a similar periodic activation of the IP_3 receptor. These changes in the level of IP_3 are thought to arise from a positive feedback loop involving induction of IP_3 synthesis through calcium, and degradation of IP_3 through IP_3 3-kinase, resulting in temporary increases in IP_3 degradation [23, 24]. However, other studies have demonstrated that calcium oscillations can occur with a constant IP_3 level, suggesting that this alternate mechanism does not apply to some situations [24]. There are additional methods of regulating calcium release through the IP_3 receptor, including phosphorylation by calmodulin-dependent kinase II, PKC, cGMP-dependent protein kinase, and cAMP-dependent protein kinase (PKA) [23], but additional research is needed to better define the mechanism for producing regenerating calcium waves.

Following calcium signaling, various pumps and exchangers are activated to remove calcium from the cytoplasm to restore the resting level of calcium and to reload internal calcium stores [23]. Four different mechanisms have been shown to be important in this end phase of calcium signaling: the plasma membrane calcium ATPases (PMCAs), the mitochondrial uniporter, sodium-calcium exchangers (NCXs), and sarco(endo)plasmic reticulum calcium ATPases (SERCAs) [23].

These mechanisms have different thresholds for activity, and the pumps have different calcium transport rates and affinities [23]. As a result, activation of different combinations of these pumps and exchangers enables the various cell types to meet their specific calcium signaling requirements [23].

A number of critical regulators and proteins involved in cellular movement react to changes in intracellular calcium. Notable examples include the IQGAP family of proteins, which associate with the calcium-sensitive calmodulin (CaM) protein when calcium levels increase [25]. IQGAP binds to and stabilizes the GTP-bound conformation of Rho GTPases such as Cdc42 and Rac [25]. Since Rac and Cdc42 are critical in regulating forward membrane protrusion and adhesion, association with IQGAP would be important at the lamella for lamellipodia formation, whereas dissociation from IQGAP at the rear of the cell would be important for the detachment of adhesions. Furthermore, several Rho GTP exchange factors (RhoGEFs) and Rho GTPase activating proteins (RhoGAPs), which regulate the transition of Rho GTPases to the active GTP-bound and inactive GDP-bound forms respectively, have been reported to contain sites for direct calcium binding [25]. In addition, Myosin II, which is responsible for generating contractile forces for movement, can be positively regulated by myosin light chain kinase (MLCK), which is regulated by intracellular calcium [11]. Finally, a number of proteins implicated in rear detachment are affected by calcium concentrations. These include: the calpain group of proteases, which can cleave focal adhesion proteins [11], calcineurin, a phosphatase which been demonstrated to be responsible for detachment of integrin-mediated adhesion as well as recycling of integrins to the leading edge [21], and gelsolin, an actin depolymerization factor [20].

1.1.4 Cell Surface Receptors and transduction of a signal across the cell membrane

Cell to cell communication is mediated by signaling molecules, which vary widely in composition, and include proteins, peptides, steroids, nucleotides, and small organic molecules. Some can pass through the membrane to initiate a signal

intracellularly, like the small hydrophobic steroids. Others, however, cannot freely pass through the cell membrane and must bind to a cell surface receptor to transduce a signal. These receptors operate through a large number of diverse mechanisms, but many seem to propagate their signals in a stereotypical manner conforming to the mechanisms employed by a few types of receptors. The most common of these are: the receptor tyrosine kinases (RTKs), the receptors bound to nonreceptor tyrosine kinases (NRTKs), and the G-protein-coupled receptors (GPCRs).

RTKs are transmembrane proteins that have intrinsic tyrosine kinase activity. They consist of an extracellular ligand-binding domain that may be glycosylated, a single transmembrane domain, and a cytoplasmic domain, which contains a conserved protein tyrosine kinase and phosphorylatable regulatory sequences [26]. RTKs can be classified according to their ligand, biological function, or primary structure – examples include the epidermal growth factor receptor (EGFR) family and the platelet-derived growth factor receptor (PDGFR) family [27] (Figure 1.5). For the majority of RTKs, activation and initiation of signal transduction follows a common pattern. Binding of an extracellular ligand to the extracellular domain of the receptor leads to receptor clustering or, in the case of preclustered receptors, a conformational change or relocalization in the membrane [26, 27]. Receptor dimerization can be induced in several ways, including interaction with a bivalent ligand, homodimeric ligand, or stimulation with two different ligands [27]. Clustering of the receptor induces autophosphorylation of the receptor's catalytic and non-catalytic domains, where tyrosine residues on the receptor's cytoplasmic domain are either phosphorylated by its own enzymatic activity (*cis*), or by an identical neighboring receptor (*trans*). Phosphorylation of the catalytic domain generally enhances the catalytic activity of the receptor's intrinsic kinase, and phosphorylation of non-catalytic domains can result in the creation of docking sites for cytoplasmic proteins. These proteins dock via Src homology 2 (SH2 - binds phosphotyrosines) or phosphotyrosine binding (PTB) motifs [26], and recruitment of additional docking proteins and effectors leads to potentiation of the signal.

Other transmembrane receptors lack intrinsic tyrosine kinase activity, but still couple ligand binding to tyrosine phosphorylation. Notable examples include

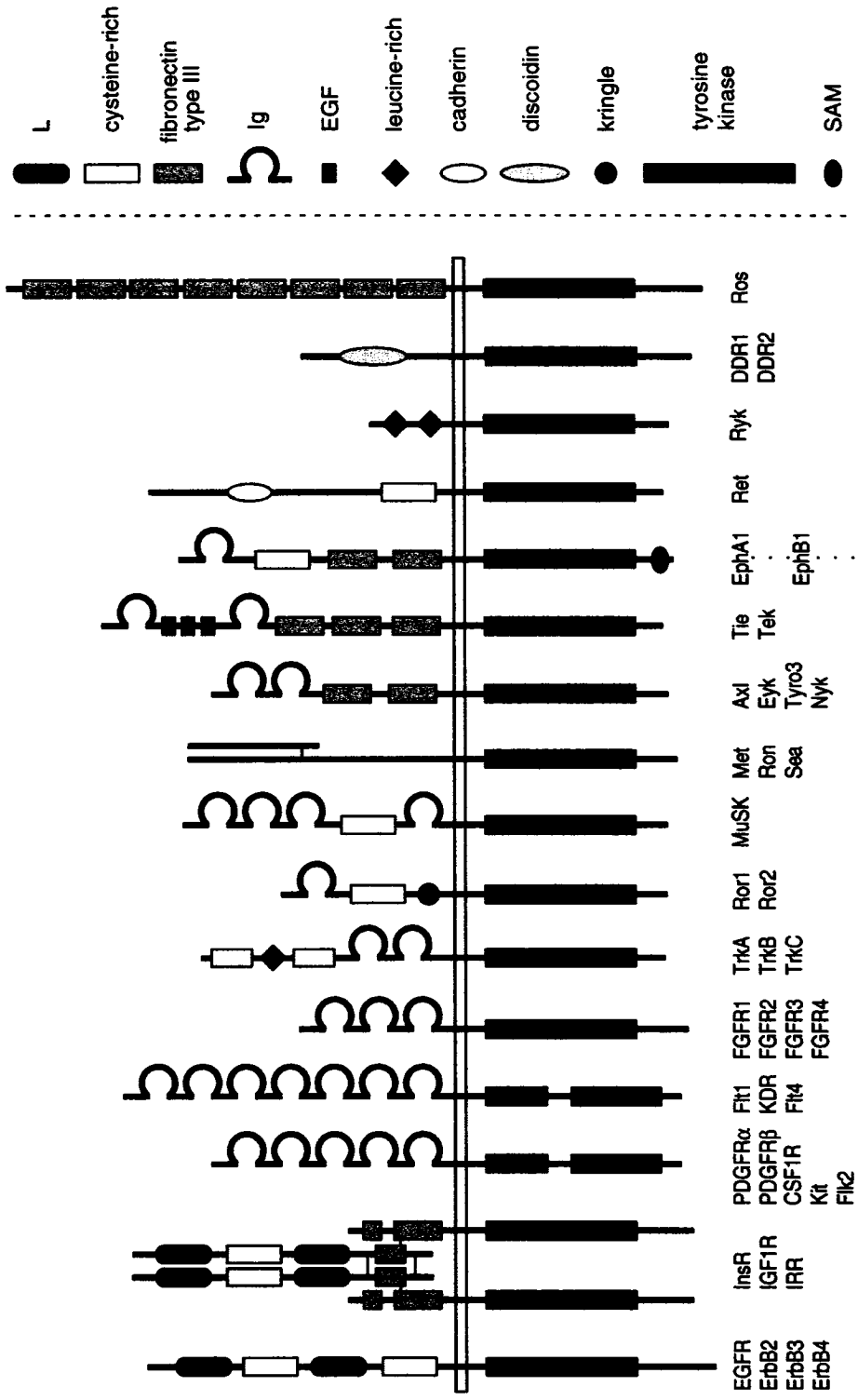

Figure 1.5 Examples of receptor tyrosine kinases. Common features include an extracellular domain, a single transmembrane domain, and a cytoplasmic domain that contains a tyrosine kinase and phosphorylatable sequences involved in regulation of downstream signaling and intrinsic kinase activity. (Adapted from [28])

the CD4 and CD8 receptors on T lymphocytes, integrins, and cytokine receptors such as interleukin-2 (IL-2). Similar to RTK activation, binding of a ligand to the extracellular domain of the receptor can induce receptor oligomerization [28, 29]. Phosphorylation of the receptor or downstream targets, however, is performed by nonreceptor tyrosine kinases (NRTKs), which associate with, and act as a subunit of the receptor. These protein kinases lack the extracellular and transmembrane domains found in receptor tyrosine kinases, and most are found in the cytoplasm, although some are associated with the membrane through a myristoyl or palmitoyl group [28]. NRTKs contain a tyrosine kinase domain, in addition to diverse protein-protein interaction domains, such as phosphotyrosine-binding SH2 and polyproline-binding SH3 domains [28] (Figure 1.6). Two prominent examples of NRTKs include the Src family kinases and the Janus kinase (JAK) family. Ligand-induced receptor oligomerization leads to the activation of the non-covalently bound NRTKs, which results in phosphorylation of tyrosine residues on the receptors and/or downstream targets [28]. Signal transduction continues though the recruitment of proteins to the phosphorylated docking sites and activation of additional downstream molecules.

G-protein-coupled receptors (GPCRs) are transmembrane receptors that contain 7 transmembrane domains connected by 3 extracellular and 3 intracellular loops, with an extracellular N-terminus and a cytoplasmic C-terminus [30, 31]. The classical example of a G-protein coupled receptor is the β-adrenergic receptor. These seven-transmembrane receptors are named G-protein-coupled receptors because the majority of them signal through heterotrimeric G proteins (Figure 1.7). They are called G proteins because the α subunit can bind to and hydrolyze GTP. In the absence of agonist, the heterotrimeric G protein is inactive and consists of 3 subunits (α, β, and γ) that is bound to GDP through the α subunit, and may associate with a GPCR on the cytoplasmic face of the plasma membrane [31, 32]. Upon binding to ligand, the receptor changes conformation, and serves as a guanosine exchange factor to enable the G proteins to release GDP and bind GTP [31]. This activated heterotrimer splits into two parts: the α subunit, and the βγ heterodimer,

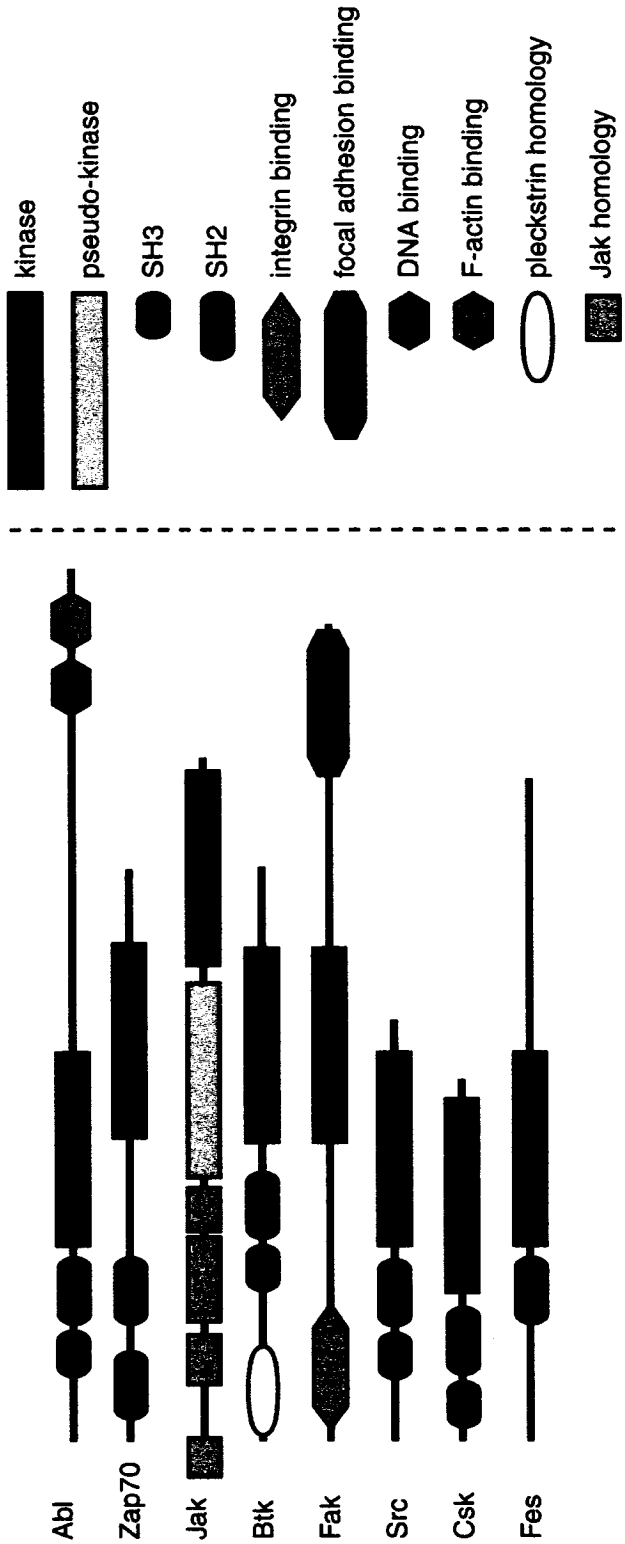

Figure 1.6 Major subfamilies of nonreceptor tyrosine kinases. Common features include a tyrosine kinase domain and protein-protein interaction domains. (Adapted from [28])

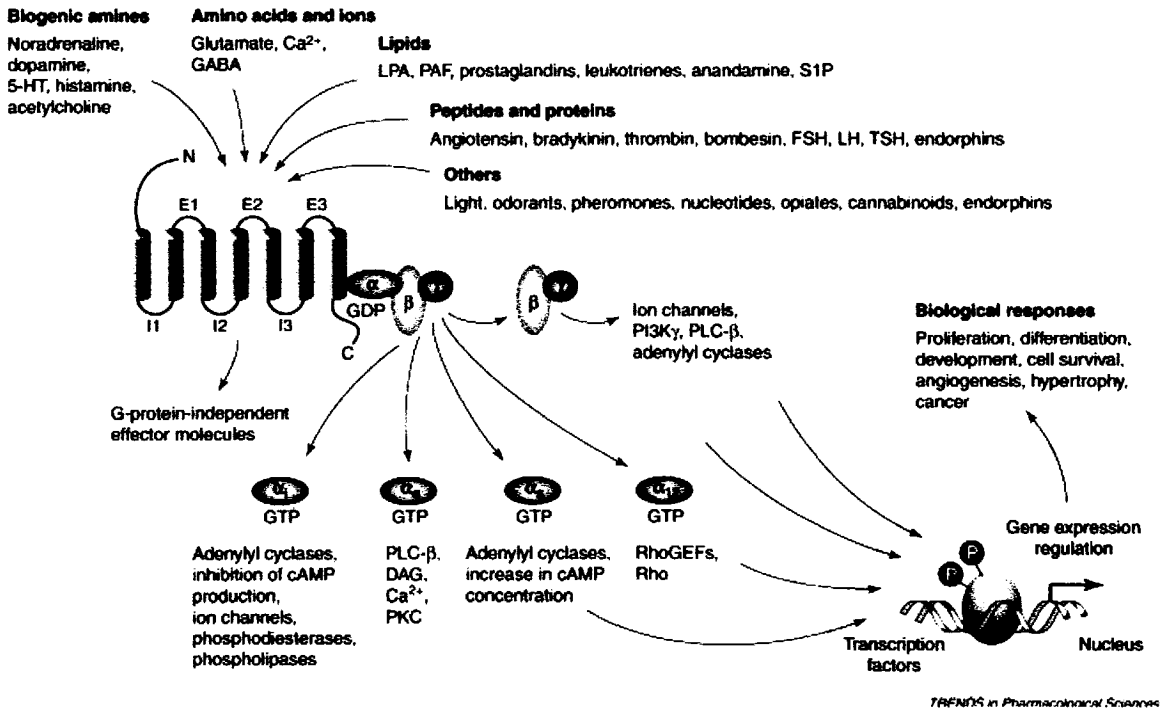

Figure 1.7 Structure and signaling of the majority of G-protein-coupled receptors. G-protein-coupled receptors consist of 7 transmembrane domains connected by 3 extracellular and 3 intracellular loops. Most of these receptors signal through heterotrimeric G proteins, which exchange GDP for GTP upon binding of a variety of ligands to the receptor. Activation of the G protein leads to dissociation of the G protein from the receptor, and dissociation of the trimer into an α subunit and a βγ dimer, which can act on different targets independently. (Adapted from [32])

which dissociate from the receptor and can act independently on different downstream targets [31].

It should be noted that there are numerous other mechanisms of transducing a signal through the membrane. Several examples include: receptor serine/threonine kinases, which may undergo ligand-induced heterodimerization and transphosphorylation (like the TGF-β receptor), ion-channel receptors where ligand-induced conformation changes enables specific ions to move across the membrane (like the nicotinic acetylcholine receptor), and receptors that undergo ligand-induced endocytosis and translocation to the nucleus, where they may influence transcription (like the NOTCH receptor).

1.1.5 Lipid Rafts and their participation in signaling

The plasma membrane is not homogenous in composition, and clustering of certain lipids leads to the formation of specialized microdomains in the lipid bilayer. Lipid rafts are a subset of these microdomains. They are found in the exoplasmic leaflet of the bilayer, and have increased concentrations of cholesterol and sphingolipids [33]. Since these sphingolipids have saturated hydrocarbon chains that are straight, this enables cholesterol to be tightly intercalated, forming a relatively solid platform in the membrane [33]. Furthermore, due to the detergent resistance of saturated sphingolipids and cholesterol, these regions are detergent insoluble [34]. In contrast, the exoplasmic leaflet surrounding these rafts is more fluid, since the majority of the phospholipids are unsaturated, resulting in a kinked structure that does not pack tightly [33]. Lipid rafts are approximately 50 nm in diameter, and contain an estimated 10 to 30 proteins, depending on packing density [33]. They are differentially distributed depending on the cell type. For example, rafts are found on the apical surface in polarized epithelial cells, the axonal plasma membrane in neurons, and all over the surface in lymphocytes and fibroblasts [33].

Lipid rafts are dynamic in a number of ways. First, they can include or exclude proteins to variable extents [33]. Some proteins have a naturally high affinity for raft localization, and include doubly acylated proteins such as Src family

kinases and the α subunit of heterotrimeric G proteins, palmitoylated and cholesterol-linked proteins such as Hedgehog, glycosyl-phosphatidylinositol-anchored (GPI-anchored) proteins, and certain transmembrane proteins [33]. In addition, a given protein can alter its affinity for raft localization. For example, a protein in monomeric form may only have a short residency in lipid rafts, but its affinity may increase following dimerization or oligomerization [33]. Second, rafts undergo continuous endocytosis from the cell surface. Once incorporated into early endosomes, lipid rafts either directly recycle back to the plasma membrane, or indirectly recycle through delivery to the Golgi [33]. The latter route allows the incorporation of new proteins into the rafts, and is also used as a method for polarized delivery of proteins to the lipid bilayer in many cell types [33]. Third, separate rafts carrying different proteins can merge. This creates new microdomains in the plasma membrane that are enriched in specific enzymes, and potentially brings together molecules that can interact with each other [33].

Because of these properties, lipid rafts have diverse functions in a cell. They have been reported to play a role in endocytosis, transcytosis (the internalization and excretion of extracellular material from different sides of the cell membrane), potocytosis (sequestration and transport of molecules by caveolae, flask-shaped invaginations in lipid rafts composed mainly of caveolins), internalization of bacteria, viruses and toxins, protein sorting, calcium homeostasis, and signal transduction [34]. The role of lipid rafts in signal transduction is of particular interest. Studies characterizing raft proteins have shown that a wide range of receptors and signaling molecules are incorporated or concentrated into these microdomains [34]. By compartmentalizing the signaling components of a given signaling pathway, an appropriate stimulus could lead to a specific and efficient response [34]. Segregation of signaling molecules from the general membrane may protect the signaling complex from inappropriate protein interactions, and also promote interactions between molecules involved in the pathway. Movement of some of these proteins into or out of rafts could determine which pathways are activated in response to a particular stimulus. In addition, re-localization of signaling complexes is facilitated since the signaling complexes are already pre-

assembled in lipid rafts. Furthermore, spatial regulation of cross-talk between pathways or higher order signaling could be regulated through clustering of specific subsets of rafts containing different pre-assembled signaling complexes [34]. Although several models of signal initiation through lipid rafts have been hypothesized, the precise contributions of raft dynamics to signaling remain unclear. Nevertheless, a number of signaling pathways have been demonstrated to require these detergent-insoluble microdomains, including growth receptor signaling (via stimulation with EGF, PDGF, FGF-2, and insulin), glial-cell-derived neurotrophic factor (GDNF) signaling, Ras signaling, Hedgehog signaling, GPI-linked protein signaling, and multicomponent immune receptor signaling (which includes IgE receptor, T-cell receptor, B-cell receptor, and the interleukin-2 receptor) [33, 34].

1.2 Structure and Function of the MUC1 mucin

The MUC1 protein belongs to a family of mucins that are characterized by dense O-glycosylation of simple core-type glycans on serine- and threonine-rich clusters [35]. There are currently more than 15 classified mucins, which are classified according to their repeat domains and chromosomal locations [35] (Figure 1.8). Mucins line glandular epithelia as part of the protective biofilm on their surface where the secreted mucins, such as MUC2, are a component of the viscoelastic gel. Membrane-tethered mucins, such as MUC1, are implicated in additional roles mediated by protein-protein interactions that are not yet clearly defined.

1.2.1 Structure and molecular functions of MUC1

MUC1 is a type I transmembrane protein consisting of two non-covalently bound subunits [36]. The smaller subunit consists of the cytoplasmic domain, the transmembrane domain, and a short piece of the extracellular sequence, whereas the larger subunit consists of the extracellular mucin (Figures 1.9 and 1.10). Structurally, the extracellular domain consists of non-repeating sequences flanking

Cysteine-rich domain
This is cysteine rich and is not heavily glycosylated.

Cysteine-rich/cysteine-knot domain
A domain that is conserved with von Willebrand factor and the cysteine knot of TGF-β that mediates dimerization of mucin molecules.

Cytoplasmic tail
This domain is found on the cytoplasmic side of the cell-surface membrane. It often contains sites of phosphorylation that interact with mediators of signal transduction and might mediate association with cytoskeletal elements.

D domain (D1, D2, D′, D3)
These show sequence homology to the von Willebrand factor 'dimerization' domain and mediate trimerization of secreted mucin core proteins such as MUC2.

D domain (D4)
A region of sequence homology to the D4 dimerization domain of von Willebrand factor; includes the GDPH autocatalytic site near the amino terminus of MUC2 and MUC5AC.

Epidermal-growth-factor (EGF)-like domains
Show homology to EGF and related growth factors and cytokines (for example, Cripto). They are believed to mediate interactions between mucin subunits and ERBB receptors.

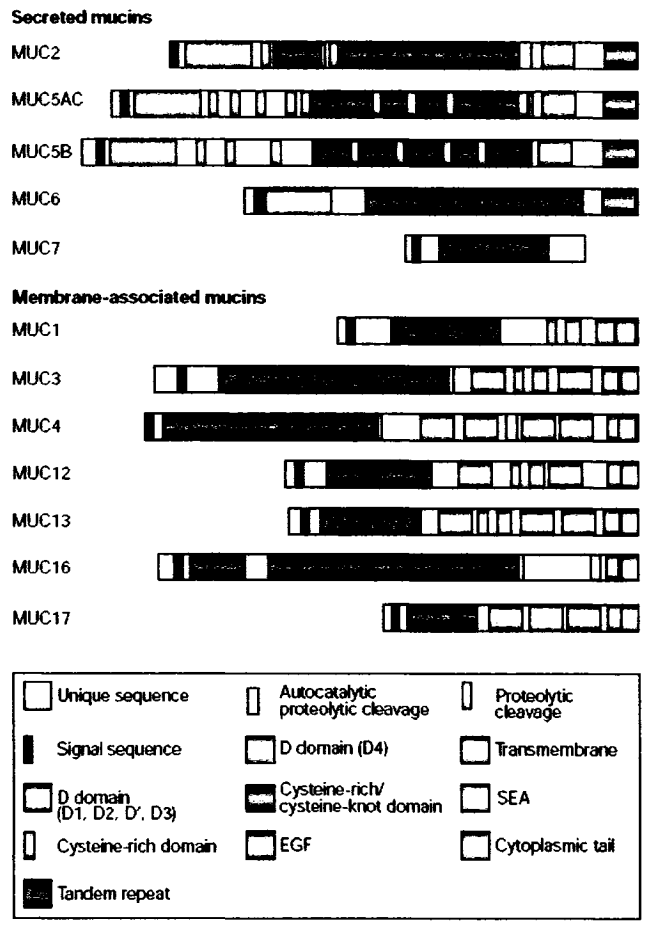

GDPH autocatalytic proteolytic cleavage site
An autocatalytic proteolysis site in some mucins (demonstrated for MUC2, conserved in MUC5AC and MUC4) that cleaves between GD and PH residues. A second step might involve formation of an autocatalytic ester linkage between the α carbon of the carboxy-terminal D residue and an internal *N*-acetylgalactosamine moiety on a chondroitin-sulphate glycosaminoglycan on the other subunit, forming a unique covalent bond by which mucin subunits are linked to other secreted molecules.

SEA domain
Named for a common domain found in sperm protein, enterokinase and agrin that was identified by sequence homology. It is widely distributed among cell-surface-associated proteins that are heavily *O*-glycosylated and is postulated to function in protein binding to carbohydrate moieties. Among mucins, this domain was originally identified in MUC1 and has subsequently been found in MUC3, MUC12, MUC13 and MUC17.

Signal sequence
Directs insertion into the endoplasmic reticulum for secretion or cell-surface delivery.

Tandem repeat
Rich in serine, threonine and proline residues. They are heavily *O*-glycosylated and are characteristic of mucin core proteins. There is a high degree of sequence similarity within any one repeat, but very little sequence conservation between different repeats or between orthologues. They can be highly polymorphic for length and sequence variability.

Transmembrane domain
Membrane-spanning domain that creates an integral membrane protein, which is found in cell-surface-associated mucins.

Proteolytic cleavage site
Conserved proteolytic cleavage site that is found within the SEA domains of some mucins and outside of the SEA domains in others. It facilitates the creation of mucin subunits that remain associated.

Figure 1.8 Cell surface-associated and secreted mucins. Mucins are characterized by dense O-glycosylation of simple core-type glycans on serine- and threonine-rich clusters. There are currently more than 15 classified mucins, which are classified according to their repeat domains and chromosomal locations. Mucins not shown include MUC8, a secretory mucin, MUC11, MUC15 and MUC20, membrane-tethered mucins, and MUC9. (Adapted from [37])

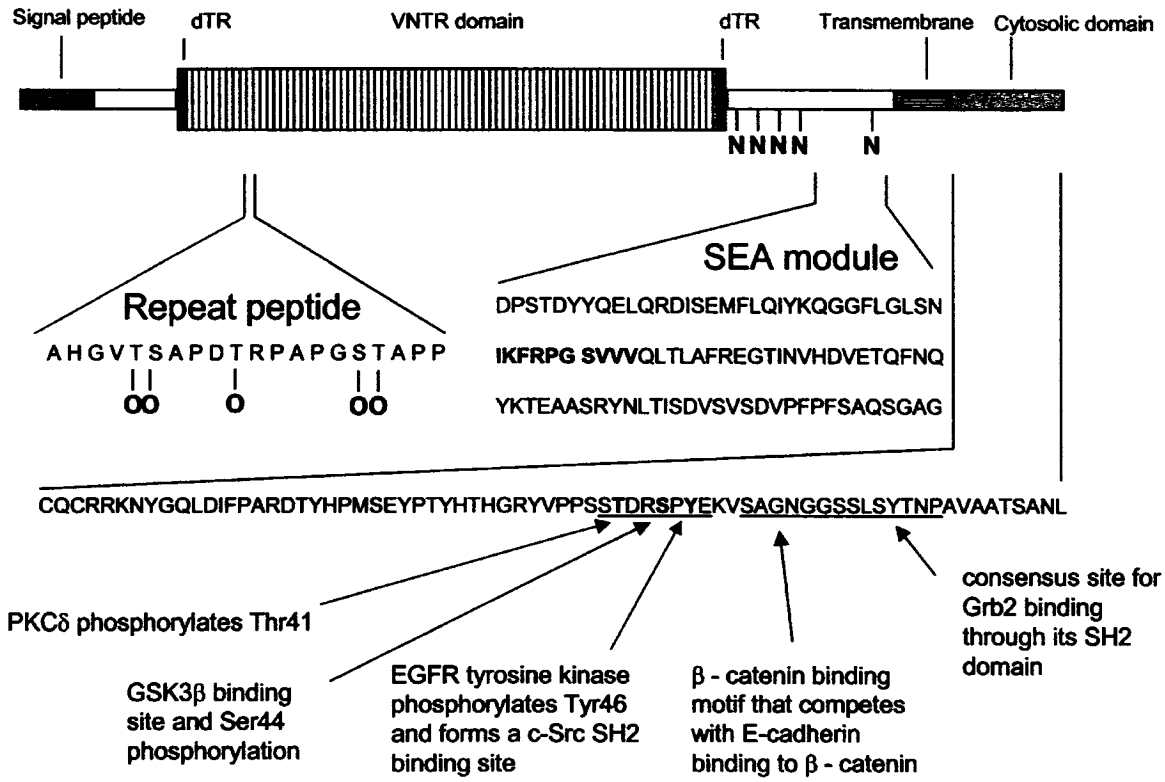

Figure 1.9. Structure of the MUC1 protein. Key features from the extracellular N-terminus (left) to the cytoplasmic C-terminus (right) are as follows: a signal peptide for apical localization, a region of VNTRs (variable number of tandem repeats) with 5 O-glycosylatable residues (represented by O's), 5 N-glycosylation sites (represented by N's), an SEA module that contains a cleavage site, a 31 amino acid transmembrane domain, and a 69 amino acid cytoplasmic domain. (Adapted from [35])

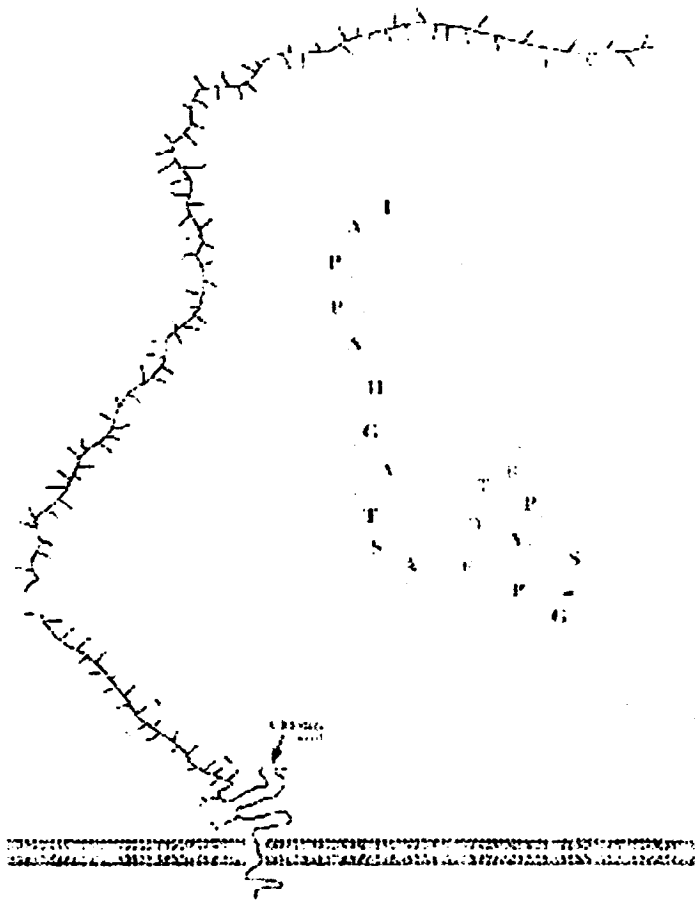

Figure 1.10 Three-dimensional schematic of MUC1. The MUC1 extracellular domain is rod-shaped and extends 200 – 500 nm from the cell surface. It contains 20 – 120 tandem repeats of a 20 amino acid sequence that tends to be heavily O-glycosylated. The extracellular domain is associated with the second MUC1 subunit consisting of the membrane-spanning transmembrane domain and the cytoplasmic domain through tight non-covalent interactions following cleavage of the extracellular SEA module. (Adapted from [38])

both ends of a region of tandem repeats. There are several notable features in this domain. First, it has a signal peptide that directs insertion of the MUC1 precursor peptide into the endoplasmic reticulum for delivery to the cell surface [37]. Second, there are 20 – 120 repeats of a 20 amino acid sequence, where the number is determined by genetic polymorphism [39]. Each repeat contains 3 threonines and 2 serines which tend to be heavily O-glycosylated, although the degree of glycosylation appears to vary depending on the organ, reflecting the distinct requirements of these environments [37]. Specifically, normal glycosylation levels vary from 50% of the available sites in the mammary gland to 80% in the pancreas [40]. Third, the extracellular domain has 5 sites for N-glycosylation. Glycosylated regions in mucins are crucial for mucin function, and are thought to play a number of roles, including binding to proteins and molecules, providing hygroscopic properties, and maintaining the rigidity of the MUC1 extracellular fragment [35, 37]. In addition, O-glycosylations are thought to be involved in apical targeting, as decreases in the amount of these saccharides results in an increased rate of MUC1 endocytosis and subcellular redistribution [41]. Finally, the MUC1 extracellular domain has an SEA module (sea urchin Sperm protein, Enterokinase, Agrin) that contains a cleavage site [42]. Following self-cleavage catalyzed by conformational stress, the extracellular domain forms a tight non-covalent bond with the short extracellular sequence on the smaller membrane-tethered subunit [36, 43, 44]. Three-dimensionally, the extracellular domain is rod-shaped and extends from 200 to 500 nm from the cell surface, a significant distance compared to the 10 nm height of the glycocalyx [40].

The second subunit of MUC1 contains the transmembrane domain, a hydrophobic helix that is 31 amino acids in length, and the cytoplasmic domain [35]. At present, 2 functions have been attributed to the transmembrane and cytoplasmic domains. First, it might be necessary for movement of MUC1 into the detergent-insoluble lipid raft regions of the cellular membrane, as deletion of the cytoplasmic domain resulted in an inability to isolate MUC1 from the detergent-soluble regions of the membrane, suggesting that MUC1 was still present in the lipid rafts [45]. Second, the transmembrane domain contains a C-Q-C motif at the junction between

the transmembrane and cytoplasmic domains. This motif is necessary for localization to the cellular membrane, as changes to the sequence result in relocalization of the protein to the cytoplasm [45].

MUC1 has a 69 amino acid cytoplasmic domain with features supporting a role in movement and signaling. In terms of movement, the cytoplasmic domain is believed to bind to actin, since disruption of actin filaments with cytochalasin D alters the polarization of the mucin [46]. In addition, MUC1 has been demonstrated to co-localize with ezrin, a cytoskeletal anchor protein [47]. In terms of signaling, MUC1 has 7 conserved tyrosines, of which 4 have been reported to be phosphorylated [48]. Since phosphorylatable tyrosines are common in signal transduction pathways, the presence of these residues implies that MUC1 may be involved in signaling. MUC1, however, does not have an intrinsic kinase to phosphorylate these residues, but several extrinsic kinases, such as c-Src [49], EGFR [50], and GSK3β [51], have been shown to be capable of performing this function. Furthermore, a number of tyrosine kinases have been coimmunoprecipitated with MUC1, including lck, syk, and ZAP-70 [40].

MUC1 protein synthesis is coupled to insertion into the endoplasmic reticulum [35]. While translation is occurring, mannose-rich glycans are transferred to the growing peptide, resulting in N-glycosylation of asparagine residues [35]. Immediately after translation, a site in the SEA module is cleaved [43], and the two fragments reassociate to form a heterodimer [35]. Subsequently, the peptide is transported to the Golgi apparatus, where processing of N-glycans continues and O-glycosylation of serine and threonine residues is initiated [35]. However, one passage through the Golgi is not sufficient to fully glycosylate the mucin, and the initial appearance of MUC1 on the cell surface is in an immature form. Maturation is completed through multiple cycles of clathrin-coated endocytosis and sialylation in the *trans* Golgi, resulting in a final molecular mass of 300 – 600 kDa [35]. The mature glycoform can remain tethered to the cell membrane, where it may participate in signal transduction leading to behavioral changes for the cell [35]. Alternatively, the extracellular mucin subunit can be released from the membrane, by conformational stress [44], TACE/ADAM17 [52], or MT1-MMP [53], thereby

regulating signal transduction by preventing extracellular ligand binding [35, 40]. In addition, dissociation of the mucin fragment enables it to function like a secretory mucin.

1.2.2 Alternative splicing of MUC1

Alternative splicing patterns of MUC1 pre-mRNA leads to the generation of several different mature mRNA molecules that are translated and processed into various protein isoforms (Figure 1.11). MUC1/SEC is a secreted form of MUC1 that lacks the cytoplasmic and hydrophobic transmembrane domains of the full length protein [40]. The other 2 isoforms, MUC1/Y and MUC1/X (which is also called MUC1/Z) lack the tandem repeat domains and part of the SEA motif, preventing cleavage of the molecule. The difference between the two isoforms is that MUC1/X contains 18 more amino acids in its extracellular domain than MUC1/Y [40]. The function of these proteins is currently not known. MUC1/Y, however, is preferentially expressed in breast carcinomas, and overexpression of this protein is correlated with increased tumorigenic potential in mouse DA3 cells [40]. MUC1/SEC has been implicated in promoting MUC1/Y signaling, by binding to the MUC1/Y extracellular domain and inducing phosphorylation of its cytoplasmic domain [40].

1.2.3 Biological functions of MUC1 at the cellular level

MUC1 is found on the apical surface of glandular and ductal epithelial cells in many organs, including the breast, pancreas, and the respiratory and gastrointestinal tracts. MUC1 is also found in non-epithelial cells such as activated T cells, plasma cells, and dendritic cells [35, 40, 54].

It was originally thought that MUC1 would be similar to other members of the secretory mucin family, in that it would have functions linked to the protection of epithelia. Some of these functions include: acting as a barrier by binding to cellular debris and pathogens, providing lubrication, maintaining hydration, and

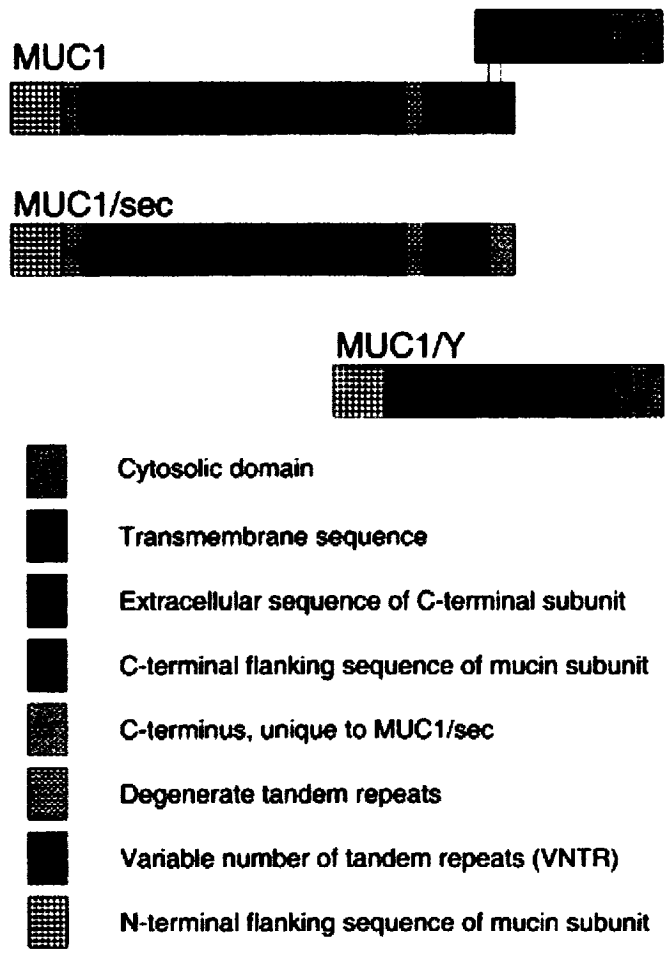

Figure 1.11 Protein architecture of MUC1 isoforms. Alternative splicing of the MUC1 gene results in the generation of different proteins. MUC1 is the full length heterodimeric protein, MUC1/sec is missing the transmembrane and cytoplasmic domains, and MUC1/Y is missing the extracellular tandem repeats and part of the SEA module. MUC1/X (a.k.a MUC1/Z), which is not shown, is similar to MUC1/Y, but has an additional 18 amino acids in the extracellular domain. (Adapted from [35])

participating in mucociliary clearance [35, 40]. Although MUC1 may contribute to these functions, numerous studies have determined that the glycoprotein has a number of additional functions. First, the glycoprotein seems to be involved in sensing and responding to the surrounding microenvironment. For example, the binding of MUC1 to bacteria leads to increased phosphorylation of tyrosine residues on the cytoplasmic domain and results in alterations to cellular adhesion [40]. Furthermore, MUC1 appears to be crucial in immune responses and development. MUC1-null mice have T cells that do not proliferate following activation, natural killer and dendritic cells that show defects, and thymocytes that halt in development before the double positive $CD4^+CD8^+$ stage (reviewed in [40]). In addition, MUC1 is thought to have both adhesive and anti-adhesive properties. Specifically, the presence of sialyl $Lewis^{x/a}$ carbohydrates on the MUC1 O-linked glycans provide ligands for selectin-like molecules on nearby cells, thereby increasing intercellular adhesion. Conversely, the extended conformation and charge of the MUC1 extracellular domain may destabilize interactions with the matrix and other cells, resulting in decreased intercellular adhesion [40]. These examples illustrate adhesive and anti-adhesive effects mediated by the extracellular domain. The cytoplasmic domain, however, might drive different effects by signal transduction through a number of pathways.

1.2.4 Signaling molecules associated with MUC1

An enlarging body of literature is developing for signaling molecules that bind to the cytoplasmic domain of MUC1. Much of the focus has been on β-catenin and molecules that can impact its localization, but several other pathways have been investigated as well.

β-catenin is a component of adherens junctions that indirectly links the actin cytoskeleton to cadherin cell-surface adhesion molecules [55]. The MUC1 cytoplasmic tail contains a binding site for β-catenin (SXXXXXSSL) (Figure 1.9), and *in vitro* experiments demonstrate that β-catenin can bind to this site [56]. The degree of binding can be influenced by glycogen synthase kinase 3β (GSK-3β),

which binds to MUC1 at the STDRSPYE sequence [51]. GSK-3β phosphorylates the second serine in the sequence, and this decreases binding between MUC1 and β-catenin [51]. As a result, a larger pool of β-catenin is available to interact with E-cadherin, which is involved in intercellular adhesion. Conversely, the degree of binding between MUC1 and β-catenin can be increased in two known ways. First, phosphorylation of the YEKV motif in the MUC1 cytoplasmic domain (by c-Src or EGFR) allows c-Src to bind to MUC1 via its SH2 domain [49, 57]. Binding of c-Src decreases the affinity between MUC1 and GSK-3β, resulting in an increase in affinity between MUC1 and β-catenin [49, 57]. Second, phosphorylation of the TDR sequence next to the β-catenin by protein kinase C δ (PKCδ) increases MUC1-β-catenin binding, and this interaction can be abrogated by mutating the PKCδ phosphorylation site [58]. Furthermore, MUC1 has been found to colocalize with β-catenin in the nucleus, where it coactivates transcription of β-catenin-Tcf-binding sites and is involved in upregulating the activation of the cyclin D1 promoter [59].

In addition, MUC1 has been found to participate in a number of other signaling pathways. EGFR has been found to coimmunoprecipitate and phosphorylate MUC1 following EGF stimulation, and this leads to activation of the ERK 1/2 pathway, which is involved in regulation of cell differentiation and physiology [50, 60]. Grb2/Sos binds to MUC1 through its SH2 domain [61], and subsequent interaction with Ras might lead to changes in cytoskeletal integrity, proliferation, cell adhesion, apoptosis, and cell migration. Association of the MUC1 cytoplasmic domain with p120(ctn) leads to translocation of the complex into the nucleus, suggesting a role in nuclear signaling [62]. Stimulation with 17beta-estradiol (E2) allows MUC1 to bind to and stabilize the estrogen receptor alpha, thereby promoting E2-mediated growth [63]. Stimulation with heregulin induces binding of MUC1 to γ-catenin, an effector in the tumorigenic Wnt pathway [64]. In addition, heregulin also induces the formation of a complex containing the MUC1 cytoplasmic fragment, HSP70, and HSP90. Translocation of this complex to the mitochondrial outer membrane results in inhibition of stress-induced activation of the intrinsic apoptotic pathway [65].

These pathways are important in regulating many important cellular processes. Changes in MUC1 expression and behavior, consequently, could lead to dysfunction in these pathways, and thereby contribute to carcinogenesis.

1.2.5 MUC1 expression in breast cancer and clinical implications

Mucins have been implicated in carcinogenesis for many years. MUC1 expression is maintained or increased in greater than 90% of breast cancers. Early clinical studies in breast cancer patients found that high concentrations of mucins in patient serum positively correlated with tumor burden and poor prognosis [37]. Interestingly, although tumor cells with high levels of MUC1 show increased invasion *in vitro*, generalized overexpression has no effect on the clinical prognosis of a breast cancer patient [54, 66]. Increasing amounts of cytoplasmic MUC1, however, correlates with poorer survival, independently of an increase in tumor grade [66]. Excessive MUC1 can also be shed or secreted into serum, and the presence of this soluble MUC1 near tumor cells is capable of inhibiting infiltration of lymphocytes into those tissues [35]. Similarly, tumor cells expressing membrane-tethered MUC1 are able to block attachment and killing by cytotoxic T cells and to inhibit the activity of natural killer cells [40]. Tumor cell adhesion is also affected by changes in MUC1 expression, as the addition of underglycosylated MUC1 peptide *in vitro* inhibited the attachment of breast cancer cells to immobilized extracellular matrix proteins [67]. Furthermore, circumferential membrane staining is a marker for a high risk of metastasis, as it is associated with positive lymph node status (reviewed in [35]).

In breast cancer, MUC1 displays several aberrant properties (Figure 1.12). First, it is overexpressed, which can be attributed to several factors, such as amplification of the number of MUC1 gene copies, which results in increased transcription and translation of the glycoprotein [68]. In some B-cell lymphomas, the MUC1 gene is translocated near the Ig heavy chain enhancer near the origin of chromosomal DNA replication, which has relatively high activity [40]. In addition, MUC1 expression is upregulated by STAT factors, interferons, prolactin, and steroid

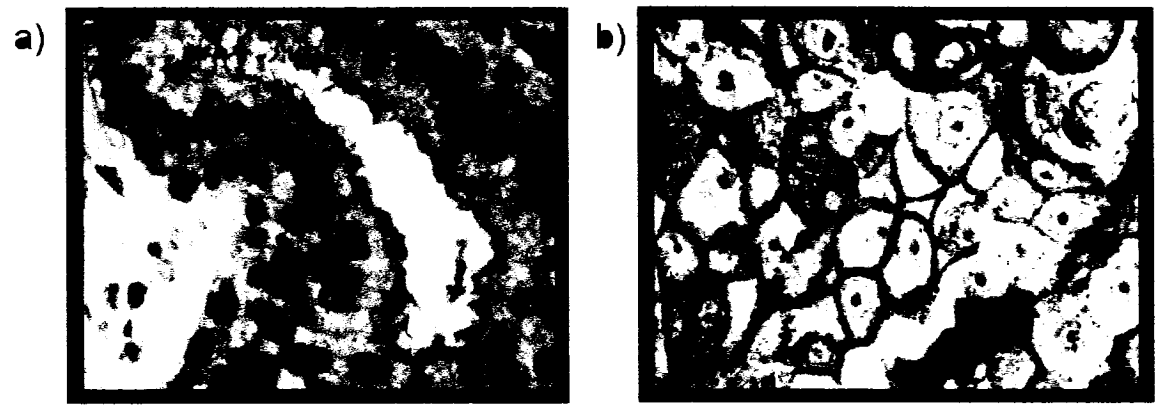

Figure 1.12 Localization of MUC1 on breast epithelia. a) MUC1 is located on the apical surface of normal breast epithelia. **b)** In breast cancer, MUC1 is overexpressed, underglycosylated, and loses its apical polarization.

hormones [40]. Second, the tandem repeats on the extracellular domain of MUC1 are underglycosylated. This is due to defects in saccharide biosynthesis, resulting in the production of shorter, less branched O-glycan chains [69, 70]. Finally, in some higher grade tumors with loss of tumor cell polarity, MUC1's intracellular localization becomes cytoplasmic or circumferential around the plasma membrane [66].

Breast cancer mortality is caused by the growth of metastases in distant organs. The movement of cells from tissue into the circulatory system and vice versa is essential for this process, and the data implicate the MUC1 protein in adhesion and cellular movement. The question then becomes: how might MUC1 mediate this increase in metastatic potential on the molecular level? Earlier work from our lab demonstrated that tumor cell MUC1 could bind to endothelial ICAM-1 [71]. Since leukocyte extravasation involves an interaction between leukocyte LFA-1 and endothelial ICAM-1, we questioned whether tumor cells expressing MUC1 might utilize a similar mechanism for transmigration.

1.3 Structure and Function of the ICAM-1 glycoprotein

There are several families of membrane-tethered adhesion molecules that mediate adhesion to other cells or to the extracellular matrix. The Intercellular Adhesion Molecule 1 (ICAM-1) belongs to the immunoglobulin supergene family. It is a transmembrane glycoprotein with a 28 amino acid cytoplasmic domain, a 24 amino acid transmembrane domain, and a 453 amino acid extracellular domain that contains 5 immunoglobulin-like repeats [72, 73]. These repeats have a β sheet structure, and stabilization of this structure occurs through a combination of disulfide bonds and hydrophobic interactions [72]. As a result, the extracellular domain is shaped like a hinged rod (Figure 1.13). The ICAM-1 molecule is 505 amino acids in length, but differences in glycosylation in various cell types results in a molecular weight between 80 – 114 kDa (reviewed in [72]). The majority of ICAM-1 is expressed on the cell surface in a homodimeric form, and, although the

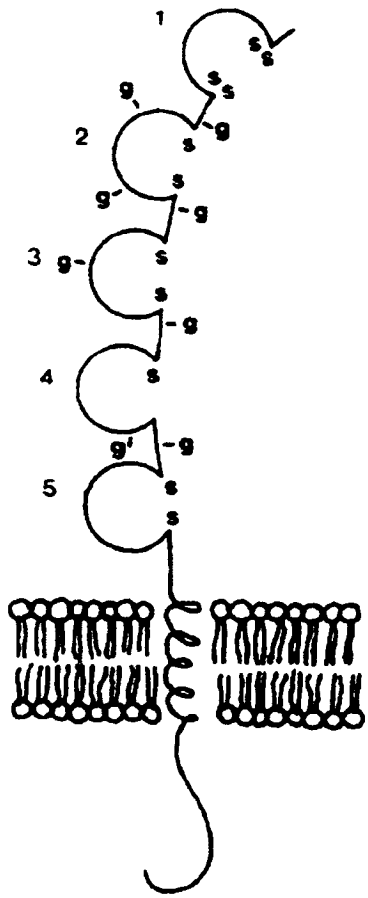

Figure 1.13 Structure of the Intercellular Adhesion Molecule-1. ICAM-1 consists of a 453 amino acid extracellular domain with 5 Ig-like domains, a 24 amino acid transmembrane domain, and a 28 amino acid cytoplasmic tail. Each Ig domain consists of two sheets of anti-parallel strands. Disulfide bonds are formed between B and F strands, except for the fourth domain, which is stabilized by hydrophobic amino acids and α disulfide bonds formed with cysteines in flanking strands. The extracellular domain is shaped as a slightly bent rod-like structure. It rises 18.7 nm from the cell surface. "g's" represent N-glycosylation sites. (Adapted from [72])

monomeric form is still functional, it performs at a reduced efficiency when compared to the dimer [74].

ICAM-1 is constitutively expressed on the surface of epithelial and endothelial cells, dermal fibroblasts, melanocytes, and leukocytes [74]. These levels can be increased through stimulation by inflammatory cytokines, such as Tumor Necrosis Factor α (TNFα), Interleukin 1 (IL-1), and Interferon γ (IFN-γ) [73]. ICAM-1 binds to the heterodimeric β2 integrins LFA-1 (CD11a/CD18) and MAC-1 (CD11b/CD18) found on leukocytes [73]. In addition to these major ligands, ICAM-1 has also been reported to bind to CD43 on leukocytes and platelets, soluble fibrinogen, the extracellular matrix component hyaluronan, rhinoviruses, and the coxsackie A13 virus [72]. ICAM-1 mediates intercellular adhesion and is essential in leukocyte trafficking (see section 1.3.1), as well as mediating leukocyte effector functions, microbial pathogenesis, adhesion to T cells during antigen presentation, and signal transduction initiated by external events [73]. Furthermore, the ICAMs in general are important in immune response, inflammation, development of the nervous system, and development during the embryonic stage [73].

1.3.1 Transendothelial Migration Mediated by ICAM-1

Leukocytes migrate from the blood into tissues during inflammation and immune surveillance [75]. Transmigration by circulating leukocytes can be divided into several steps: 1. rolling on the endothelium, 2. attachment to endothelial cells, and 3. transmigration through this layer of endothelial cells (Figure 1.14). In the first step, leukocytes contact the luminal side of the blood vessel and begin rolling on the surface through low-affinity interactions between leukocyte carbohydrates and endothelial selectins and addressins, or through interactions between leukocyte $\alpha_1\beta_1$-integrin and endothelial vascular intercellular adhesion molecule-1 (VCAM-1) [75]. These weak associations slow the leukocyte down, allowing for additional bonds to form between the leukocyte and the endothelium. In the second step, the selectin/addressin interaction induces signal transduction in the leukocyte, leading to an increase in the affinity of leukocyte integrins to their ligands [75]. Integrin

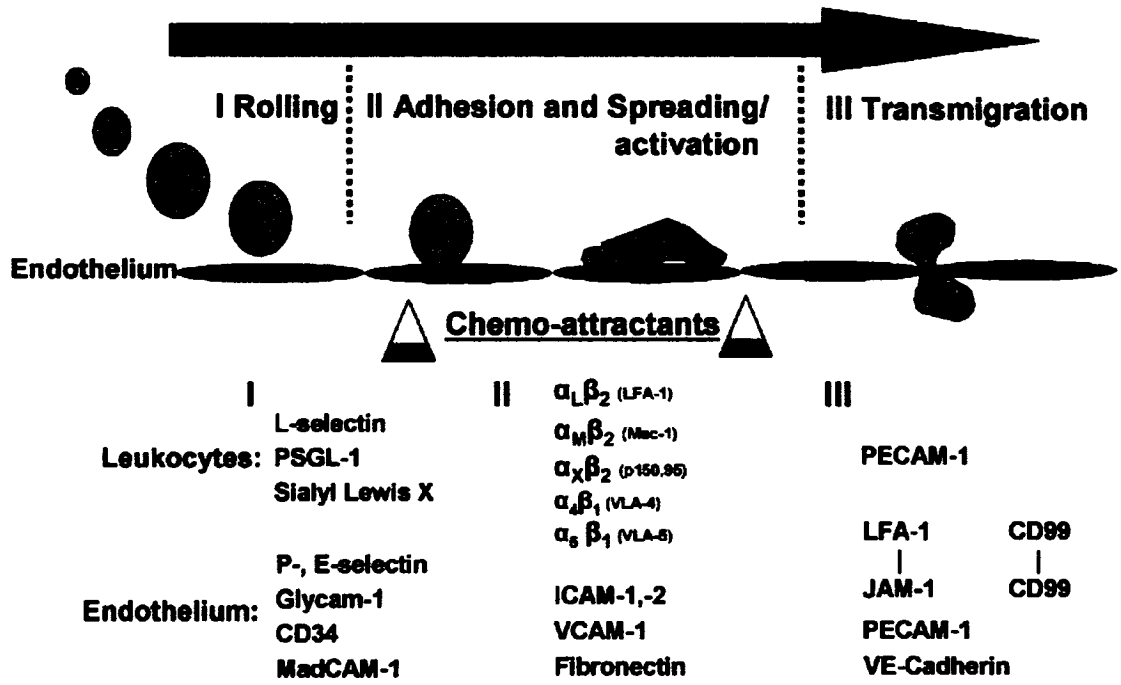

Figure 1.14 Overview of the steps that comprise leukocyte transendothelial migration. Step I represents rolling of leukocytes on the endothelium and involves adhesion molecules such as selectins on the leukocytes or endothelial cells and their ligands on the cellular counterparts. **Step II** represents firm adhesion, mediated through immobilized chemoattractants on the endothelium and adhesion molecules such as integrins on the leukocytes and CAMs on the endothelium. **Step III** represents the diapedesis of the leukocytes through the endothelial cell–cell junctions, in which homophilic binding molecules are involved. (Adapted from [76])

affinity is further augmented by chemokines produced by the endothelial cells [75]. As a result, the leukocyte integrin LFA-1 is able to tightly bind to additional adhesion molecules on the endothelium, such as VCAM-1 and ICAM-1 [75]. These tight interactions cause the leukocyte to stop rolling along the surface of the endothelium.

Adhesion of a ligand to ICAM-1 causes intracellular calcium flux and activation of protein kinase C (PKC) in the endothelial cell, and subsequent downstream signaling alters the cytoskeleton and behavior of cell junction proteins [75]. Localized retraction at lateral junctions creates an opening between the endothelial cells, and adhesion and transmembrane molecules in the junctions provide attachment points for leukocytes to complete their migration [75] (Figure 1.15). As mentioned earlier, tumor cell MUC1 also binds ICAM-1, and the next section will outline the reasons why MUC1-mediated tumor cell extravasation may be similar to the leukocyte migration model.

1.4 Review of MUC1-ICAM-1 binding and associated signaling

Similar to leukocyte extravasation, tumor cells can contact endothelial cells and begin rolling along the surface through interactions between tumor cell carbohydrates (such as the sialic acids on the MUC1 extracellular domain) and endothelial selectins [77, 78]. Subsequently, tighter adhesion occurs between tumor cell MUC1 and endothelial cell ICAM-1, and this adhesion between MUC1-expressing transfectants or breast cancers cells with ICAM-1-expressing HUVEC cells can be disrupted with antibodies to either molecule [71]. Furthermore, the interaction is strong enough to withstand shear stresses caused by physiological fluid flow conditions [79]. The MUC1/ICAM-1 interaction is also involved in cell motility and migration. ICAM-1 stimulation of MUC1-expressing cells with fluorescently labeled actin showed lamellipodia formation (unpublished) (Figure 1.16). In contrast, when either MUC1 or ICAM-1 were missing, no signs of significant cytoskeletal reorganization was detected (unpublished). These data support the role of MUC1 in tumor cell motility. Studies from this lab have also

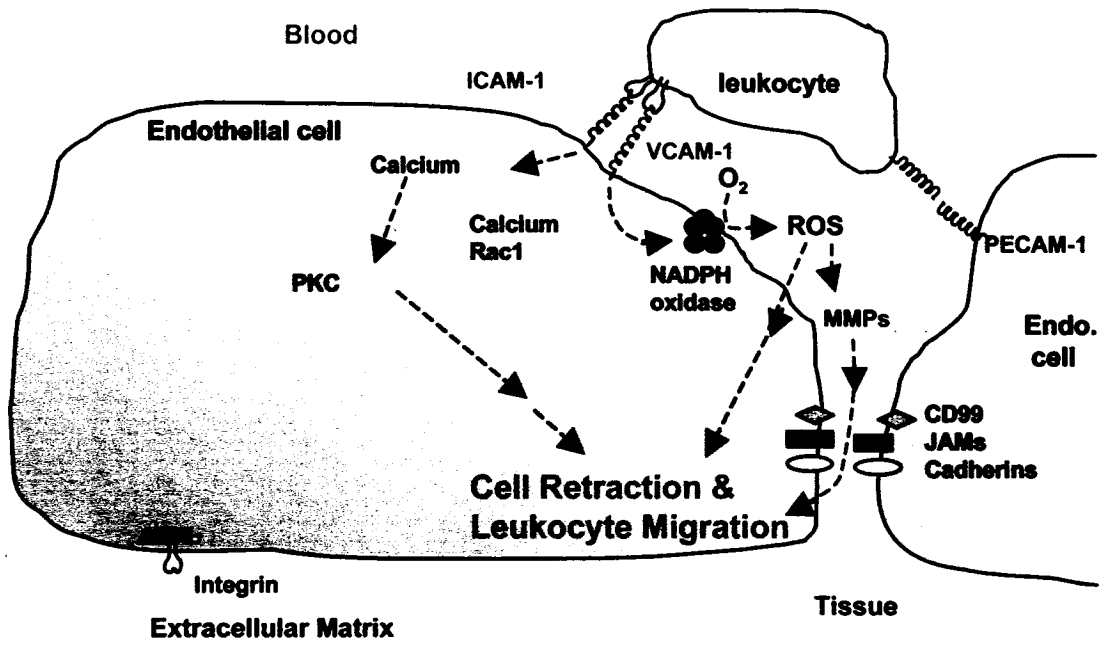

Figure 1.15 Overview of the signaling pathways and events that occur during transendothelial migration in endothelial cells. Stimulation of ICAM-1 and VCAM-1 activates "outside-in" signals, which are required for leukocyte migration. Intracellular calcium or PKC in brain endothelial cells is necessary for ICAM-1-dependent lymphocyte migration but not lymphocyte adhesion. Lymphocyte binding to VCAM-1 activates release of intracellular calcium, calcium channels, and Rac1. Stimulation of NADPH oxidase is required for the VCAM-1-dependent activation of endothelial cell-associated matrix metalloproteinases (MMPs). Alteration of the cytoskeleton and junctional adhesion molecules (JAMs) leads to localized retraction at lateral junctions. (Adapted from [75])

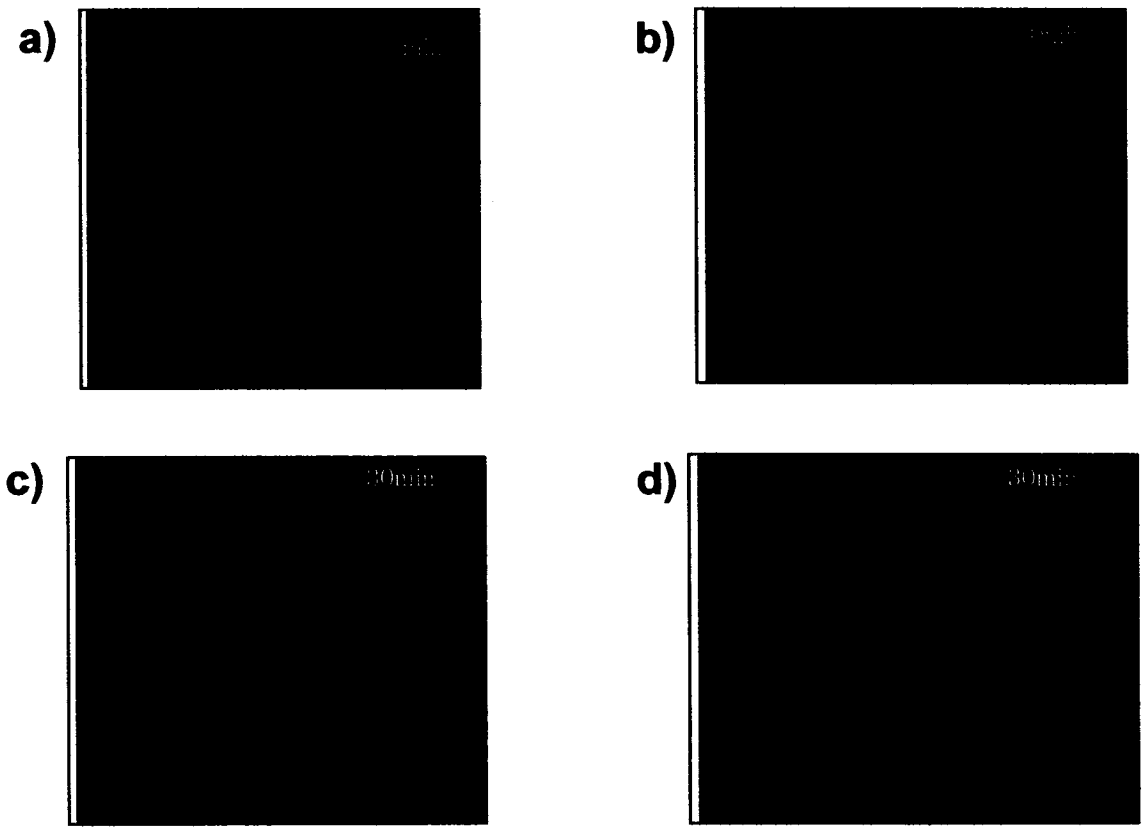

Figure 1.16 Cytoskeletal rearrangement mediated by the MUC1/ICAM-1 interaction. HEK 293T cells were doubly transfected with MUC1 and EGFP-actin. NIH 3T3 cells either expressing ICAM-1 **(a)** and **(c)** or lacking ICAM-1 **(b)** and **(d)** were dropped over the transfectants, and the MUC1 transfectants were visualized after 30 minutes. Only MUC1 cells stimulated by ICAM-1 formed lamellipodia, as depicted by the red arrows **(c)**. This experiment was done by Qiang Shen.

documented MUC1's role in cell migration. A blood vessel wall with underlying stroma was simulated in a transwell system, where ICAM-1-expressing HUVECs were plated on the upper surface of the transwell, and fibroblasts or ICAM-1-expressing NIH-3T3 cells were plated on the lower surface (Figure 1.17). Cells were dropped into the upper chamber, and their ability to migrate through the transwell was monitored. Dropped cells expressing MUC1 showed increased migration, and antibody blockade with antibody to either MUC1 or ICAM-1 decreased their migration by 60 – 70% [80]. This indicates that although the MUC1/ICAM-1 is clearly important in mediating migration of MUC1-expressing breast cancer cells, it is not the only mechanism used for movement through an endothelial cell-lined membrane.

There are several things known about the mechanism by which ICAM-1-induced MUC1-mediated migration may occur. For adhesion, MUC1 must express at least 2 tandem repeats, and the first immunoglobulin domain of ICAM-1 must be intact [81, 82]. Following contact between MUC1-expressing cells and ICAM-1-expressing cells, intracellular calcium oscillations are induced in the MUC1-expressors [83] (Figure 1.18). One requirement for these oscillations to occur is the presence of intact lipid rafts, detergent-insoluble regions of the membrane with high concentrations of signaling molecules [83]. It should be noted that MUC1 is also present in the rafts, suggesting an association with a signaling complex in the lipid rafts (Figure 3.1b). Release of calcium is mediated by the phospholipase C-IP_3 pathway, and inhibitors of phospholipase C, phosphoinositol 3-kinase, the IP_3 receptor, and Src family kinases are able to reduce calcium oscillations to levels seen in the negative controls [83]. This data suggests that a number of possible downstream targets relevant to cytoskeletal reorganization and cell motility could be activated, such as gelsolin [84], calpain [85], and calmodulin [86]. This is consistent with the known ability of MUC1 to interact with signaling molecules associated with motility, including GSK3β, Src, PKCδ, β-catenin, Grb/Sos, and EGFR (reviewed in [80]). Taken together, the MUC1/ICAM-1 interaction generates a signal that may be important in tumor cell migration.

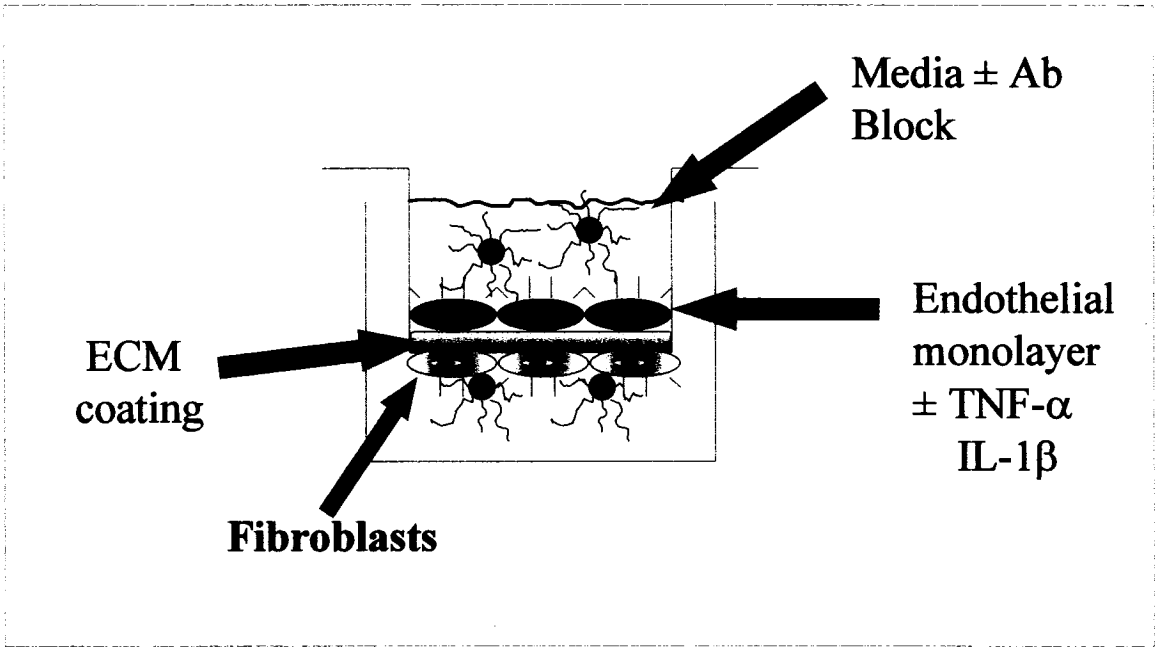

Figure 1.17 Schematic of the transwell model used to measure transendothelial migration. ICAM-1-expressing HUVECs were plated on the top side of the transwell chamber, while fibroblasts or ICAM-1-expressing NIH-3T3 cells were plated on the bottom side of the chamber. ICAM expression could be upregulated with inflammatory cytokines, and antibodies could be added to block specific interactions. Tumor cells were dropped into the top chamber, and the percentage that migrated to the bottom of the chamber was determined after a 24 hour incubation. (Adapted from [87])

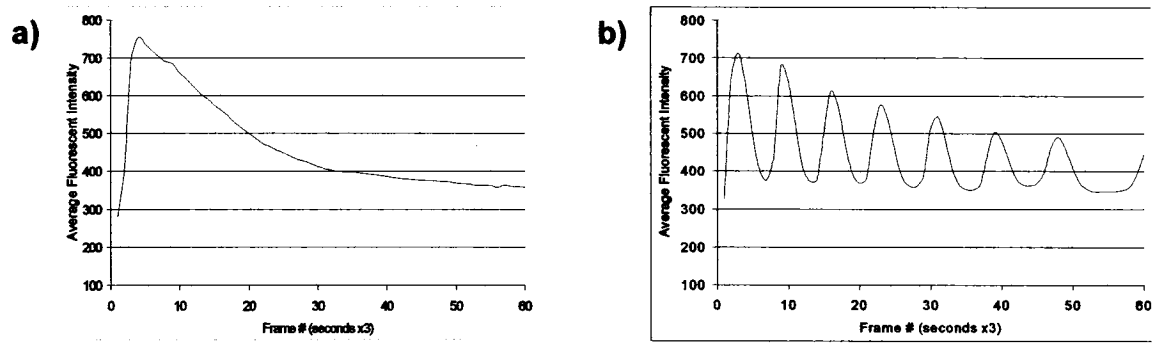

Figure 1.18 Representative calcium oscillation graphs. Cells expressing or lacking MUC1 were plated on a glass bottom dish and loaded with Fluo 3, a calcium indicator dye. Cells expressing or lacking ICAM-1 were dropped over them and the changes in intracellular calcium concentration were measured in 3 second intervals on a fluorescent microscope. Subsequently, average fluorescence intensity was plotted against time. **a)** When either ICAM-1 or MUC1 was missing, the cells loaded with Fluo 3 displayed one large spike of intracellular calcium that slowly dropped off. **b)** When both ICAM-1 and MUC1 were present, the cells loaded with Fluo 3 displayed calcium oscillations that had a regular periodicity. (Adapted from [83])

1.5 General Hypothesis and Objectives

The functional effects of the MUC1/ICAM-1 interaction have been determined in previous studies: ligation of tumor cell MUC1 to endothelial cell ICAM-1 induces calcium oscillations in the tumor cell, resulting in cytoskeletal rearrangement and transmigration through the endothelial layer. The molecular mechanisms mediating these processes, however, remain largely undefined. The purpose of this study is to examine the early molecular events that occur prior to intracellular signaling. It is currently unknown which segment(s) of the MUC1 mucin mediates ICAM-1 binding and the events leading up to calcium oscillations. To investigate this part of the mechanism, one domain of the MUC1 protein will be manipulated. It is proposed that the MUC1 extracellular domain is responsible for binding to ICAM-1 on adjacent cells, and that it mediates subsequent events leading to signal initiation. The MUC1 mucin is similar to a single pass transmembrane receptor phosphorylated by NRTKs. A common mechanism of signal initiation for these receptors is ligand-induced dimerization followed by altered partitioning in lipid rafts. Preliminary data from our lab supports this model as MUC1 has been found to homodimerize and is present in lipid rafts (Figure 3.1). Therefore, the specific objectives of the thesis are as follows:

1. To determine if the MUC1 tandem repeats are necessary for ICAM-1-induced MUC1 signaling;
2. To determine if binding of ICAM-1 to MUC1 is necessary for MUC1 homodimer formation; and
3. To determine if the MUC1 extracellular domain is necessary for movement of MUC1 homodimers into lipid rafts.

Chapter 2: Role of the MUC1 extracellular domain (ECD) in ICAM-1-induced MUC1 signaling

2.0 Introduction

Previous work from our lab has demonstrated that ligation of MUC1 to ICAM-1 leads to transendothelial migration in a transwell system, where migration was influenced by both MUC1 and ICAM-1 levels, and could be inhibited with antibodies to either protein [80, 83]. To examine the mechanisms behind this phenomenon, we looked for a signal that was initiated by the MUC1/ICAM-1 interaction. Since a number of calcium-sensitive regulators are involved in cellular movement, we examined whether the MUC1/ICAM-1 interaction could generate a calcium-based signal. We noticed that contact between ICAM-1-expressing cells and MUC1-expressing cells resulted in the induction of calcium oscillations, and that the oscillations were not present when either MUC1 or ICAM-1 was missing [83]. In addition, these oscillations could be inhibited by antibodies to either molecule, and inhibition of PI3K or the IP_3 receptor also abolished the signal, demonstrating the involvement of intracellular calcium through the IP_3 pathway [83].

The mechanism by which MUC1 initiates this calcium-based signal, however, remains unclear. To investigate the role of the MUC1 extracellular domain in signal initiation, we tested the ability of a MUC1 splice variant lacking tandem repeats, MUC1/Y, to generate a similar pattern of calcium oscillations to that seen with full length MUC1.

2.1 Methods and Materials

2.1.1 Reagents

DMEM, FBS, G418, 2-mercaptoethanol, blasticidin, and LMP agarose were from Invitrogen (Carlsbad, California, USA). Xho I, Sac II, Not I and T4 DNA ligase were from New England Biolabs (Ipswich, Massachusetts, USA). DMSO, luria agar, sodium butyrate, RIPA buffer, phosphatase inhibitor cocktail II, protease inhibitor cocktail (P8340), and pluronic F-127 were from Sigma-Aldrich (Oakville,

Ontario, Canada). High strength analytical grade agarose and precision plus all blue protein standards were from Bio-Rad (Mississauga, Ontario, Canada). Kanamycin was from Fisher Scientific (Ottawa, Ontario, Canada). The Immobilon-P membrane was from Millipore (Billerica, Massachusetts, USA). Fluo-3 AM was from Molecular Probes (Burlingon, Ontario, Canada). The PCR primers were synthesized by Integrated DNA Technologies (Coralville, Iowa, USA). The pCINeoMUC1TR+FLAG plasmid and CT2 antibody against the MUC1 cytoplasmic tail were generously provided by Dr. Sandra Gendler, Mayo Clinic, Scottsdale, Arizona, USA. The pUC-CVM-MUC-1Y plasmid was from Gene-Therapeutics Luckenwalde (Luckenwalde, Germany). B27.29 antibody against the MUC1 extracellular domain was from Fujirebio Diagnostics Inc. (Malvern, Pennsylvania, USA). The HRP-conjugated secondary antibodies (goat anti-mouse and goat anti-Armenian hamster) were from Jackson ImmunoResearch (West Grove, Pennsylvania, USA).

2.1.2 Cells

293T human embryonic kidney cells were obtained from ATCC and were maintained in DMEM + 10% (v/v) FBS. SYM25 cells are a single-cell clone (clone 25) of 293T cells expressing full length MUC1 with an extracellular N-terminal yellow fluorescent protein tag. This transfectant was generated prior to this study [87]. 293T MUC1-CFP cells are 293T cells expressing full length MUC1 with a cytoplasmic C-terminal cyan fluorescent protein tag. 293T MUCY-YFP cells are 293T cells expressing MUC1/Y with a cytoplasmic C-terminal yellow fluorescent protein tag. All three 293T transfectants were selected in DMEM + 10% FBS + 1200 μg/ml G418, and maintained in DMEM + 10% FBS (v/v) + 200 μg/ml G418. NIH ICAM and NIH mock cells are transfected NIH 3T3 mouse fibroblasts that were a generous gift from Dr. Ken Dimock, University of Ottawa, Ontario. They express or lack ICAM-1 respectively, and were maintained in DMEM + 10% FBS (v/v) + 5 μg/ml blasticidin. T47D cells are a human breast cancer cell line from ATCC. They were maintained in DMEM + 10% FBS (v/v) + 0.1 mg/ml insulin.

2.1.3 Plasmid Construction

The goal was to construct a MUC1 and MUC1/Y plasmid where the expressed protein would express a cytoplasmic C-terminal cyan or yellow fluorescent protein (CFP and YFP), respectively (Figure 2.1). Therefore, the plan was to insert the MUC1 and MUC1/Y genes immediately before the CFP or YFP genes in mammalian vectors that already contained one of the fluorescent protein genes (the pECFP and pEYFP plasmids from Clontech).

2.1.3.1 Primer Design for the MUC1 and MUC1/Y Genes

The cloning strategy was to engineer unique cut sites in the regions flanking the MUC1 and MUC1/Y genes so that they could be inserted into the multiple cloning site (MCS) located immediately upstream from the fluorescent protein gene in the mammalian pECFP and pEYFP vectors. Primers were designed to be in-frame to the fluorescent protein sequences, and the forward and reverse primers were designed to generate sticky ends compatible with Xho I and Sac II restriction sites, respectively. Primer sequences are as follows, where capitalized letters are overhang residues, and lowercase letters are complementary to the MUC1 sequence: MUC1 forward primer - ATA CCC TCG AGT gcc tgc ctg aat ctg; MUC1 reverse primer - ACT ATA CCG CGG Atg ccc **ata** caa gtt gg; MUC1/Y forward primer – GTA GCC CTC GAG Tat tca cca tga cac cg; MUC1/Y reverse primer – ATA ACA TTA CCG CGG ATa ccc caa caa gtt gg.

2.1.3.2 PCR of MUC1 genes

pCINeoMUC1TR+FLAG is a plasmid that is approximately 10 kb in size with a 3.5 kb MUC1 insert. Since a small linear DNA template generates PCR products with a high percentage of full-length amplified template, the MUC1 gene

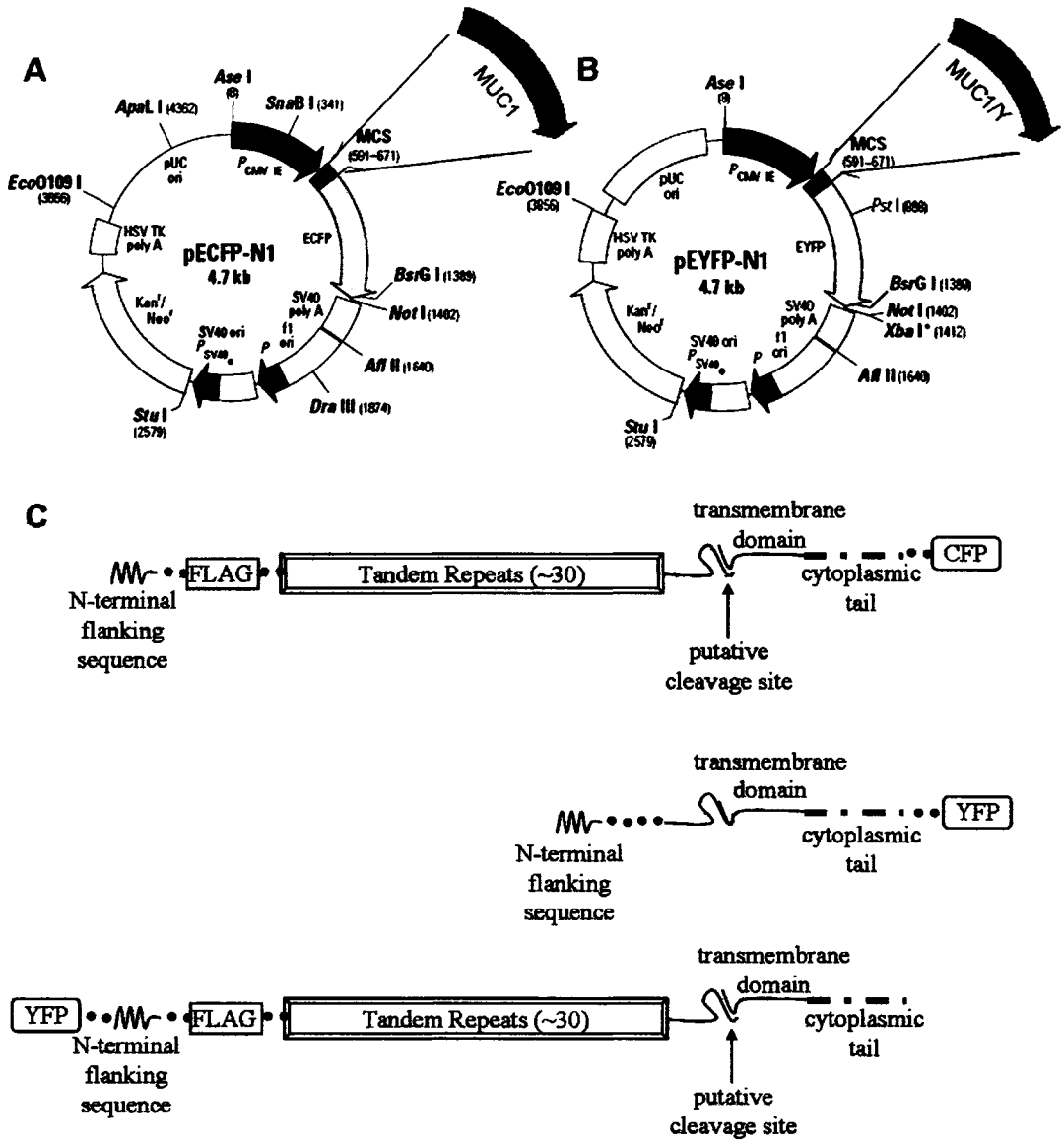

Figure 2.1 Plasmid design and expected protein structures. A. Strategy for the construction of a C-terminally labeled MUC1 protein. The MUC1 gene lacking its stop codon was inserted into the multiple cloning site of the pECFP-N1 plasmid in-frame with the 3' enhanced cyan fluorescent protein (ECFP) gene. **B.** Strategy for the construction of a C-terminally labeled MUC1/Y protein. The MUC1/Y gene lacking its stop codon was inserted into the multiple cloning site of the pEYFP-N1 plasmid in-frame with the 3' enhanced yellow fluorescent protein (EYFP) gene. **C.** Constructs of MUC1 variants used in the experiments. From top to bottom: MUC1-CFP (MUC1 with a C-terminal CFP tag), MUCY-YFP (MUC1/Y with a C-terminal YFP tag), and SYM (MUC1 with a N-terminal YFP tag). The MUC1-CFP and

Figure 2.1 continued: SYM proteins have two subunits due to cleavage in the SEA module. The subunits separate after exposure to SDS. Extracellular fragments are expected to run between 200 – 500 kDa on SDS-PAGE, depending on the degree of glycosylation. Cytoplasmic fragments are expected to run between 16 – 30 kDa for SYM, and approximately 50 kDa for MUC1-CFP due to the attachment of the 27 kDa fluorescent tag. MUCY-YFP is expected to run at approximately 75 kDa due to the attachment of the 27 kDa fluorescent tag and the inclusion of the extracellular domain, since the protein lacks the cleavage site that is present in the other two proteins. (Adapted from [88] and [83])

was excised from the parental plasmid prior to PCR – 4 μg of the parental plasmid was digested with Not I, which digested the plasmid in the regions flanking the MUC1 gene, and the gel slice containing the 3.5 kb MUC1 fragment was isolated following gel purification on a 1% (w/v) low melting point agarose gel. No further purification was done – the gel slice was simply melted at 70 °C to enable transfer of the template DNA into the PCR reaction mixture. In contrast, the plasmid containing the MUC1/Y gene was only 4.2 kb in total, so no manipulations were done to it prior to addition to the PCR reaction mixture.

The MUC1 gene is extremely GC-rich, where approximately 82% of the sequence consists of guanines and cytosines. Previous attempts to amplify MUC1 by PCR demonstrated that secondary structures caused by GC interactions interfered with the reaction, resulting in the generation of a large amount of truncated DNA product. Consequently, several adjuvants were added to the PCR reaction mixture to improve amplification efficiency. The final PCR mixtures were:

5.0 μl of Invitrogen High Fidelity PCR Buffer
2.0 μl of 50 mM magnesium sulfate (adjuvant – stabilizes primer-DNA interactions)
2.0 μl of 25 nmol/ml Forward primer
2.0 μl of 25 nmol/ml Reverse primer
1.0 μl of 10 mM Invitrogen dNTP mix
2.5 μl of DMSO (adjuvant – destabilizes secondary structure)
10 μl of Qiagen Q solution (5M betaine; adjuvant – destabilizes secondary structure)
0.5 μl of Invitrogen Platinum Taq DNA polymerase (High Fidelity)
24 μl of distilled de-ionized water (ddH_2O)
1.0 μl of MUC1 liquefied gel slice, or 1.0 μl of MUC1/Y plasmid

PCR was done in an Applied Biosystems 2400 thermal cycler, and the following cycling parameters were used:

1 cycle at 96 °C for 10 minutes (initial denaturation)

25 cycles of:

94 °C for 15 seconds (denaturation)

47 °C for 60 seconds (annealing)

69 °C for 13 minutes (extension)

1 hold at 4 °C

2.1.3.3 Insertion of PCR product into a plasmid

To prepare the mammalian vectors for ligation, 4 μg of pECFP or pEYFP plasmid was digested with Xho I and Sac II, followed by purification on a 1% low melting point agarose gel. Following excision of the appropriate DNA band, the linearized plasmid was recovered by melting the gel slice at 70 °C, snap-freezing in a dry ice/acetone bath for 5 minutes, thawing the gel slice, centrifuging at 14k rpm for 5 minutes in an Eppendorf 5415C centrifuge, and removing the pelleted agarose. The concentration of the vector was determined by UV spectroscopy (1 Ab_{260} = 50 μg/ml double-stranded DNA).

To prepare the MUC1 insert for ligation, the PCR product was digested with Xho I and Sac II, and was purified using the Invitrogen ChargeSwitch kit. The principle of the kit is: First, DNA is bound to positively charged magnetic beads, which are then immobilized against a magnet. Next, non-nucleic acids are washed away, and the pH is finally raised to negate the charge on the beads, eluting the bound DNA is back into solution. Following UV spectroscopy to determine the concentration of the insert, the insert was mixed with the pECFP vector in a molar ratio between 3:1 and 5:1. Ligation was done with T4 ligase at 4 °C overnight.

Since the efficiency of this method of plasmid construction was low, the MUC1/Y plasmid was generated differently. In this case, the PCR product was purified with the Invitrogen ChargeSwitch kit and ligated into the pGEM-T vector from Promega, which ligates anything with a poly-A terminal sequence (generated during PCR). Following transformation (using the protocol from section 2.1.3.4) and amplification with the Qiagen QIAprep Spin miniprep kit (modified alkaline

lysis), the plasmid was digested with Xho I and Sac II. Following purification on a 1% (w/v) low melting point agarose gel, the appropriate DNA fragment was excised, and isolated using the freeze-thaw procedure listed above. The DNA concentration was determined by UV spectroscopy, and the MUC1/Y insert was mixed with the pEYFP vector in a molar ratio between 3:1 and 5:1. Ligation was done with T4 ligase in a total volume of 20 µl at 4 °C overnight.

2.1.4 Transformation, selection, and amplification of plasmids

The MUC1 plasmid was transformed in DH5α cells prepared with the $CaCl_2$ method by our lab, and the MUC1/Y plasmid was transformed in DH5α cells prepared with the Inoue method by Dr. Gordan Chan's lab. The main difference between the two methods is in the preparation of competent cells. In the Inoue method, the transformation buffer consists of 55 mM $MnCl_2*4H_2O$, 15 mM $CaCl_2*2H_2O$, 250 mM KCl, and 10 mM PIPES (0.5 M, pH 6.7) [89]. Furthermore, growth of the culture is done at a lower temperature (18 – 22 °C) than the $CaCl_2$ method (37 °C).

Transformation for both methods is as follows: Cells were thawed on ice, and 10 µl of the ligation mixture was added to 100 µl of cells. Following a 30 minute incubation on ice, cells were heat-shocked at 42 °C for 30 – 45 seconds. Cells were placed back on ice for 2 minutes, and then 900 µl of 37 °C SOB broth was added. After incubation at 37 °C with shaking (~225 rpm) for 1 hour, 250 µl of the transformation mixture was plated onto LB agar plates containing 30 µg/ml kanamycin. Plates were incubated overnight at 37 °C.

After incubation, tubes containing 2 ml of LB broth with 30 µg/ml kanamycin were inoculated with individual colonies. The tubes were incubated at 37 °C with shaking (~225 rpm) overnight. The plasmids were isolated with the Qiagen QIAprep Spin miniprep kit (modified alkaline lysis), using the manufacturer's protocol, and DNA concentrations were determined by UV spectroscopy.

2.1.5 Verification of insertion

Plasmids were digested with Xho I and Sac II, and the fragments were run on a 1% (w/v) agarose gel. One plasmid with the proper size digestion fragments was further amplified using the Qiagen HiSpeed Plasmid maxi kit (modified alkaline lysis), as per the manufacturer's protocol. Subsequently, the DNA concentration was once again determined by UV spectroscopy. The MUC1 C-terminus was sequenced with the 1081F primer (See section AII.2.6) to ensure that the reading frame between the MUC1 gene and the fluorescent protein gene was correct.

2.1.6 Transfection of HEK 293T cells and selection of transfectants

Transfection was done using the Invitrogen Lipofectamine 2000 kit (liposome-based using cationic lipids), in a 6 well plate following the manufacturer's protocol. To boost expression of the plasmid, the transfection mixture was aspirated 6 hours into the final incubation step. Two milliliters of regular growth medium was added (DMEM), and the plate was incubated at 37 °C and 5% (v/v) CO_2 for 1 hour. FBS and sodium butyrate (promotes transcription) were subsequently added, to give final concentrations of 10% (v/v) and 2mM respectively, and the plate was incubated overnight at 37 °C and 5% (v/v) CO_2. The sodium butyrate solution was aspirated, and replaced with DMEM + 10% FBS (v/v).

The following day, the cells were trypsinized, pelleted at 2500 xg for 2.5 minutes, and resuspended in 1 ml of ice cold PBS + 1 mM EDTA. The MUC1/Y transfectants could be sorted by flow cytometry at this point, as the flow cytometer had a filter for YFP, but the MUC1 transfectants required additional steps, as the flow cytometer did not have a filter for detecting CFP. As a result, the suspension of MUC1 transfectants was incubated with a B27.29 antibody (binds to MUC1 tandem repeats) conjugated to FITC on ice for 60 minutes. Following pelleting at 2500 xg for 2.5 minutes, the cells were resuspended in 1 ml PBS + EDTA. This wash step was repeated twice more, and the cells were sorted by flow cytometry. Positive cells were selected in DMEM + 10% FBS (v/v) + 1200 μg/ml G418 (since the plasmid

backbones had a neomycin resistance gene) until there were enough cells to form a confluent monolayer in a T-75 flask. Cells were subsequently maintained in DMEM + 10% FBS (v/v) + 200 μg/ml G418.

2.1.7 Verification of MUC1 and MUC1/Y expression

MUC1 expression was verified by Western blotting. Transfectants were lysed using RIPA buffer and 0.25% (v/v) phosphatase and 0.25% (v/v) protease inhibitors. Following the addition of loading buffer (4x buffer: 0.5 M Tris (pH 6.8), 0.1% bromophenol blue (w/v), 4.0% (v/v) glycerol, 8% (w/v) SDS) and 2-mercaptoethanol, samples were loaded onto a 4-20% polyacrylamide gradient gel with a 4% (v/v) stacking gel. The Mini-PROTEAN II Western apparatus was run with 2 gels (one unloaded) at 80V and 120 mA until the sample had entered the resolving gel, and then the voltage was increased to 110V. The apparatus was turned off once the dye line was within 1 cm of the bottom of the gel. Transfer of the proteins to an Immobilon-P membrane was done at 100V and 350 mA for 1 hour.

Immunoblotting was done with an Armenian hamster CT2 antibody (which binds near the end of the MUC1 cytoplasmic domain) as the primary antibody, and a goat anti-Armenian hamster antibody conjugated to horse radish peroxidase (HRP) as the secondary antibody. Detection was done with the Amersham ECL Plus kit (chemiluminescent detection), using the manufacturer's instructions (Figure 2.2).

2.1.8 Calcium oscillation assay

50 μl of 0.1% (w/v) gelatin was spread on the glass section of 35 mm dishes with a 10 mm microwell from MatTek Cultureware and allowed to dry in a laminar flow hood. Then, the dishes were UV-irradiated for 15 – 60 minutes. Cells to be plated were trypsinized and counted on a hemocytometer. After diluting to a density that will result in approximately 50 – 80% confluence, 200 μl of the cell suspension was pipetted onto the gelatin-covered glass section of the dishes. The dishes were

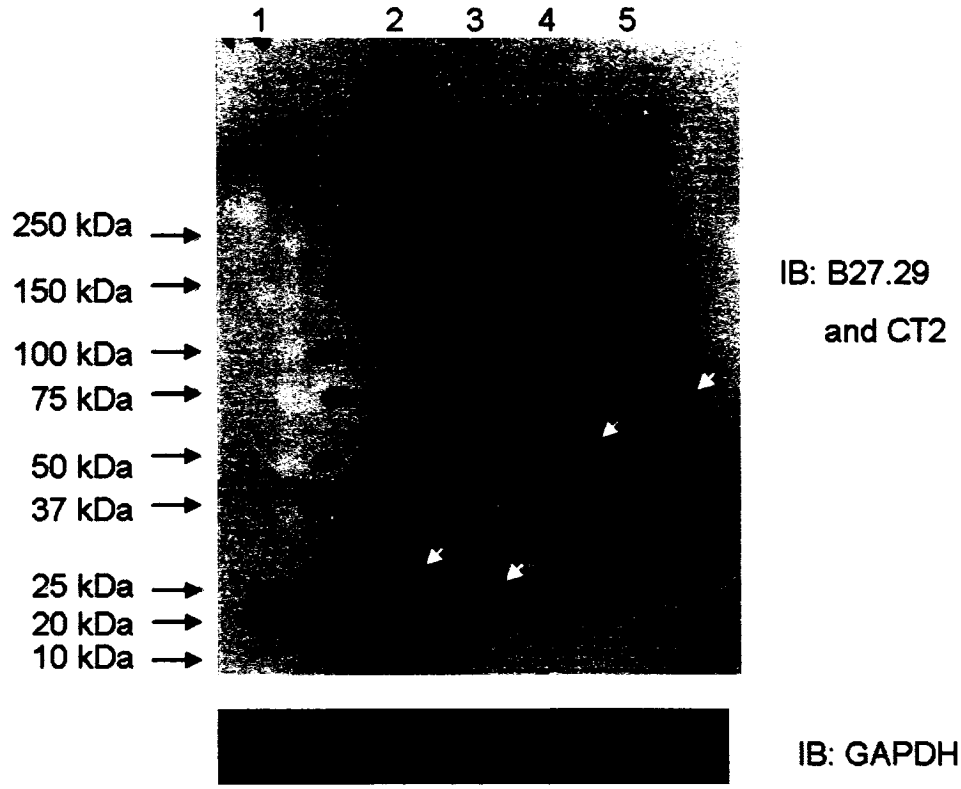

Figure 2.2 Comparison of total MUC1 in whole cell lysates. Lysates from MUC1 transfectants were separated on SDS-PAGE. GAPDH was used as a loading control. Probing was done against both the MUC1 extracellular domain with B27.29 antibody and the MUC1 cytoplasmic domain with CT2 antibody. Lanes were as follows: 1. 293T, 2. T47D, 3. SYM25, 4. 293T MUC1-CFP, and 5. 293T MUCY-YFP cells (see section 2.1.2). MUC1 was not detected in untransfected 293T cells. The MUC1 extracellular domain appeared as a doublet running above 150 kDa in T47D cells, SYM25 cells, and 293T MUC1-CFP. The B27.29 antibody did not detect the extracellular domain in 293T MUCY-YFP cells, as this MUC1 isoform lacked the binding site in the tandem repeats. CT2 staining showed the MUC1 cytoplasmic subunit as a doublet between 10 – 25 kDa in T47D cells, and as a singlet between 20 – 25 kDa in SYM25 cells, 50 kDa in 293T MUC1-CFP cells, and the MUC1/Y protein at just under 75 kDa in 293T MUCY-YFP cells. Cytoplasmic subunit dimers were evident at 100 kDa in 293T MUC1-CFP cells, and MUC1/Y dimers were evident at 150 kDa in 293T MUCY-YFP cells. Cytoplasmic MUC1 subunit monomers are indicated with white arrows, and dimers are indicated with black arrows. Additional bands are currently unidentified. This experiment was done by Brian Maciejko. (n = 3)

incubated at 37 °C and 5% (v/v) CO_2 for approximately 4 hours, to allow the cells to adhere to the bottom of the dish. 2 ml of the appropriate media (see section 2.1.2) was added to each dish, and the dishes were placed back into the incubator. The addition of media was done to prevent excess evaporation of the media.

The next day, loading media was prepared by mixing 2 ml of the appropriate media with 2 µl of 5 mM fluo-3 stock, and 2 µl of pluronic stock (20% w/v Pluronic F-127 in DMSO). The media was aspirated from the dishes and replaced with 200 µl of loading media. The dishes were placed back into the incubator for 1 hour.

Half an hour before the end of the incubation period, one confluent T150 flask of NIH-ICAM-1 or NIH mock cells was trypsinized for every 6 dishes that will be tested. Following centrifugation at 2500 xg for 2.5 minutes, the supernatant was aspirated, and the cells were resuspended in 550 µl (multiplied by the number of flasks) of imaging buffer, which should represent conditions close to physiological conditions (152 mM 5.4 mM KCl, 0.8 mM $MgCl_2*6H_2O$, 1.8 mM $CaCl_2$, 10 mM HEPES, 5.6 mM D-glucose, final pH 7.2).

After the incubation period, the loading media was aspirated from the dishes. The cells were washed once with imaging buffer, and approximately 200 µl of imaging buffer was added over the cells. The dishes were then placed in the 37 °C incubator at the imaging facility of the Cross Cancer Institute.

To prepare the Zeiss Axioscope Digital Imaging microscope for imaging, the objective was set on 20x, the condenser was set to PH2, and the heated stage was set to 37 °C. After placing a dish on the stage, the field of view was focused on an area of the dish that was over 70% confluent, but under 90% confluent. A picture was taken under the DIC filter, and then the filter was changed to FITC. After refocusing, the time course was started using the Metamorph program (Version 7.0 R2) (Sunnyvale, California, USA). Pictures were taken every 3 seconds for 60 time points. 100 µl of the NIH-ICAM or NIH-mock suspension was dropped onto the dish after the first time point. Afterwards, a final picture was taken under the DIC filter.

2.1.9 Calcium oscillation assay analysis

The images for each time point were merged into a stack using Metamorph software (Molecular Devices. 5 random cells in the field of view were chosen per condition, and the changes in their average fluorescence intensity was graphed over time and exported to Microsoft Excel. Each condition was repeated at least 3 times. Graphs that were not representative of the majority of graphs for that condition were discarded, resulting in 8 – 21 useful graphs per condition.

Excel was used to determine the oscillation factors, which are calculated by multiplying the amplitude factor by the number of oscillation cycles for each graph. The amplitude factor is defined as the sum of the differences between the plotted data and the trend line for that data. It was worked out using the LOGEST trend line function ($y = \text{intercept} * \text{slope}^x$) from the beginning of the calcium oscillations to the last time point, and then calculating the absolute value of the difference between the data and the trend line for each time point (Figure 2.3).

2.1.10 Statistical analysis

The mean ± the standard error was graphed (Figures 2.6 and 2.8). Statistical significance was determined using the Student's t-test at $P = 0.05$.

2.2 Results

2.2.1 Verification of the ability of NIH 3T3 cells transfected with human ICAM-1 to induce calcium oscillations in 293T cells transfected with human MUC1

Previous work had demonstrated that NIH 3T3 cells expressing human ICAM-1 could induce calcium oscillations in 293T cells expressing human MUC1 (Figure 2.4) [83]. To ensure that the calcium oscillation assay was working correctly, untransfected 293T cells and SYM25 cells, which are 293T cells expressing human MUC1 with a YFP tag on the extracellular N-terminus, were

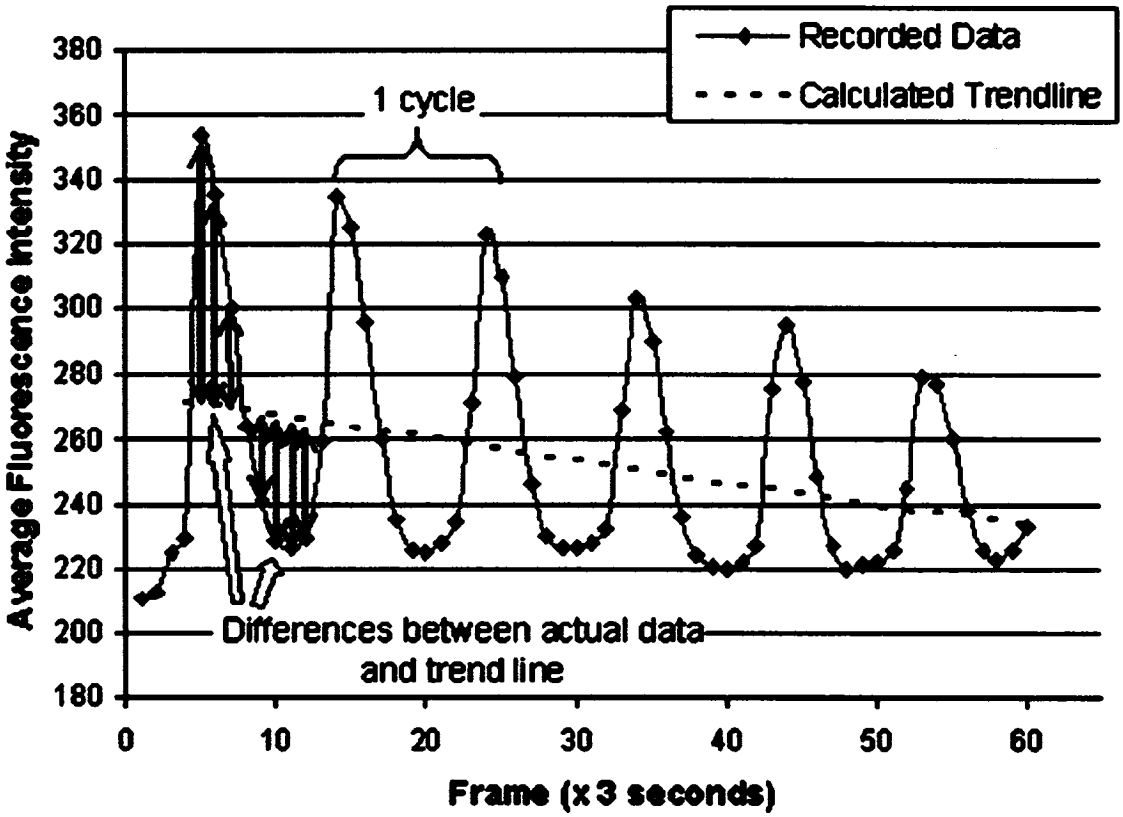

Figure 2.3 Oscillation Factor Calculation. The oscillation factor is defined as the amplitude factor multiplied by the number of oscillation cycles for each graph. The amplitude factor is defined as the sum of the differences between the plotted data and the trend line for that data for each time point. The trend line was calculated with the LOGEST trend line function ($y = \text{intercept} * \text{slope}^x$) from the beginning of the calcium oscillations to the last time point. (Adapted from [83])

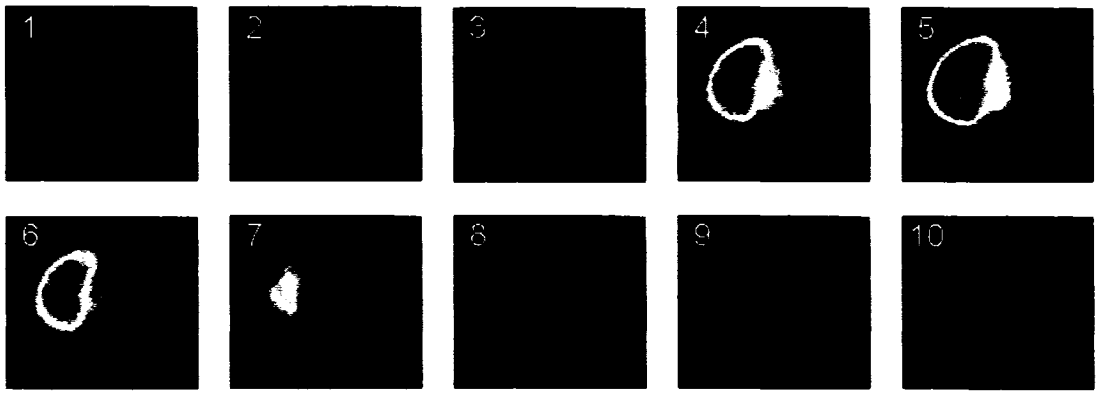

Figure 2.4 Example of a single calcium oscillation. Adherent MUC1-expressing SYM25 cells were loaded with the fluo 3 calcium indicator dye, and cells expressing human ICAM-1 were subsequently dropped on top of them. Numbered pictures were taken sequentially on a fluorescent microscope, and each frame represents a picture taken every 3 seconds. The periodicity of an oscillation cycle is approximately 30 seconds.

tested for their ability to generate oscillatory signals following contact with ICAM-1- or mock-transfected NIH 3T3 cells (NIH ICAM and NIH mock, respectively). MUC1-expressing SYM25 cells exposed to NIH ICAM cells showed multiple oscillation cycles that diminished in amplitude over time (Figure 2.5). The oscillation period appeared to be approximately 10 frames, which translates to 30 seconds. Conversely, when ICAM-1 was absent (NIH mock cells), SYM25 cells were not induced to generate calcium oscillations. Similarly, calcium oscillations were not detected when MUC1 was absent (293T cells exposed to NIH ICAM cells), or when both MUC1 and ICAM-1 were absent (293T cells exposed to NIH mock cells). In the three conditions where both MUC1 and ICAM-1 were not present, the 293T cells and the transfectant displayed a single calcium spike that peaked before 15 seconds after initiation and diminished over time.

Cell responses in any given experiment, however, showed variations in both synchronization and amplitude of the calcium peaks. To correct for this, the signals were averaged into oscillation factors, which represent a sum of the absolute differences between the plotted data and the trend line of the graph at each time point. In so doing, data between different conditions could be compared quantitatively. Comparison between the two SYM25 conditions showed that stimulation with ICAM-1 was able to induce a significantly higher calcium response from the MUC1-expressing cells when compared to stimulation from ICAM-1-null cells (1305 ± 349 versus 23 ± 9) (Figure 2.6). On the other hand, 293T cells not expressing MUC1 responded no differently to NIH ICAM and NIH mock cells (84 ± 43 versus 27 ± 22).

2.2.2 NIH 3T3 cells transfected with human ICAM-1 are not able to induce calcium oscillations in 293T cells transfected with MUC1/Y

To determine if the MUC1 extracellular domain is necessary for ICAM-1-induced calcium oscillations in MUC1-expressing cells, 293T cells expressing MUC1/Y with a cytoplasmic C-terminal YFP tag (293T MUCY-YFP) were tested for calcium oscillations following stimulation with NIH ICAM and NIH mock cells.

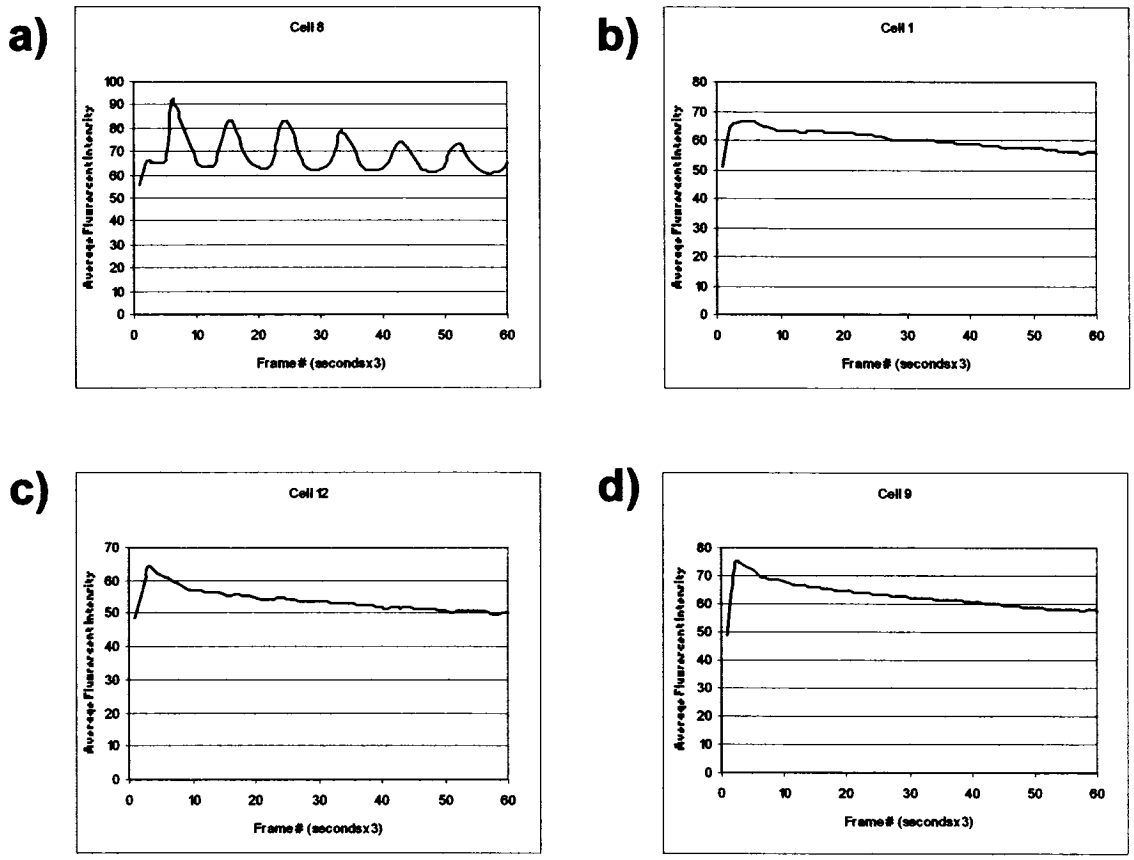

Figure 2.5 Representative Calcium Oscillation Graphs for SYM25 and 293T cells. Average fluorescence intensity was plotted against frames, where each frame represents a 3 second interval. MUC1-expressing SYM25 cells stimulated with NIH ICAM cells showed a number of distinct calcium peaks (a). SYM25 cells stimulated with NIH mock cells (b), or MUC1-null 293T cell stimulated with either NIH ICAM or NIH mock cells (c and d), showed a single calcium peak with no, or very small oscillations. (n >3)

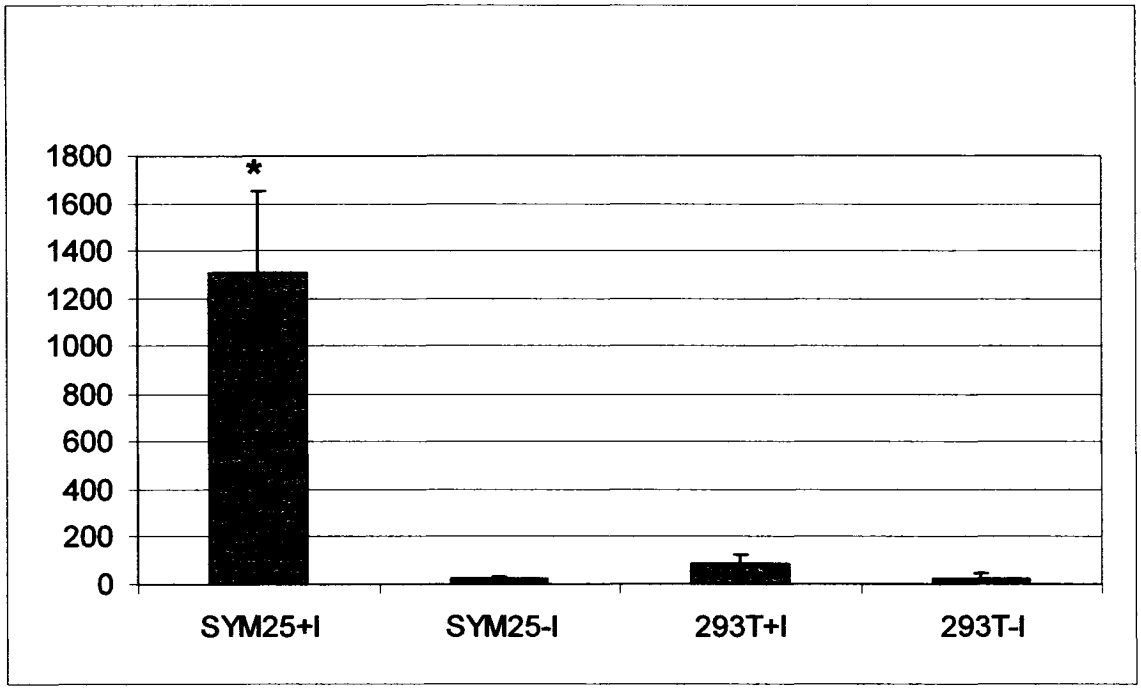

Figure 2.6 Calcium oscillation factors for N-terminally tagged 293T transfectants and untransfected 293T cells. From left to right: SYM25 cells stimulated with NIH ICAM cells, SYM25 cells stimulated with NIH mock cells, 293T cells stimulated with NIH ICAM cells, and 293T cells stimulated with NIH mock cells. Bars marked with a * show a significant difference between the two conditions for that cell type (P = 0.05).

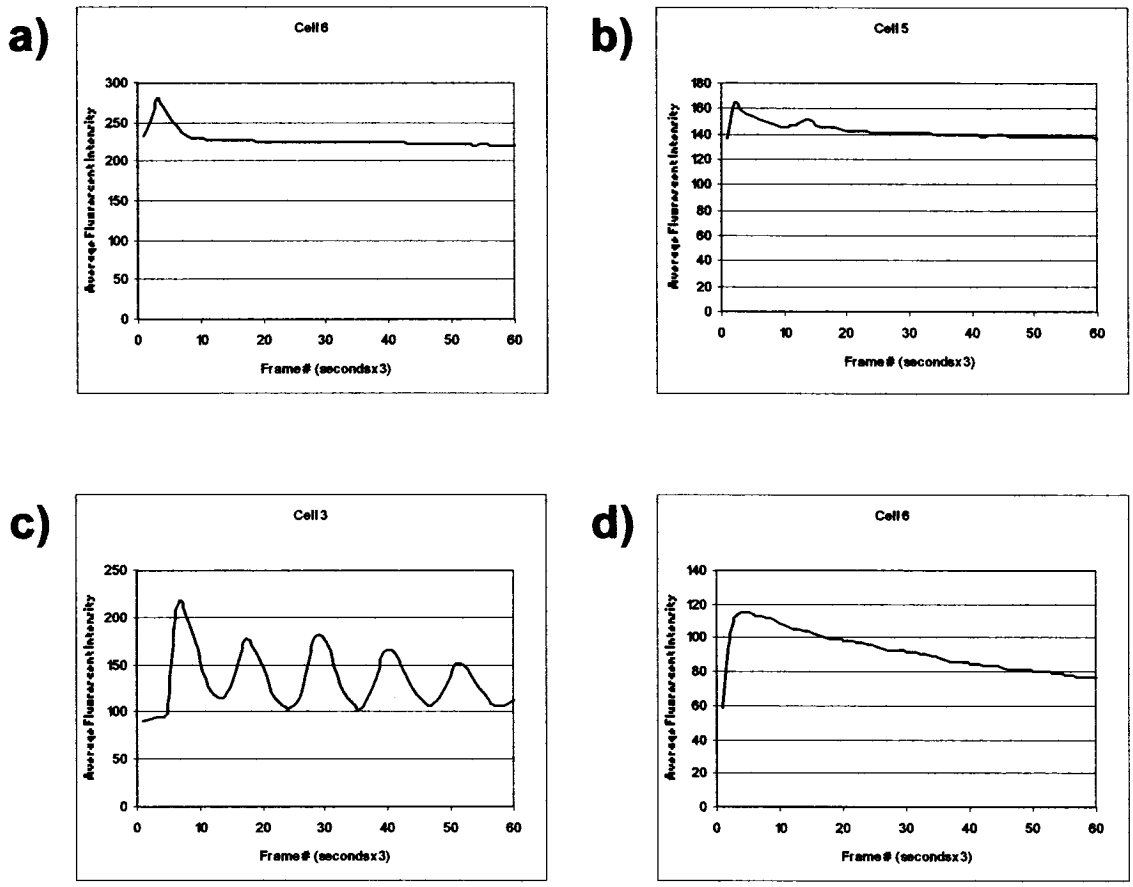

Figure 2.7 Representative Calcium Oscillation Graphs for MUCY-YFP and MUC1-CFP cells. Average fluorescence intensity was plotted against frames, where each frame represents a 3 second interval. MUCY-YFP cells (lacking the MUC1 tandem repeats) stimulated with either NIH ICAM or NIH mock cells (a and b), showed a single calcium peak with no, or very small oscillations. MUC1-expressing MUC1-CFP cells stimulated with NIH ICAM cells showed a number of distinct calcium peaks (c), whereas MUC1-CFP cells stimulated with NIH mock cells (d) showed a single calcium peak. ($n > 3$)

In both scenarios, 293T MUCY-YFP cells displayed a single calcium spike that peaked before 15 seconds after initiation and gradually diminished over time (Figure 2.7a and 2.7b). These results are consistent with a negative oscillatory response. However, since there was a bulky extraneous protein attached to the MUC1 cytoplasmic tail, there was a chance that the placement of the tag in this location was interfering with MUC1 function.

Therefore, to eliminate this possibility, 293T cells expressing full length MUC1 with a cytoplasmic C-terminal CFP protein (293T MUC1-CFP) were stimulated with NIH ICAM and NIH mock cells to see if calcium oscillations were also inhibited. Multiple calcium peaks were seen when 293T MUC1-CFP cells were exposed to NIH ICAM cells. Like the interaction between SYM25 cells and NIH ICAM cells, the amplitude of the peaks decreased over time, and had a period of approximately 30 seconds (Figure 2.7c and 2.7d). Exposure of 293T MUC1-CFP cells to NIH mock cells, on the other hand, resulted in a negative oscillatory response.

Comparisons between the calculated oscillation factors demonstrated that 293T MUC1-CFP cells exposed to NIH ICAM cells had a significantly higher calcium response compared to exposure to 293T mock cells (2494 ± 445 versus 202 ± 122) (Figure 2.8). 293T MUCY-YFP cells exposed to NIH ICAM cells, conversely, displayed a response that was only marginally higher than exposure to NIH mock cells (107 ± 44 versus 32 ± 10). Interestingly, the calcium oscillation factors of the conditions that produced large calcium peaks, SYM25 and 293T MUC1-CFP following contact with NIH ICAM cells, varied noticeably (1305 ± 349 versus 2494 ± 445). This may be indicative of differences between the two transfectants or experimental conditions.

2.3 Summary

Earlier work had demonstrated that cells expressing MUC1 would generate repetitive calcium spikes with a period of approximately 30 seconds following contact with cells expressing ICAM-1 [83]. This effect was not seen when at least

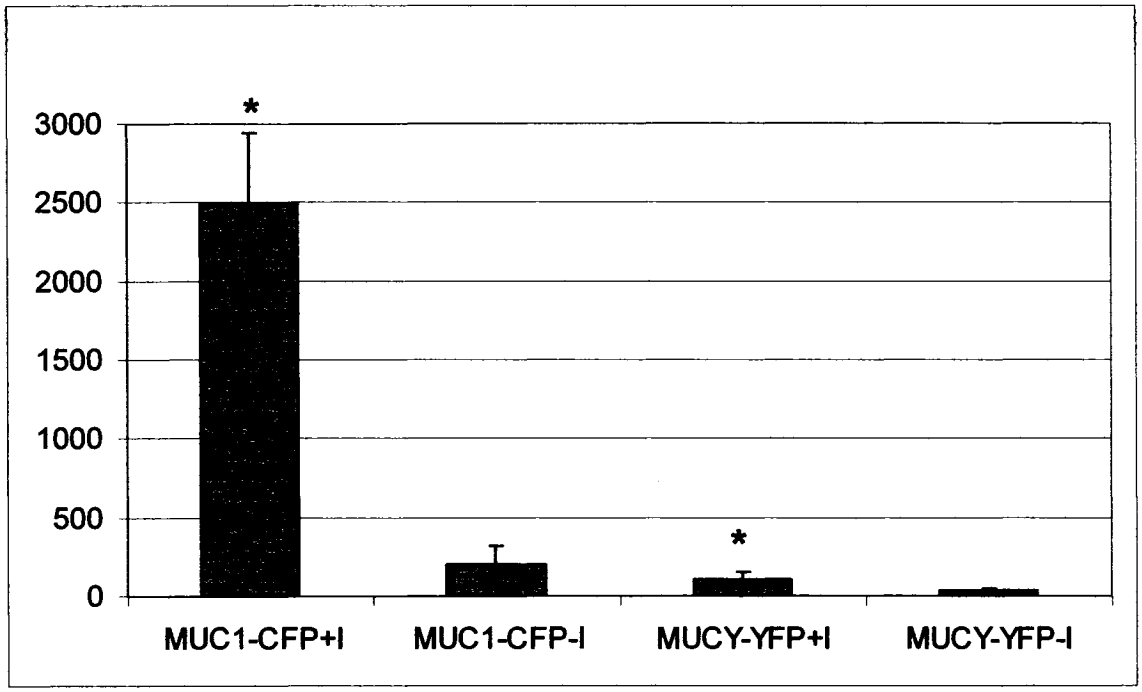

Figure 2.8 Calcium oscillation factors for C-terminally tagged MUC1-CFP and MUCY-YFP transfectants. From left to right: MUC1-CFP cells stimulated with NIH ICAM cells, MUC1-CFP cells stimulated with NIH mock cells, MUCY-YFP cells stimulated with NIH ICAM cells, and MUCY-YFP cells stimulated with NIH mock cells. Bars marked with a * show a significant difference between the two conditions for that cell type (P = 0.05).

one of these molecules was absent. Under these latter conditions, the majority of the MUC1 positive cells only displayed a single calcium spike with no subsequent oscillations. Since antibody blockade against either MUC1 or ICAM-1 inhibited both calcium oscillations and transendothelial migration, changes in intracellular calcium were used as an indicator of ICAM-1-induced MUC1 signaling. In this study, 293T cells transfected with MUC1/Y, a splice variant of MUC1 lacking the tandem repeats, were subjected to a calcium assay to determine if the tandem repeats were needed for this form of signaling.

The data showed that cells expressing this truncated form of MUC1 were incapable of producing calcium oscillations following stimulation with NIH ICAM cells, generating only one calcium spike similar to the conditions where either MUC1 or ICAM-1 was missing. The MUC1/Y protein also had a fluorescent protein attached to the cytoplasmic tail which could have potentially interfered with calcium signaling. However, 293T cells transfected with a similarly tagged full length MUC1 molecule were fully capable of generating intracellular calcium oscillations, thereby supporting the importance of the MUC1 extracellular tandem repeats in ICAM-1-induced signal initiation.

Chapter 3: Role of the MUC1 extracellular domain in MUC1 homodimerization

3.0 Introduction

So far, the MUC1 extracellular tandem repeats have been demonstrated to be necessary for ICAM-1-induced MUC1 signaling. The question, however, is how they are involved in the signaling pathway. Structurally, the MUC1 protein is similar to a receptor associated with a nonreceptor tyrosine kinase. It is a single transmembrane section protein with a cytoplasmic domain containing tyrosine residues that can be phosphorylated. Although MUC1 does not have intrinsic tyrosine kinase activity, it has been shown to co-immunoprecipitate with nonreceptor tyrosine kinases such as c-Src [49]. In addition, recent data from our lab has demonstrated that MUC1 homodimerizes (Figure 3.1a). Ligand-induced receptor dimerization is a common mechanism for induction of phosphorylation of residues in the cytoplasmic domain. ICAM-1, the known ligand for MUC1, functions as a physiologic dimer [90], which suggests a possible mechanism for receptor dimerization. Evidence suggests that MUC1 homodimers may play a role in ICAM-1-induced signaling, as disruption of lipid rafts with methyl-β-cyclodextrin or nystatin abrogates signaling [83], and the amount of raft-localized MUC1 dimer increases upon ICAM-1 stimulation (compared to unstimulated cells), whereas the amount of raft-localized monomer remains unchanged (Figure 3.1 and unpublished). It is currently unknown, however, whether MUC1 homodimerization is a consequence of binding to ICAM-1, or whether it happens independently. As a result, the objective of this chapter is to determine if the binding of ICAM-1 to the MUC1 extracellular tandem repeats is necessary for MUC1 homodimerization.

3.1 Methods and Materials

3.1.1 Reagents

See section 2.1.1. Disuccinimidyl suberate (DSS) was from Pierce (Rockford, Illinois, USA). Mouse anti-α-Tubulin was from Sigma Aldrich (Oakville, Ontario,

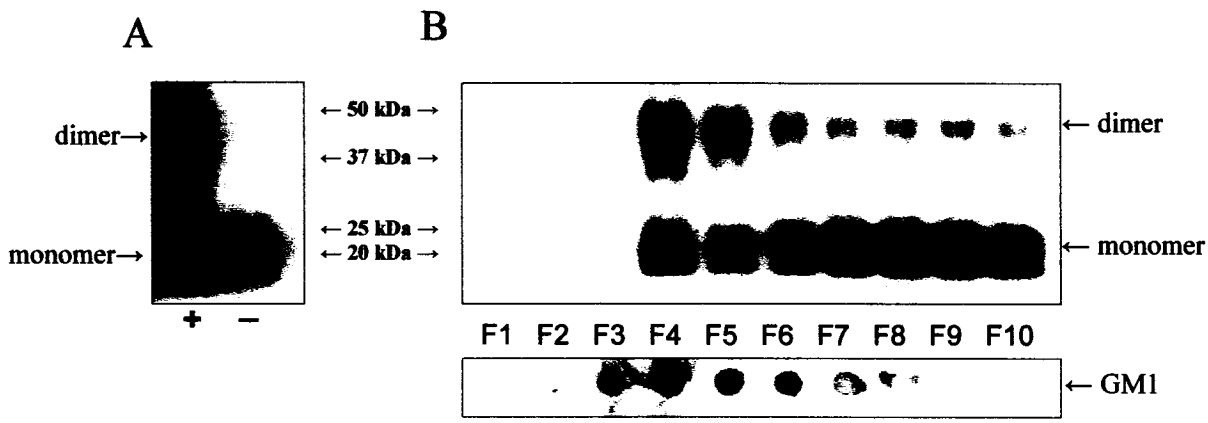

Figure 3.1 Evidence of MUC1 homodimerization. Whole cell lysates of T47D breast tumour cells were separated on SDS-PAGE following incubation of live cells with (+) or without (-) the membrane-permeable DSS cross-linker. (**A**) Probing with MUC1 CT2 antibody reveals the presence of the dimerized cytoplasmic domain in the chemically crosslinked sample. (**B**) Further processing of the chemically crosslinked lysate by sucrose gradient centrifugation reveals the presence of the dimer predominantly in the lipid raft fractions. Localization of the lipid rafts is determined using dot blots of the fractions and probing for the lipid raft marker GM1-ganglioside. This experiment was done by Sue Szigety.

Canada). HRP-conjugated goat anti-mouse antibody was from Jackson ImmunoResearch (West Grove, Pennsylvania, USA). X-ray film was from Kodak (Toronto, Ontario, Canada).

3.1.2 Cells

See section 2.1.2.

3.1.3 Cross-linking

Falcon tissue culture dishes (35 x 10 mm) were coated with 0.1% (w/v) gelatin and allowed to dry in a laminar flow hood. Sterilization was done by UV irradiation for one hour.

Adherent cells to be plated were trypsinized and resuspended in a volume of media four-times the volume of trypsin used. The cell density was determined on a hemocytometer, and one million cells in 3 ml of appropriate media were plated on each dish. This density gave approximately 50 – 80% confluence in a dish for HEK 293T parental and transfected cells. The cells were allowed to settle overnight.

On the day of the experiment, the media was aspirated from the dishes, washed once with imaging buffer, and the cells were incubated in imaging buffer at 37 °C and 5% (v/v) CO_2 for 45 minutes, to serum starve the cells in conditions close to physiological conditions. 15 minutes before the end of this incubation period, one confluent T-75 flask of NIH ICAM and/or NIH mock cells was trypsinized for each 10 mm dish to be tested. The NIH cells were resuspended in media, and the suspensions of each type of NIH cell were combined in a single 50 ml centrifuge tube (i.e. all NIH mock cells in one tube, and all NIH ICAM cells in another tube). The cells were pelleted at 2500 xg for 2.5 minutes, and resuspended in PBS, at a volume of 2 ml multiplied by the number of T-75 flasks used (e.g. if 2 flasks were used, then the cells were resuspended in 4 ml PBS).

Following the 45 minute incubation period, the imaging buffer was aspirated, and 2 ml of NIH cells were added to the dishes. After a 1 minute incubation, the NIH cells were aspirated, and the dishes were placed on ice. One gentle wash was done with ice-cold PBS, and 2 ml of 1 mM membrane-permeable DSS cross linker was added. The cross-linking solution was aspirated after 10 minutes, and replaced with 1.5 ml of ice-cold quenching solution (20 mM Tris buffer). The cell monolayer was then scraped off the dish with a rubber policeman, and transferred to a 1.5 ml Eppendorf tube. The cells were pelleted at 13.5k rpm for 1 minute at 4 °C in an Eppendorf 5415C centrifuge, and the supernatant was aspirated. The pellet was resuspended in ice-cold lysis buffer (200 µl RIPA + 0.5 µl protease inhibitor cocktail + 0.5 µl phosphatase inhibitor cocktail). Following a 15 minute incubation on ice, the cells were disrupted with 5 strokes in a 26G 5/8 syringe, and were incubated for an additional 30 – 60 minutes on ice. The lysate was centrifuged at 13.5k rpm for 1 minutes at 4 °C in an Eppendorf 5415C centrifuge, and the supernatant was transferred to a new eppendorf tube. The original tube with the pellet of cell debris and intact cells was discarded.

3.1.4 Protein Assay

The assay used was a modified Lowry assay. Samples were diluted 1/4 in distilled and de-ionized water in a total volume of 20 µl. Protein standards were prepared from a solution of 1.5 mg/ml BSA in 1/4, 1/2, 3/4, and 1/1 dilutions in total volumes of 20 µl. All protein standards and samples were transferred in triplicate to a 96 well plate. 25 µl of Bio-Rad DC Protein Assay reagent A and 200 µl of reagent B were added to each well, and the plate was incubated at room temperature for 30 minutes. The protein concentrations were determined on a Bio-Rad Benchmark multiplate reader at a 655 nm wavelength.

3.1.5 Western Blotting

Equal amounts of protein in total volumes of 15 µl were combined with 5 µl of 5x loading buffer and 1 µl of 2-mercaptoethanol. Samples were boiled for 10 minutes, and then briefly centrifuged to collect the steam droplets. Subsequently, the samples were loaded onto a 4-20% polyacrylamide gradient gel with a 4% stacking gel. The Mini-PROTEAN II Western apparatus was run with 2 gels in the apparatus at 80V and 120 mA until the sample had entered the resolving gel, and then the voltage was increased to 110V. The apparatus was turned off once the dye line was within 1 cm of the bottom of the gel. Transfer of the proteins to an Immobilon-P membrane was done at 100V and 350 mA for 1 hour.

Immunoblotting was done with an Armenian hamster CT2 antibody (which binds near the end of the MUC1 cytoplasmic domain) as the primary antibody, and a goat anti-Armenian hamster antibody conjugated to horse radish peroxidase (HRP) as the secondary antibody. Tubulin blotting was done with a mouse antibody against α-tubulin as a primary antibody, and a goat anti-mouse antibody conjugated to HRP as the secondary antibody. Detection of CT2 was done by chemiluminescence using the Amersham ECL Plus kit (chemiluminescent detection), and detection of tubulin was done with the Amersham ECL kit, using the manufacturer's instructions. These systems are based on the oxidation of the cyclic Diacylhydrazide, luminol(1,2), in the presence of HRP and peroxide, where one of the products produces a high intensity chemiluminescence that can be detected on autoradiography film.

3.1.6 Density Analysis of protein bands

Chemiluminescent detection was done on X-ray film, and the films were scanned into Adobe Photoshop. Scans were saved in .bmp format and protein band densities were analyzed using NIH Scion Image software. Results from 3 separate experiments were combined and plotted in Microsoft Excel.

3.1.7 Statistical analysis

The mean ± the standard error was graphed (Figure 3.3). Statistical significance was determined using the Student's t-test at P = 0.05.

3.2 Results

3.2.1 The MUC1 tandem repeats and human ICAM-1 are not required for MUC1 homodimerization

To determine if ICAM-1 was required to induce dimerization of MUC1, both N-terminally and C-terminally fluorescently labeled MUC1 transfectants were stimulated with NIH ICAM or NIH mock cells, and then tested for their ability to dimerize (Figure 3.2). Cytoplasmic MUC1 monomer was detected in lanes containing SYM25 lysate (~25 kDa) and 293T MUC1-CFP lysate (~50 kDa, due to the addition of a ~27 kDa fluorescent tag to the cytoplasmic tail), but not in lanes containing 293T lysate, which do not express MUC1 - this demonstrates the specificity of the CT2 antibody to the cytoplasmic fragment of MUC1.
Both the N-terminally tagged SYM25 cells and the C-terminally tagged 293T MUC1-CFP cells displayed a low level of constitutive dimer formation, at approximately 50 kDa and 100 kDa respectively. Stimulation of these MUC1 transfectants with NIH ICAM cells, however, noticeably increased the amount of dimer that was formed (lanes 2 and 8). Stimulation with NIH mock cells lacking human ICAM-1 also resulted in an increase in the amount of dimer (lanes 3 and 9). In all cases, the amount of MUC1 monomer was clearly greater than the amount of MUC1 dimer. In addition, minor bands larger than the MUC1 dimer complexes appeared at approximately 75 kDa and 100 kDa in the stimulated SYM25 lanes, and at approximately 150 kDa in the stimulated 293T MUC1-CFP lanes, implying that MUC1 might cluster into trimers, tetramers, and possibly larger complexes.

To verify that MUC1 homodimerization was not mediated by binding to ICAM-1, 293T MUCY-YFP cells were stimulated with NIH ICAM and NIH mock

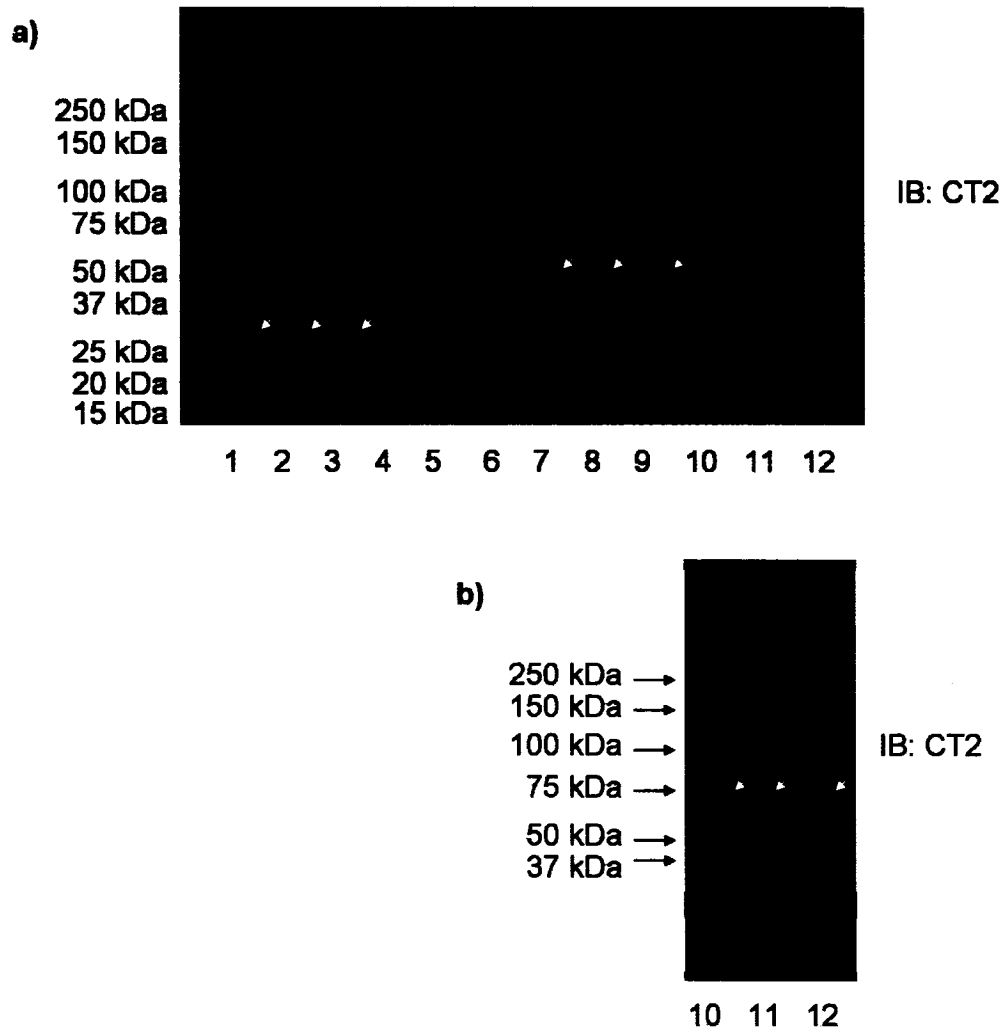

Figure 3.2 Cross-linking of MUC1 and MUC1/Y transfectants following stimulation with NIH transfectants. SYM25, 293T, 293T MUC1-CFP, and 293T MUCY-YFP cells were stimulated for 0 or 10 minutes with NIH ICAM or NIH mock cells, and then incubated with DSS cross-linker. Lysates were separated on SDS-PAGE and probed with the MUC1 CT2 antibody. Blots were exposed for **a)** 10 seconds, or **b)** 1 second. 1. SYM25 unstimulated, 2. SYM25 + NIH ICAM, 3. SYM25 + NIH mock, 4. 293T unstimulated, 5. 293T + NIH ICAM, 6. 293T + NIH mock, 7. 293T MUC1-CFP unstimulated, 8. 293T MUC1-CFP + NIH ICAM, 9. 293T MUC1-CFP + NIH mock, 10. 293T MUCY-YFP unstimulated, 11. 293T MUCY- YFP + NIH ICAM, and 12. 293T MUCY-YFP + NIH mock. MUC1 monomer and dimers ran at ~25 kDa and ~50 kDa for SYM25 cells, ~50 kDa and ~100 kDa for 293T MUC1-CFP cells, and ~75 kDa and ~150 kDa for 293T MUCY-YFP cells. Cytoplasmic MUC1 subunit monomers are indicated with white arrows, and dimers are indicated with black arrows. (n = 3)

cells, and the presence of dimers was examined. Since the 293T MUCY-YFP cells lack the MUC1 tandem repeats, ICAM-1 should not be able to bind, since its binding site is in the tandem repeat region of MUC1 [81, 82]. The CT2 antibody was able to detect MUC1/Y, showing the presence of the monomer at just under 75 kDa (~42 kDa MUC1/Y with an additional ~27 kDa fluorescent tag) (lane 10). Like the full length MUC1 transfectants, the 293T MUCY-YFP cells had a low level of constitutive dimer formation, at just under 150 kDa (Figure 3.2b). Stimulation with either NIH ICAM or NIH mock cells significantly increased the amount of dimer formed (lanes 11 and 12). Of note were one or two distinct bands smaller than the MUC1/Y monomer band that appeared to be between the 37 and 50 kDa. Similarly, two small bands appeared in the 293T MUC1-CFP lanes under the MUC1-CFP band that were between 25 and 37 kDa. Proteins at these sizes may represent artifacts created during lysate preparation, or may represent intermediates formed during metabolic processing of the protein. Taken together, these data suggest that other factors besides ICAM-1 in cell-to-cell contact are responsible for inducing MUC1 homodimerization.

3.2.2 Human ICAM-1 does not increase the level of MUC1 homodimerization caused by cellular contact

To determine if ICAM-1 was able to influence MUC1 dimer formation, quantitative data was generated by performing density analysis on the MUC1 bands for SYM25 cells, 293T MUC1-CFP cells, and 293T MUCY-YFP cells. Analysis was done on three sets of experiments, and the data was combined and graphed (Figure 3.3). As a confirmation of the visual analysis of the Western blot, the MUC1 dimer to monomer ratio increased when comparing unstimulated cells to NIH ICAM- and NIH mock-stimulated cells – this was true for both of the MUC1 transfectants and the MUC1/Y transfectant. MUC1 dimer to monomer comparison between ICAM-1 and mock stimulation, however, showed no difference between the two conditions. Consequently, these data demonstrate that ICAM-1 is not likely

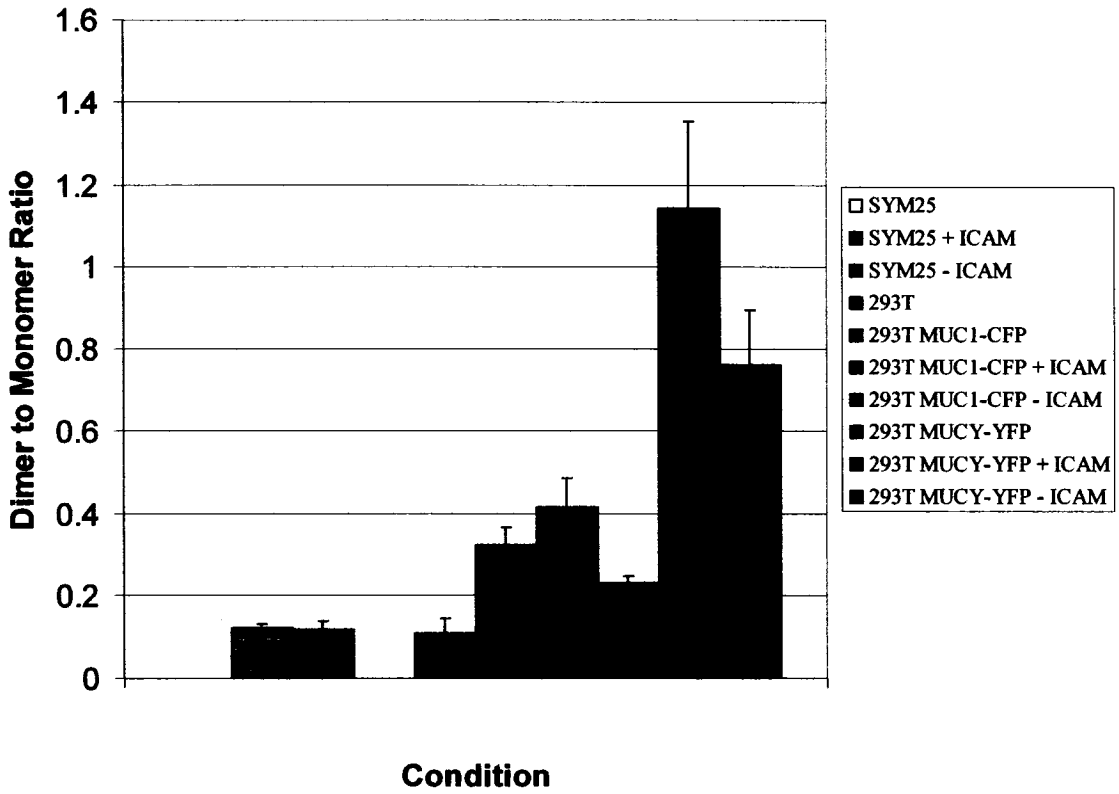

Figure 3.3 MUC1 dimer to monomer analysis of MUC1 and MUC1/Y transfectants following contact with NIH cells. MUC1 dimer and monomer band density analysis was done on 3 sets of cross-linking blots similar to figure 3.2. Dimer to monomer ratios were calculated, and the results were combined and graphed. Conditions for the cell lines were graphed in sets of 3. From left to right for each cell line: Unstimulated, stimulated with NIH-ICAM cells, and stimulated with NIH mock cells.

to participate in ligand-induced MUC1 dimerization. Thus, homodimerization is caused by other interactions that occur between the MUC1-expressing cell and the cell that comes into physical contact with it.

The graph brings up one more point of interest: there seems to be a correlation between the length or bulkiness of the MUC1 extracellular domain and the amount of dimer formed. With the SYM25 cells, the MUC1 protein has a full length extracellular domain with an attached YFP protein. In these scenarios, the ratio of MUC1 dimer to monomer is very low. With the 293T MUC1-CFP cells, with a full length MUC1 extracellular domain but no extracellular fluorescent protein tag, there is a moderate dimer to monomer ratio. Finally, with the 293T MUCY-YFP cells, with a truncated MUC1 extracellular domain, there is a relatively high MUC1 dimer to monomer ratio (see figure 2.1 for a schematic of the lengths). Whether these results have any significance, however, is unknown.

3.3 Summary

Since the MUC1 dimer, but not the monomer, displays increased localization in lipid rafts upon stimulation with ICAM-1, and that disruption of rafts inhibits ICAM-1-induced calcium oscillations, the ability of MUC1 to homodimerize was the first concept examined in the investigation of the mechanism of ICAM-1-induced MUC1 signal initiation. Data generated from the crosslinking experiments showed that there was a constitutive level of dimerization that was noticeable for the 293T MUC1-CFP and 293T MUCY-YFP cells, but that these dimers are likely to be in an inactive state or below the threshold for meaningful activity, since unstimulated MUC1 293T transfectants do not migrate efficiently [80]. Subsequently, after stimulating SYM25 cells, 293T MUC1-CFP cells, and 293T MUCY-YFP cells with NIH ICAM or NIH mock cells, the formation of MUC1 homodimers increased, regardless of ICAM-1 expression on the dropped cells (Figure 3.3). In addition, the increase in homodimerization was similar following stimulation with either NIH transfectant. These data indicate that ICAM-1 and the

missing ECD in the MUC1-Y molecule are not required to induce MUC1 homodimerization.

Chapter 4: Effect of the MUC1 extracellular domain on the distribution of MUC1 monomers and dimers in the cellular membrane

4.0 Introduction

The next area of investigation after the discovery that ICAM-1 was not required for MUC1 homodimerization was the localization of these MUC1 dimers. One aspect of signal regulation is spatial orientation – if the components of a signaling pathway cannot interact, then a signal cannot be transduced. Lipid rafts, which are liquid-ordered microdomains in the exoplasmic leaflet of the plasma membrane, are capable of performing this spatial orientation function. Lipid rafts are composed of a unique combination of saturated sphingolipids and cholesterol, and contain numerous proteins that are involved in a wide variety of signaling pathways (reviewed in [33, 34]). As a result, they are able to segregate proteins from the bulk of the lipid bilayer, and concentrate molecules in a small area, thereby promoting interaction between them. Previous work had demonstrated that the MUC1 monomer was present in both the raft fractions and the non-raft fractions, regardless of the ICAM-1 status of the stimulating cells (data not shown). MUC1 homodimers, however, were present mainly in the detergent-insoluble lipid rafts following ICAM-1 stimulation (Figure 3.1). In addition, disruption of these rafts, by cholesterol extraction with methyl-β-cyclodextrin or by membrane sequestration of cholesterol with nystatin, inhibited ICAM-1-induced calcium oscillations [83]. These data indicate that the lipid rafts are essential for ICAM-1-induced MUC1 signal transduction, and suggest that MUC1 dimers are necessary for the process. It is still unclear, however, whether MUC1 homodimerization occurs in or out of the lipid rafts, and whether the MUC1 extracellular domain is involved in movement of the protein into or out of lipid rafts. Therefore, the objective of this chapter is to determine if the MUC1 tandem repeats are necessary for the translocation of MUC1 homodimers into lipid rafts.

4.1 Methods and Materials

4.1.1 Reagents

See sections 2.1.1 and 3.1.1. 55 cm^2 tissue culture dishes and Triton-X 100 were from Fisher Scientific (Ottawa, Ontario, Canada). Insulin and methyl-β-cyclodextrin was from Sigma Aldrich (Oakville, Ontario, Canada). Omni-pur sucrose was from EMD Biosciences (San Diego, California, USA). HRP-conjugated cholera toxin B was from List Biological Laboratories (Hornby, Ontario, Canada).

4.1.2 Cells

See section 2.1.2.

4.1.3 Cross-linking

Similar to section 3.1.3, but all volumes and amounts were scaled up, as more cells were required in order to detect proteins from the fractions of a surcrose gradient. 55 cm^2 tissue culture dishes were coated with 0.1% (w/v) gelatin and allowed to dry in a laminar flow hood. Sterilization was done by UV irradiation for one hour.

Adherent cells to be plated were trypsinized and resuspended in a volume of media four-times the volume of trypsin used. The cell density was determined on a hemocytometer, and 5.0 to 5.5 million cells in 6.5 ml of appropriate media (see section 2.1.2) were plated on each dish. This density gave approximately 50 – 80% confluence in a dish for HEK 293T parental and transfected cells. The cells were allowed to settle overnight.

On the day of the experiment, the media was aspirated from the dishes, washed once with imaging buffer, and the cells were incubated in imaging buffer at 37 °C and 5% (v/v) CO_2 for 45 minutes. Imaging buffer was used since it

represented conditions that were close to physiological conditions. 15 minutes before the end of the incubation period, 2 confluent T-150 flasks of NIH ICAM or NIH mock cells was trypsinized for each 55 cm^2 dish to be tested. The NIH cells were resuspended in media, and the suspensions of each type of NIH cell were combined in a single 50 ml centrifuge tube. The cells were pelleted at 2500 xg for 2.5 minutes, and resuspended in PBS, in a volume of 3 ml for every two T-150 flasks used.

Following the 45 minute incubation period, the imaging buffer was aspirated, and a 3 ml suspension of NIH cells were added to each dish. After a 1 minute incubation period, the NIH cells were aspirated, and the dishes were placed on ice. One gentle wash was done with ice-cold PBS, and 3 ml of 1 mM membrane-permeable DSS cross linker was added. The cross-linking solution was aspirated after 10 minutes and replaced with 1.5 ml of ice-cold quenching solution (20 mM Tris buffer). The cell monolayer was then scraped off the dish with a rubber policeman and transferred to a 1.5 ml Eppendorf tube. The cells were pelleted at 13.5k rpm for 1 minute at 4 °C in an Eppendorf 5415C centrifuge, and then the supernatant was aspirated. The pellet was resuspended in ice-cold lysis buffer (2 ml 1% Triton-X 100 (v/v) + 5 µl protease inhibitor cocktail + 5 µl phosphatase inhibitor cocktail) and transferred to a 15 ml centrifuge tube. Following a 15 minute incubation on ice, the cells were disrupted with 5 strokes in a 26G 5/8 syringe, and were incubated for an additional 30 – 60 minutes on ice. The lysate was centrifuged at 13.5k rpm for 1 minutes at 4 °C in an Eppendorf 5415C centrifuge, and the supernatant was transferred to a new 15 ml centrifuge tube. The original tube with the pellet of cell debris and intact cells was discarded.

4.1.4 Fractionation of cell lysate on a sucrose gradient

3 concentrations of sucrose were prepared in lipid raft buffer (25 mM Tris, 150 mM NaCl, 5 mM EDTA*$2H_2O$, final pH 7.5): 5% (w/v), 30% (w/v), and 80% (w/v). Immediately before the experiment, 0.25% (v/v) of the phosphatase inhibitor

cocktail and 0.25% (v/v) of the protease inhibitor cocktail were mixed into each sucrose solution. The solutions were then put on ice.

In a cold room, a maximum of 2 ml of cell lysate was transferred into the bottom of a Beckmann 14 x 89 mm polyallomer ultracentrifuge tube. 3 ml of 80% (w/v) sucrose was thoroughly mixed with the lysate, and 3 ml of 30% (w/v) sucrose was carefully layered on top. A final layer of 3 ml 5% (w/v) sucrose was layered over the 30% (w/v) sucrose, and these steps were repeated for each of the lysates used in the experiment.

Opposing tubes were balanced to within 0.01g of each other using 5% sucrose, and placed in the pre-cooled tube holders for a pre-cooled Beckman SW Ti 41 rotor. The rotor was then moved into a pre-cooled Beckman ultracentrifuge. Following a spin at 40k rpm (197.5k xg average) at 4 °C for 16 hours, ten 1.1 ml fractions were collected from each tube, going from the top to the bottom. The fractions were vortexed vigorously, and frozen until needed.

4.1.5 Dot blot

A nitrocellulose membrane was soaked in TBS (10x = 500 mM Tris, 1.5 M NaCl, final pH 7.5) and transferred to a BioRad Bio-Dot microfiltration apparatus. Sample fractions were diluted to 1/5 and 1/15 in a 50 µl total volume using ddH_2O. Diluted samples were added to separate wells of the dot blot apparatus, and the remaining wells were filled with 50 µl of ddH_2O. The vacuum was applied for 2 minutes, and then the wells were washed once by adding 50 µl of TBS and applying the vacuum briefly. The membrane was removed from the dot blot apparatus, and incubated in 5% (w/v) skim milk made in T-TBS (TBS with 0.05% (v/v) Tween 20) overnight.

The next day, the membrane was probed for the GM1 lipid raft marker using cholera toxin B conjugated to HRP (CTB-HRP). The membrane was incubated with 0.1 µg/ml CTB-HRP for 3 hours. Following two 10 minute washes with TBS and one 10 minute wash with T-TBS, detection was done by chemiluminescence with the Amersham ECL kit, using the manufacturer's instructions.

4.1.6 Western blotting

See section 3.1.5. Equal volume loading was done instead of equal protein loading to objectively measure the distribution of proteins by density, with 15 µl of sample, 5 µl of 4x loading buffer, and 1 µl of 2-mercaptoethanol.

4.1.7 Disruption of lipid rafts with methyl-β-cyclodextrin (MBCD)

A 10 – 20 mM solution of MBCD was made in imaging buffer. For conditions that required lipid raft disruption, 3 ml of the MBCD solution was added to a 55 cm^2 dish already containing settled cells for 30 – 60 minutes at 37 °C. This step replaced the initial 45 minute incubation with imaging buffer in the cross-linking protocol.

4.2 Results

4.2.1 The MUC1 extracellular tandem repeats are necessary for MUC1 homodimer localization in lipid rafts following stimulation with human ICAM-1

MUC1 dimers are found in lipid rafts, but it is unknown how they localize there. To determine if the MUC1 extracellular domain is required for movement of MUC1 dimers into lipid rafts, 293T cells expressing full length MUC1 (293T MUC1-CFP) or extracellularly-truncated MUC1 (293T MUCY-YFP) were stimulated with NIH ICAM cells, incubated with a membrane-permeable crosslinker, and fractionated on a sucrose gradient. Fractions were probed for the GM1-ganglioside lipid raft marker and the MUC1 cytoplasmic fragment to establish which fractions contained lipid rafts and MUC1 dimers, respectively. For both 293T MUC1-CFP and 293 MUCY-YFP transfectants, the majority of the GM1 staining was in fractions 3 – 5, and these fractions will therefore be considered to be the lipid rafts (Figure 4.1 and 4.2). CT2 staining for the MUC1 cytoplasmic fragment in

293T MUC1-CFP cells showed the presence of the MUC1-CFP monomer at approximately 50 kDa, and the dimer at approximately 100 kDa (Figure 4.1). The amount of monomer was clearly greater than the amount of dimer. MUC1-CFP monomers were present in both the lipid raft and non-raft fractions, and the distribution between the two categories (fractions 3 – 5 versus 6 – 10) seemed to be relatively even. No staining was seen in fractions 1 and 2. Dimers, however, were predominantly in the lipid raft fractions, and this distribution was similar to the pattern seen in T47D cells (Figure 3.1), illustrating that the behavior of the transfected MUC1 protein was similar to endogenous MUC1.

In contrast, CT2 staining of 293T MUCY-YFP fractions showed a markedly different pattern. MUC1/Y-YFP monomers were evident at 75 kDa and dimers were at 150 kDa (Figure 4.2). Similar to full-length MUC1, the amount of monomer was much greater than the amount of dimer. Unlike the full-length MUC1 in the transfectant and the endogenous expresser, the MUC1/Y-YFP monomer was concentrated in the lipid raft fractions (fractions 3- 5), but the significance of this observation is unclear. And, similar to full-length MUC1, no staining was seen in fractions 1 and 2. The MUC1/Y dimer, conversely, localized entirely out of the lipid rafts (fractions 6 – 10). This observation offers a possible explanation for the lack of calcium oscillations seen in these cells following NIH ICAM stimulation. Since lipid rafts are necessary for inducing intracellular calcium signaling, and full-length MUC1 dimers are found in lipid rafts after ICAM-1 stimulation, then MUC1 dimers in lipid rafts are likely to be required for the induction of the calcium signal. Furthermore, as MUC1/Y should not be capable of binding to ICAM-1, this suggests that ICAM-1 is involved in relocalizing MUC1 dimers from the mostly fluid portion of the lipid bilayer to the detergent-insoluble lipid raft microdomains. However, since the MUC1/Y protein not only lacks the tandem repeats, but also lacks additional residues in the extracellular domain, another possibility is that a segment of these missing residues is required for raft localization.

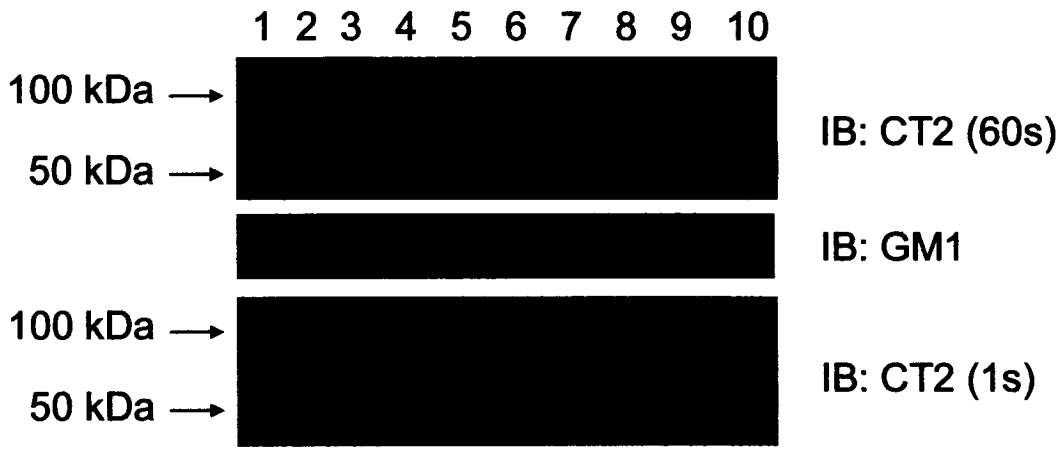

Figure 4.1 MUC1-CFP distribution following ICAM-1 stimulation. 293T MUC1-CFP cells were stimulated with NIH ICAM cells, incubated with DSS crosslinker, and fractionated on a sucrose gradient. Fractions were probed for GM1 and the MUC1 cytoplasmic subunit (using the CT2 antibody) to determine the location of the lipid rafts and the distribution of MUC1, respectively. Exposure times for the CT2 blots are listed on the right side. GM1 staining showed that lipid rafts were mainly in fractions 3 – 5. CT2 staining showed that the MUC1-CFP monomer appeared at approximately 50 kDa, and the homodimer appeared at approximately 100 kDa. (n=1)

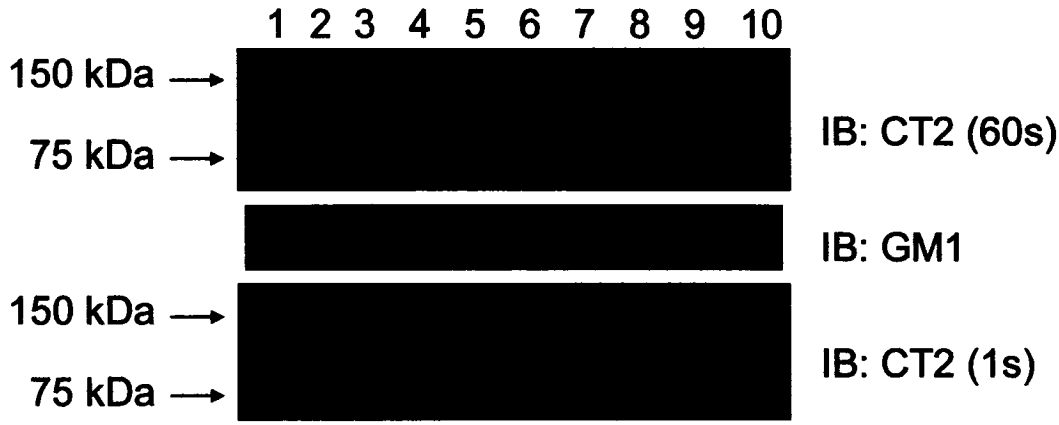

Figure 4.2 MUC1/Y distribution following ICAM-1 stimulation. 293T MUCY-YFP cells were stimulated with NIH ICAM cells, incubated with DSS crosslinker, and fractionated on a sucrose gradient. Fractions were probed for GM1 and the MUC1 cytoplasmic subunit (using the CT2 antibody) to determine the location of the lipid rafts and the distribution of MUC1/Y, respectively. Exposure times for CT2 blots are listed on the right side. GM1 staining showed that lipid rafts were mainly in fractions 3 – 5. CT2 staining showed that the MUC1/Y-YFP monomer appeared at approximately 75 kDa, and the homodimer appeared at approximately 150 kDa. (n = 1)

4.2.2 MUC1 homodimer formation is not dependent on the presence of lipid rafts

The MUC1 monomer is found in both raft and non-raft fractions. As a result, there is the possibility that lipid rafts are required for MUC1 homodimer formation. To determine if MUC1 homodimer formation is dependent on the presence of lipid rafts, T47D cells were incubated with methyl-β-cyclodextrin to disrupt lipid rafts, and then stimulated with NIH ICAM cells, incubated with a membrane-permeable crosslinker, and fractionated on a sucrose gradient. A higher number of fractions were taken compared to the previous experiment due to changes in the centrifugation equipment (i.e. different centrifuge, and an SW Ti 40 rotor). Fractions were probed for the GM1-ganglioside lipid raft marker and the MUC1 cytoplasmic fragment to establish which fractions contained lipid rafts and MUC1 dimers, respectively. When lipid rafts are intact, lipid rafts were predominantly in fractions 4 – 6 (Figure 4.3A). CT2 staining of the MUC1 cytoplasmic domain indicated the presence of MUC1 monomers between 20 – 25 kDa, and MUC1 dimers between 37 – 50 kDa. Both the monomer and the dimer were located predominantly off the rafts, and appeared to be concentrated in the heavier higher-numbered fractions. MUC1 was not detected in fractions 1 – 3.

When lipid rafts were disrupted, the GM1 distribution changed, shifting to fractions 4 – 5 (Figure 4.3B). Probing for the MUC1 cytoplasmic domain showed a similar pattern to the non-disrupted condition. The MUC1 monomer appeared between 20 – 25 kDa, and the MUC1 dimer was evident close to 50 kDa. In addition, both the monomer and the dimer were predominantly off the rafts, although the distribution appears to have shifted even further towards the heavier fractions compared to the non-disrupted condition. Similarly, MUC1 could not be detected in fractions 1 – 3. Taken together, these data indicate that the formation of MUC1 homodimers can form independently of lipid rafts.

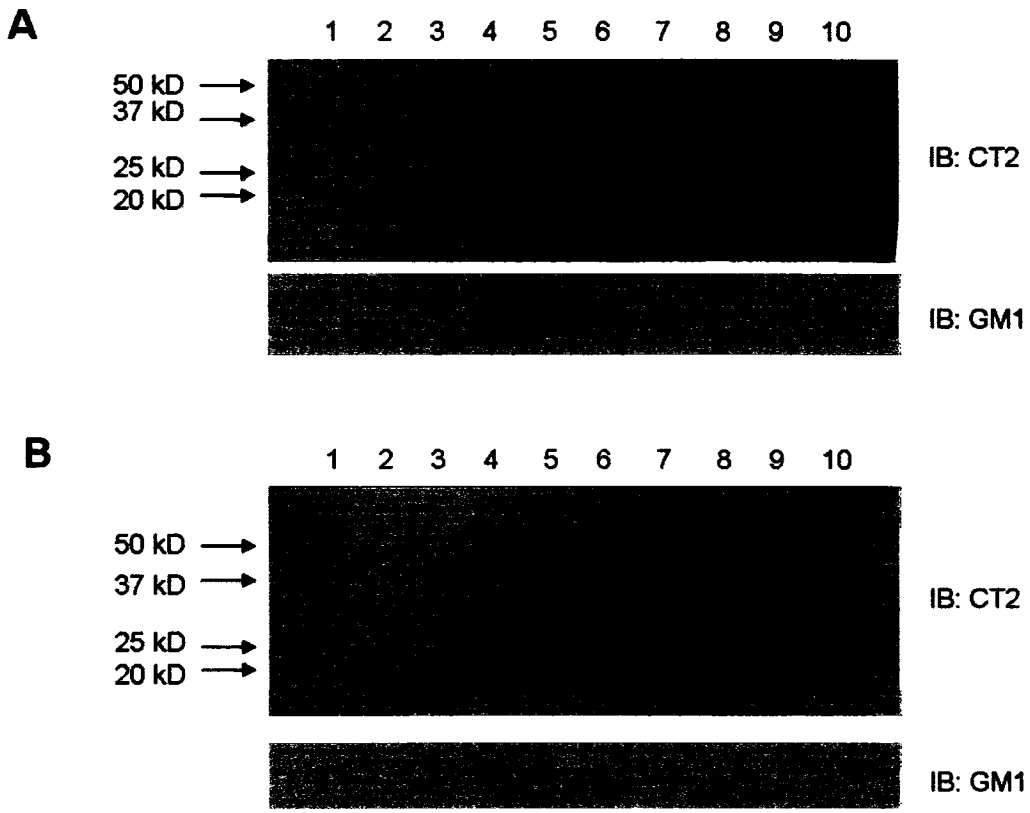

Figure 4.3 Formation of MUC1 homodimers following lipid raft disruption. T47D cells were stimulated with NIH ICAM cells, incubated with DSS crosslinker, and fractionated on a sucrose gradient. Fractions were probed for GM1 and the MUC1 cytoplasmic subunit (using the CT2 antibody) to determine the location of the lipid rafts and the distribution of MUC1, respectively. (**A**) GM1 staining showed that lipid rafts were mainly in fractions 4 – 6. CT2 staining showed the MUC1 monomer between 20 – 25 kDa, and the MUC1 dimer between 37 – 50 kDa. (**B**) Cells were incubated with methyl-β-cyclodextrin for 1 hour prior to stimulation. GM1 staining showed that lipid rafts were mainly in fractions 4 – 5. CT2 staining showed the MUC1 monomer between 20 – 25 kDa, and the MUC1 dimer between 37 – 50 kDa. This experiment was done by Lindsay Finnie-Carvalho. (n = 2)

4.3 Summary

Since dimerization alone was not sufficient to induce signaling, another potential requirement for ICAM-1-induced MUC1 signaling was investigated. Earlier work had shown that disruption of the detergent-insoluble lipid raft microdomains of the plasma membrane resulted in the inhibition of ICAM-1-induced calcium oscillations [83]. To determine if MUC1 localization was a factor in ICAM-1-induced signaling, the distribution of full-length and extracellularly-truncated MUC1 between rafts and non-rafts was compared.

Probing for the cytoplasmic fragment of MUC1 with the CT2 antibody showed that dimers of full-length MUC1 dimers localized primarily in the lipid rafts, whereas MUC1/Y dimers localized entirely out of the lipid rafts (Figures 4.1 and 4.2). The monomers of both forms, however, were present in both types of membrane domains. Although these data imply that dimerization occurs in the bulk plasma membrane, the presence of monomers in the rafts leaves an option for dimer formation to occur on the raft followed by movement out of the rafts. To verify that lipid rafts are not needed for dimer formation, lipid rafts were disrupted with methyl-β-cyclodextran, which showed that dimerization still occurred, demonstrating that lipid rafts were not necessary for MUC1 homodimerization (Figure 4.3). Taken together, the results suggest that lipid raft localization of the MUC1 homodimer is important for ICAM-1-induced signal transduction, and that ICAM-1 or the MUC1 extracellular domain is necessary for translocation into rafts.

Chapter 5: Discussion and Conclusions

5.0 Introduction

The focus of this thesis has been on the molecular mechanism driving the initial steps of ICAM-1-induced MUC1 signaling. *In vitro*, interaction between these two proteins results in adhesion and transendothelial migration of the MUC1-expressing cell through a simulated vessel wall. *In vivo*, in order for breast cancer cells to disseminate through the body to distant sites, they must have the ability to move into and out of the circulatory system. Since the formation of secondary metastases in distant organs following tumor cell extravasation leads to impairment of organ function and mortality, one plausible method of stopping breast cancer is to prevent the entry of tumor cells into secondary sites. Understanding the molecular mechanism behind breast cancer cell locomotion would therefore potentially offer new targets for treatment.

Prior to this study, several parts of the pathway were already known. The binding sites on the MUC1 and ICAM-1 molecules have been established, and an early downstream effect of this interaction was the induction of intracellular calcium oscillations, which is significant since changes in intracellular calcium have been reported to be involved in cellular movement. In addition, several signaling molecules had been shown to either participate or be excluded from the ICAM-1-induced signaling pathway. However, the events prior to calcium signaling remain unclear. To investigate these events, the extracellular domain of MUC1 was manipulated, and the effects of this alteration on signal initiation were examined. The specific objectives of this thesis were to:

1. To determine if the MUC1 tandem repeats are necessary for ICAM-1-induced MUC1 signaling;
2. To determine if binding of ICAM-1 to MUC1 is necessary for MUC1 homodimer formation; and
3. To determine if the MUC1 extracellular domain is necessary for movement of MUC1 homodimers into lipid rafts.

5.1 Summary and discussion of the necessity of the MUC1 tandem repeats for ICAM-1-induced calcium oscillations

Earlier work had demonstrated that cells expressing MUC1 would generate repetitive calcium spikes with a period of approximately 30 seconds following contact with cells expressing ICAM-1 [83]. This effect was not seen when at least one of these molecules was absent. Under these latter conditions, the majority of the MUC1 positive cells only displayed a single calcium spike with no subsequent oscillations. Since antibody blockade against either MUC1 or ICAM-1 inhibited both calcium oscillations and transendothelial migration, changes in intracellular calcium were used as an indicator of ICAM-1-induced MUC1 signaling. In this study, 293T cells transfected with MUC1/Y, a splice variant of MUC1 lacking the tandem repeats, were subjected to a calcium assay to determine if the tandem repeats were needed for this form of signaling. The Fluo-3 calcium indicator used in the assay undergoes a structural modification upon calcium binding, where calcium binding is positively correlated with the ability of the indicator to be fluorescently excited at a particular wavelength. Consequently, changes in intracellular calcium can be tracked using time course microscopy on a fluorescent microscope.

The data showed that cells expressing this truncated form of MUC1 were incapable of producing calcium oscillations following stimulation with NIH ICAM cells, generating only one calcium spike similar to the conditions where either MUC1 or ICAM-1 was missing. The MUC1/Y protein also had a fluorescent protein attached to the cytoplasmic tail which could have potentially interfered with calcium signaling. However, 293T cells transfected with a similarly tagged full length MUC1 molecule were fully capable of generating intracellular calcium oscillations, thereby supporting the importance of the MUC1 extracellular tandem repeats in ICAM-1-induced signal initiation.

The single calcium spike might be attributed to membrane deformation due to contact with the dropped cells. Pressure from these contacting cells could cause both mechanosensitive calcium channels in the cell membrane and intracellular channels to open, increasing the concentration of intracellular calcium. This type of

response is consistent with responses seen in HUVEC endothelial cells, where mechanical perturbation lead to a transient rise in intracellular calcium [91]. Consequently, the single calcium spike could be considered a non-specific cell contact response that is independent of the MUC1/ICAM-1 interaction. In contrast, the calcium oscillations seen when MUC1 is able to interact with ICAM-1 is a specific response. The oscillation frequency graphs demonstrate that these oscillations occur regularly, and the oscillation factor graphs show that the amplitudes are far above what could be considered to be noise. Multiple reports have shown that the behavior of some proteins can be regulated through a single change in the concentration of calcium (amplitude modulation), and others that are regulated by specific frequencies of calcium oscillations (frequency modulation) (reviewed in [22]). As a result, the 30 second cycle generated from the MUC1/ICAM-1 interaction strongly implies a frequency-modulated signal. However, the precise contribution of the calcium signal to migration involving MUC1 remains unclear.

Furthermore, there were some variations in the calcium responses in any given experiment. These include variations in the latency period before the initial calcium spike and intercellular differences in the magnitude of the calcium oscillations. Differences in the times leading to the initial calcium spike might be attributed to differences in the time it took for a plated cell to properly come into contact with a dropped cell. Differences in the amplitudes, however, might be due to variations in MUC1 surface expression on the contacting cells – this would be consistent with the data from overall population differences, where cell lines with higher amounts of membrane-tethered MUC1 showed higher oscillation factors than cell lines with lower amounts of membrane-tethered MUC1 [83]. Since 293T MUC1-CFP cells generally displayed higher oscillation factors than SYM25 cells, the increased strength of the calcium oscillations might be due to a difference in the quantity of cell surface MUC1. This possibility is comparing total cellular MUC1 levels, where the 293T MUC1-CFP cells show a higher level of MUC1 expression than the SYM25 cells (Figure 2.2). A second possibility for the difference in oscillation factors is that the ratio of dimerized MUC1 to monomeric MUC1 is

higher in the 293T MUC1-CFP cells than in the SYM25 cells (Figure 3.3). Along with the data in chapter 4 that strongly suggests that the presence of MUC1 dimers in lipid rafts is necessary for ICAM-1-induced calcium signaling, the higher amount of MUC1 homodimers formed after ICAM-1 stimulation of the 293T MUC1-CFP cells may result in a signal that has greater potency. Further investigation is needed to determine the cause of this difference.

One additional point of interest is that the MUC1/Y transfectants have a higher calcium oscillation factor following stimulation with NIH ICAM cells compared to stimulation with NIH mock cells (Figure 2.8). Since the curves in the calcium frequency graphs look similar, it is difficult to determine if this is a real difference or an artifact from experimental conditions or analytical technique. If there is an actual difference, it could mean that some form of amplitude-modulated response is mediated by MUC1/Y. The more likely reason, however, is that the difference is artificial, and that it is due to the small sample size since the oscillation factor calculation is not ideal for low numbers of calcium oscillations. Specifically, the setting of the minimum size threshold of a calcium peak is subjective, and analysis for low numbers of calcium spikes can lead to noticeable changes in the oscillation factor that is computed. But regardless of the flaw, 293T MUCY-YFP cells stimulated with NIH ICAM cells did not display a curve that could be considered to contain calcium oscillations.

5.2 Summary and discussion for the effects of the MUC1 tandem repeats on MUC1 homodimer formation

Since the MUC1 dimer, but not the monomer, displays increased localization in lipid rafts upon stimulation with ICAM-1, and that disruption of rafts inhibits ICAM-1-induced calcium oscillations, the ability of MUC1 to homodimerize was the first concept examined in the investigation of the mechanism of ICAM-1-induced MUC1 signal initiation. The CT2 antibody was chosen for these experiments, since it binds to the MUC1 cytoplasmic tail, which is identical for both full length MUC1 and the truncated MUC1/Y. The other MUC1 antibody available

to the lab, B27.29, binds to the MUC1 extracellular tandem repeats, and would therefore have been useless for detecting dimerization of the MUC1/Y splice variant, which lacks the tandem repeats. Full-length MUC1 is cleaved in the extracellular SEA motif and the two subunits subsequently associate non-covalently in physiological conditions, but separate after exposure to sodium dodecyl sulfate. Consequently, the CT2 antibody will only detect the smaller subunit containing the transmembrane and cytoplasmic domains following SDS-PAGE. In contrast, since the MUC1/Y splice variant is missing the cleavage site in the SEA module, the protein runs as one species on SDS-PAGE. The MUC1 cytoplasmic fragment has been reported to run between 16 – 30 kDa in the literature [50, 83, 92, 93]. In addition, multiple groups have found that the CT2 antibody detects protein bands smaller than the MUC1 monomer [50, 83, 92]. Furthermore, these bands are not non-specific, as they do not appear in lysates with no MUC1 (Figure 3.2). At present, these small proteins have not been conclusively identified, but they have been speculated to be artifacts from lysate preparation, degradation products, different glycoforms, or intermediate products generated during metabolic processing [42, 50, 83, 92].

To prevent the separation of dimers in SDS-PAGE, disuccinimidyl suberate (DSS) was used to cross-link the proteins prior to cell lysis. The cell permeable DSS was chosen instead of a cell impermeable crosslinker, as a percentage of MUC1 subunits are separated by SDS and a cell impermeable crosslinker is not able to enter the cell to efficiently crosslink the MUC1 cytoplasmic fragment. Using the cell permeable crosslinker, as a result, allows for the detection of these dimers with the CT2 antibody. It should be noted that a lower amount of MUC1 homodimers can be detected in the absence of crosslinker (unpublished, data not shown), but the reason for this SDS resistance has yet to be determined. Data generated from the crosslinking experiments showed that there was a constitutive level of dimerization that was noticeable for the 293T MUC1-CFP and 293T MUCY-YFP cells, but that these dimers are likely to be in an inactive state or below the threshold for meaningful activity, since unstimulated MUC1 293T transfectants do not migrate efficiently [80]. This is not a unique phenomenon, as receptors such as EGFR and

the erythropoietin receptor have been shown to undergo ligand-independent dimerization [94, 95]. Subsequently, after stimulation with dropped cells, the formation of MUC1 homodimers increased, regardless of the level of ICAM-1 expression on the dropped cells (Figure 3.3). Since dimerization was not induced by ICAM-1, the response must have been mediated in a different manner. Stimulation can come from two directions: for instance, an external source, such as a protein from the dropped cell, might bind to the MUC1 extracellular domain to induce dimerization. This is unlikely since ICAM-1 binds to the MUC1 tandem repeats, but MUC1/Y is still capable of dimerization even though it lacks the tandem repeats. The second direction would be through an internal source, which could be illustrated by integrin clustering, since this event is partially mediated by internal signals [11]. But dimerization alone is not sufficient for ICAM-1-induced MUC1 signaling – stimulation of cells expressing full-length MUC1 with NIH mock cells and stimulation of 293T MUCY-YFP cells with both types of NIH cells results in MUC1 homodimerization, but these conditions do not generate calcium oscillations (Figures 2.5, 2.7 and 3.3). Part of the reason might be that the dimer is still in an inactive state before interacting with a ligand. The question, however, is what constitutes an inactive state. The MUC1 cytoplasmic tail has multiple tyrosine residues that can be phosphorylated, and phosphorylation of a receptor is often considered to be a shift to an active state. Studies from our lab have shown that tyrosine residues on the cytoplasmic tail are phosphorylated following stimulation with either NIH ICAM or NIH mock cells [96]. This suggests that either these initial phosphorylations do not target the correct tyrosines for ICAM-1-induced signaling, or that there are additional requirements for MUC1 activation. One of these requirements is probably the localization of the dimer, since 293T MUCY-YFP cells have MUC1 dimers that have a non-raft distribution, but do not generate any calcium oscillations following ICAM-1 stimulation (Figures 2.7 and 4.2).

Several other issues arose from these experiments. For example, the amount of MUC1 dimerization increases as the size of the MUC1 extracellular domain decreases, with the extracellularly-tagged SYM25 cells showing the least amount of dimerization and the extracellularly-truncated 293T MUCY-YFP cells showing the

most amount of dimerization (Figure 3.3). As this trend occurs even in non-stimulated conditions, it is possible that the bulkiness of the extracellular domain interferes with dimerization through a steric effect. If this is true, then deglycosylation of the MUC1 extracellular domain would also be expected to increase dimerization, and preliminary data from our lab supports the theory (data not shown). Other possibilities for this effect are charge repulsion, since the MUC1 extracellular domain is negatively charged due to the sialyl Lewis$^{a/x}$ carbohydrates on the tandem repeats, or that increased size of the extracellular domain inhibits lateral diffusion of the mucin. Finally, there was evidence of large cross-linked protein complexes that could be detected with the CT2 antibody, suggesting the presence of MUC1 oligomers (Figure 3.7). If the minimum valency to activate ICAM-1-induced signaling is a dimer, then a question that arises is whether these oligomers have an increased avidity to ICAM-1 that enables them to signal more potently than a dimer. There is also the possibility that these high molecular weight bands consist of MUC1 complexed to other proteins besides MUC1, but additional research is necessary to examine this and the other issues before conclusions can be made.

5.3 Summary and discussion for the necessity of the MUC1 tandem repeats for ICAM-1-induced movement into lipid rafts

Since dimerization alone was not sufficient to induce signaling, another potential requirement for ICAM-1-induced MUC1 signaling was investigated. Earlier work had shown that disruption of the detergent-insoluble lipid raft microdomains of the plasma membrane resulted in the inhibition of ICAM-1-induced calcium oscillations [83]. To determine if MUC1 localization was a factor in ICAM-1-induced signaling, the distribution of full-length and extracellularly-truncated MUC1 between rafts and non-rafts was compared. Lipid rafts were isolated using a sucrose gradient, and since lipid rafts have a low buoyant density, they float towards the lower density regions of the gradient. Separation of proteins on a sucrose gradient is dependent on buoyant density, and proteins travel through

the gradient until they reach a region where their own density matches that of the surrounding sucrose – for lipid rafts, this region is the interface between 5% and 30% sucrose when cells are lysed with 1% Triton-X 100 (v/v). Determination of lipid raft location following fractionation of the gradient was done by probing for the GM1 monosialoganglioside, a glycosphingolipid that is a commonly used marker for lipid rafts. Probing for the cytoplasmic fragment of MUC1 with the CT2 antibody showed that dimers of full-length MUC1 dimers localized primarily in the lipid rafts, whereas MUC1/Y dimers localized entirely out of the lipid rafts (Figures 4.1 and 4.2). The monomers of both forms, however, were present in both types of membrane domains. Although these data imply that dimerization occurs in the bulk plasma membrane, the presence of monomers in the rafts leaves an option for dimer formation to occur on the raft followed by movement out of the rafts. To verify that lipid rafts are not needed for dimer formation, lipid rafts were disrupted with methyl-β-cyclodextran, which sequesters cholesterol from the membrane, thereby depriving lipid rafts of one of their major structural components. The data indicated that dimerization still occurred, demonstrating that lipid rafts were not necessary for MUC1 homodimerization (Figure 4.3). Unfortunately, the distribution of MUC1 was inconsistent with earlier data, in that MUC1 was detected predominantly outside of the rafts instead of half within and half outside the lipid rafts. As the phenomenon is not unique to the T47D cell line (data not shown), the differences are likely due to technical issues – different equipment was used and it is also possible that there was some variation in technique as the experiment was performed by another. Neverthless, the results suggest that lipid raft localization of the MUC1 homodimer is important for ICAM-1-induced signal transduction, and that ICAM-1 or the MUC1 extracellular domain is necessary for translocation into rafts. However, an issue arises as to how MUC1 partitions into lipid rafts following ICAM-1 ligation. Preliminary work has shown that although the MUC1 extracellular fragment is present in non-raft fractions, it cannot be detected in the lipid raft fractions (Figure 5.1). Using this information, one potential mechanism is that binding of ICAM-1 to the MUC1 dimer leads to shearing of the MUC1 extracellular fragment. This event could lead to a change in the conformation of the

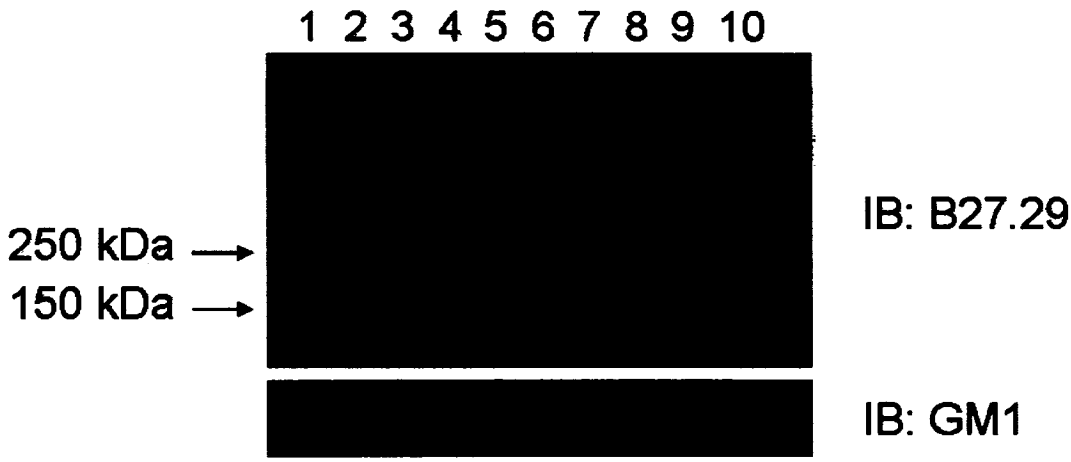

Figure 5.1 Distribution of the MUC1 extracellular subunit. T47D cells were lysed and fractionated on a sucrose gradient. Fractions were probed for GM1 and the MUC1 extracellular subunit (using the B27.29 antibody) to determine the location of the lipid rafts and the distribution of MUC1, respectively. B27.29 staining showed that the MUC1 extracellular fragment above 150 kDa. This experiment was done by Sue Szigety.

cytoplasmic fragments, resulting in an increased affinity for partitioning into lipid rafts. A precedent for subunit separation following ligand binding is well documented in the literature. One example is the NOTCH receptor that was first isolated from *Drosophila melanogaster*. This is a 300 kDa single pass transmembrane receptor that is cleaved in the trans-Golgi, and the extracellular and transmembrane subunits re-associate to form a heterodimer on the cell surface [97]. The NOTCH receptor binds to 5 known ligands (delta-like-1, delta-like-3, delta-like-4, jagged-1, and jagged-2) which are themselves single pass transmembrane proteins [97]. Binding of the receptor to a ligand on an adjacent cell is postulated to induce a conformational change in the receptor, allowing for proteolytic cleavage and release of the extracellular fragment by TACE/ADAM17 [98, 99]. In this respect, it is noteworthy that MUC1 is also cleaved by the same enzyme [52]. The second hypothesis of altered affinity for lipid rafts is also well documented, where binding of a ligand to a receptor leads to increased partitioning in detergent-insoluble microdomains [33, 34].

5.4 Partial model for ICAM-1-induced MUC1 Signal Initiation and downstream signaling

With the new data presented in this study, a possible model for ICAM-1-induced MUC1 signaling is as follows: Tumor cell MUC1 is not restricted to the apical surface, and the circumferential localization may better position the molecule to interact with ICAM-1, and might also enable associations with signaling molecules that are normally segregated from MUC1. Upon contact and adhesion to an endothelial or stromal cell expressing ICAM-1, the tumor cell expressing MUC1 would initiate general cell contact signals, resulting in events such as an influx of calcium from the environment through cell membrane ion channels [91], increased MUC1 homodimerization (Figure 3.3), and the recruitment and activation of kinases such as Src at heterotypic contact points [100]. In order to completely activate MUC1 for signaling, at least two additional events are likely to be needed: 1. phosphorylation of specific tyrosine residues on the cytoplasmic tail, and 2.

partitioning of the MUC1 dimer into lipid rafts. Some phosphorylation could potentially occur before ligand binding, as contact with a cell lacking ICAM-1 is sufficient to induce tyrosine phosphorylation on the MUC1 cytoplasmic tail [96]. Interaction between MUC1 and its ligand, ICAM-1, would subsequently lead to the release of the extracellular subunit from the cell membrane, causing conformational changes in the cytoplasmic subunit and increased partitioning into lipid rafts. Partitioning of the MUC1 cytoplasmic dimers into lipid rafts would bring them into proximity of additional activated kinases, and phosphorylation of more tyrosine residues on the cytoplasmic domain could occur.

Inhibitor experiments have demonstrated that the generation of the calcium oscillations involves Src, PI3K, phospholipase C, and the IP_3 receptor. Src is able to associate with both unphosphorylated and phosphorylated MUC1 through its SH3 and SH2 domains, respectively [49]. Phosphorylation of the potential PI3K binding site on the MUC1 cytoplasmic domain might lead to the recruitment of PI3K, and conversion of PI(4,5)P to PI(3,4,5)P by this kinase enables membrane localization of phospholipase C through its phosphoinositide-binding PH domain [101]. Tyrosine phosphorylation and binding of phospholipase C to MUC1 would meet the other requirements for phospholipase C activation, enabling the protein to cleave PIP2 into IP_3 and diacylglycerol [102]. Thus, the IP_3 generated by this enzyme would be able to bind to and activate the IP_3 receptor, allowing for release of calcium from the endoplasmic reticulum into the cytoplasm [102].

These signaling molecules and pathways offer a number of potential links to cell locomotion. Src has been shown to participate in the regulation of WASP and WAVE proteins, which are important mediators of actin polymerization [11]. In addition, Src is necessary for the formation of adhesion complexes and adhesion turnover, and it associates with FAK and is present in adhesion complexes [11]. Recruitment and activation of PI3K at points of adhesion may contribute to forward protrusion, as PI3K is a key regulator of actin polymerization at the leading edge [11]. Changes in intracellular calcium can modulate the activity of diverse proteins as well. Examples include: calmodulin, which associates with IQGAP, a protein that is involved in regulating Rho GTPases crucial to forward membrane protrusion and

adhesion, several RhoGEFs and RhoGAPs which also regulate Rho GTPase activity, MLCK, which is involved in the generation of contractile force for movement, and calpains, calcineurin, and gelsolin, proteins involved in rear detachment and adhesion turnover [11]. Further research is necessary to clearly define the details of the pathway initiated by the MUC1/ICAM-1 interaction.

5.5 Final Thoughts

Transendothelial migration is a cooperative process between a migrating cell and the endothelium. Contact between the two types of cells induces signals that result in cellular movement in the migrating cells, and signals that enhance adhesion and endothelial retraction in the endothelial cell. There are a number of known mediators for cell migration. Our lab has focused on the MUC1 mucin, which has been demonstrated to participate in bidirectional migratory signaling. In the endothelial cell, interaction of ICAM-1 with MUC1 has been demonstrated to induce signaling in ICAM-1-expressing HUVEC cells [87], and MUC1-expressing MCF-7 cells have been shown to induce endothelial retraction [103]. In the migrating tumor cell, ICAM-1 is able to halt the tumor cell's movement and promote its migration *in vitro* through a monolayer of endothelial cells [80]. The molecular details of this signal, however, are not well defined. The current study has addressed some of the missing details, and the data indicate that the MUC1 extracellular tandem repeats are necessary for ICAM-1-induced MUC1 signaling. In addition, the results strongly suggest that the normal method of signal initiation involves MUC1 homodimerization in the bulk plasma membrane and movement of the dimerized transmembrane-cytoplasmic subunit into lipid rafts. There are still many holes in the pathway, and although several downstream segments of the pathway were previously known, their overall contributions to the pro-migratory signal are still unclear. Specifically, the MUC1 molecule may signal through unique pathways that modulate cell locomotion. However, several of the proteins known to associate with MUC1 are also important regulators of cell locomotion. As lipid raft localization seems to be an important component in both ICAM-1-induced MUC1

signaling and common mechanisms of cell movement, it is possible to speculate that either the MUC1 molecule acts like a scaffold to bring proteins needed for migration into contact with raft proteins from these general migratory pathways, or that it simply requires raft localization to complete the signaling complex for its own separate pathway. Furthermore, a given protein may act in a different fashion depending on whether it is at the leading edge or at the retracting tail of the cell, and this spatial behavior may also apply to the MUC1 mucin.

Regardless of the possible scenarios, transendothelial migration of several breast tumor cell lines that endogenously express MUC1 can be inhibited by 60 – 70% by blocking the MUC1/ICAM-1 interaction [80]. Although these results clearly indicate the importance of this particular interaction to transendothelial migration *in vitro*, they also show that the cells can utilize additional methods to initiate migration. In addition, other breast cancer cell lines that express low levels of MUC1, such as MDA-MB-231 cells, can show high levels of migration in transwell assays [104, 105]. Taken together, the MUC1/ICAM-1 method of migration is likely to be a significant migration mechanism for the subset of tumor cells that show higher levels of MUC1 expression. If the behavior of these cells is similar *in vivo*, then several routes of preventative treatment could potentially be beneficial. Anti-inflammatory drugs such as NSAIDS can reduce ICAM-1 expression [106, 107], and have been documented to inhibit the onset of secondary metastases [108-110]. Furthermore, statins, which inhibit cholesterol synthesis, have been implicated in indirectly modulating the amounts of cholesterol and sphingomyelin (where both are components of lipid rafts) in several cell lines, resulting in a decrease in breast tumor cell migration [111]. In addition, statins have been shown to downregulate ICAM-1 in some systems [111]. By reducing the possibility of MUC1 interacting with ICAM-1, or signaling through lipid rafts, it might be possible to inhibit tumor cell migration. As the ICAM-1-induced MUC1 signaling pathway continues to be better elucideated, additional novel methods of metastatic prevention might emerge.

References:

1. Society, C.B.C., *Breast Cancer Facts*. 2006, Canadian Cancer Society/National Cancer Institute of Canada: Toronto.
2. Weigelt, B., J.L. Peterse, and L.J. van 't Veer, *Breast cancer metastasis: markers and models.* Nat Rev Cancer, 2005. **5**(8): p. 591-602.
3. Kumar, V., Abul K. Abbas, Nelson Fausto, *Pathologic Basis of Disease*. Seventh ed, ed. R.a. Cotran. 2005: W.B. Saunders Company.
4. Miller, K., *Estrogen and DNA damage: the silent source of breast cancer?* J Natl Cancer Inst, 2003. **95**(2): p. 100-2.
5. Fidler, I.J., *The pathogenesis of cancer metastasis: the 'seed and soil' hypothesis revisited.* Nat Rev Cancer, 2003. **3**(6): p. 453-8.
6. Crowe, D.L. and C.F. Shuler, *Regulation of tumor cell invasion by extracellular matrix.* Histol Histopathol, 1999. **14**(2): p. 665-71.
7. Egeblad, M. and Z. Werb, *New functions for the matrix metalloproteinases in cancer progression.* Nat Rev Cancer, 2002. **2**(3): p. 161-74.
8. Carter, C.L., C. Allen, and D.E. Henson, *Relation of tumor size, lymph node status, and survival in 24,740 breast cancer cases.* Cancer, 1989. **63**(1): p. 181-7.
9. Chambers, A.F., A.C. Groom, and I.C. MacDonald, *Dissemination and growth of cancer cells in metastatic sites.* Nat Rev Cancer, 2002. **2**(8): p. 563-72.
10. Muller, A., B. Homey, H. Soto, N. Ge, D. Catron, M.E. Buchanan, T. McClanahan, E. Murphy, W. Yuan, S.N. Wagner, J.L. Barrera, A. Mohar, E. Verastegui, and A. Zlotnik, *Involvement of chemokine receptors in breast cancer metastasis.* Nature, 2001. **410**(6824): p. 50-6.
11. Ridley, A.J., M.A. Schwartz, K. Burridge, R.A. Firtel, M.H. Ginsberg, G. Borisy, J.T. Parsons, and A.R. Horwitz, *Cell migration: integrating signals from front to back.* Science, 2003. **302**(5651): p. 1704-9.
12. Lodish, H., Arnold Berk, S. Lawrence Zipursky, Paul Matsudaira, David Baltimore, and James Darnell, *Molecular Cell Biolgy*. Fourth ed, ed. S. Tenney. 1999, New York: W.H. Freeman and Company.
13. Emsley, J., C.G. Knight, R.W. Farndale, M.J. Barnes, and R.C. Liddington, *Structural basis of collagen recognition by integrin alpha2beta1.* Cell, 2000. **101**(1): p. 47-56.
14. Geiger, B., A. Bershadsky, R. Pankov, and K.M. Yamada, *Transmembrane crosstalk between the extracellular matrix--cytoskeleton crosstalk.* Nat Rev Mol Cell Biol, 2001. **2**(11): p. 793-805.
15. Etienne-Manneville, S. and A. Hall, *Rho GTPases in cell biology.* Nature, 2002. **420**(6916): p. 629-35.
16. Rodriguez, O.C., A.W. Schaefer, C.A. Mandato, P. Forscher, W.M. Bement, and C.M. Waterman-Storer, *Conserved microtubule-actin interactions in cell movement and morphogenesis.* Nat Cell Biol, 2003. **5**(7): p. 599-609.
17. Cory, G.O. and A.J. Ridley, *Cell motility: braking WAVEs.* Nature, 2002. **418**(6899): p. 732-3.

18. Pollard, T.D. and G.G. Borisy, *Cellular motility driven by assembly and disassembly of actin filaments.* Cell, 2003. **112**(4): p. 453-65.
19. Welch, M.D. and R.D. Mullins, *Cellular control of actin nucleation.* Annu Rev Cell Dev Biol, 2002. **18**: p. 247-88.
20. Feldner, J.C. and B.H. Brandt, *Cancer cell motility--on the road from c-erbB-2 receptor steered signaling to actin reorganization.* Exp Cell Res, 2002. **272**(2): p. 93-108.
21. Kirfel, G., A. Rigort, B. Borm, and V. Herzog, *Cell migration: mechanisms of rear detachment and the formation of migration tracks.* Eur J Cell Biol, 2004. **83**(11-12): p. 717-24.
22. Cullen, P.J. and P.J. Lockyer, *Integration of calcium and Ras signalling.* Nat Rev Mol Cell Biol, 2002. **3**(5): p. 339-48.
23. Berridge, M.J., M.D. Bootman, and H.L. Roderick, *Calcium signalling: dynamics, homeostasis and remodelling.* Nat Rev Mol Cell Biol, 2003. **4**(7): p. 517-29.
24. Dupont, G., G. Houart, and A. Goldbeter, *From simple to complex Ca2+ oscillations: Regulatory mechanisms and theoretical models*. Lecture Notes in Physics. Understanding calcium dynamics. Experiments and theory., ed. M. Falcke, and D. Malchow. 2003, Berlin: Springer.
25. Aspenstrom, P., *Integration of signalling pathways regulated by small GTPases and calcium.* Biochim Biophys Acta, 2004. **1742**(1-3): p. 51-8.
26. Pawson, T., *Regulation and targets of receptor tyrosine kinases.* Eur J Cancer, 2002. **38 Suppl 5**: p. S3-10.
27. Schlessinger, J., *Cell signaling by receptor tyrosine kinases.* Cell, 2000. **103**(2): p. 211-25.
28. Hubbard, S.R. and J.H. Till, *Protein tyrosine kinase structure and function.* Annu Rev Biochem, 2000. **69**: p. 373-98.
29. Schenk, P.W. and B.E. Snaar-Jagalska, *Signal perception and transduction: the role of protein kinases.* Biochim Biophys Acta, 1999. **1449**(1): p. 1-24.
30. Bai, M., *Dimerization of G-protein-coupled receptors: roles in signal transduction.* Cell Signal, 2004. **16**(2): p. 175-86.
31. Pierce, K.L., R.T. Premont, and R.J. Lefkowitz, *Seven-transmembrane receptors.* Nat Rev Mol Cell Biol, 2002. **3**(9): p. 639-50.
32. Marinissen, M.J. and J.S. Gutkind, *G-protein-coupled receptors and signaling networks: emerging paradigms.* Trends Pharmacol Sci, 2001. **22**(7): p. 368-76.
33. Simons, K. and D. Toomre, *Lipid rafts and signal transduction.* Nat Rev Mol Cell Biol, 2000. **1**(1): p. 31-9.
34. Zajchowski, L.D. and S.M. Robbins, *Lipid rafts and little caves. Compartmentalized signalling in membrane microdomains.* Eur J Biochem, 2002. **269**(3): p. 737-52.
35. Baldus, S.E., K. Engelmann, and F.G. Hanisch, *MUC1 and the MUCs: a family of human mucins with impact in cancer biology.* Crit Rev Clin Lab Sci, 2004. **41**(2): p. 189-231.

36. Ligtenberg, M.J., L. Kruijshaar, F. Buijs, M. van Meijer, S.V. Litvinov, and J. Hilkens, *Cell-associated episialin is a complex containing two proteins derived from a common precursor.* J Biol Chem, 1992. **267**(9): p. 6171-7.
37. Hollingsworth, M.A. and B.J. Swanson, *Mucins in cancer: protection and control of the cell surface.* Nat Rev Cancer, 2004. **4**(1): p. 45-60.
38. Price, M.R., P.D. Rye, E. Petrakou, A. Murray, K. Brady, S. Imai, S. Haga, Y. Kiyozuka, D. Schol, M.F. Meulenbroek, F.G. Snijdewint, S. von Mensdorff-Pouilly, R.A. Verstraeten, P. Kenemans, A. Blockzjil, K. Nilsson, O. Nilsson, M. Reddish, M.R. Suresh, R.R. Koganty, S. Fortier, L. Baronic, A. Berg, M.B. Longenecker, J. Hilgers, and et al., *Summary report on the ISOBM TD-4 Workshop: analysis of 56 monoclonal antibodies against the MUC1 mucin. San Diego, Calif., November 17-23, 1996.* Tumour Biol, 1998. **19 Suppl 1**: p. 1-20.
39. Patton, S., S.J. Gendler, and A.P. Spicer, *The epithelial mucin, MUC1, of milk, mammary gland and other tissues.* Biochim Biophys Acta, 1995. **1241**(3): p. 407-23.
40. Gendler, S.J., *MUC1, the renaissance molecule.* J Mammary Gland Biol Neoplasia, 2001. **6**(3): p. 339-53.
41. Altschuler, Y., C.L. Kinlough, P.A. Poland, J.B. Bruns, G. Apodaca, O.A. Weisz, and R.P. Hughey, *Clathrin-mediated endocytosis of MUC1 is modulated by its glycosylation state.* Mol Biol Cell, 2000. **11**(3): p. 819-31.
42. Palmai-Pallag, T., N. Khodabukus, L. Kinarsky, S.H. Leir, S. Sherman, M.A. Hollingsworth, and A. Harris, *The role of the SEA (sea urchin sperm protein, enterokinase and agrin) module in cleavage of membrane-tethered mucins.* Febs J, 2005. **272**(11): p. 2901-11.
43. Levitin, F., O. Stern, M. Weiss, C. Gil-Henn, R. Ziv, Z. Prokocimer, N.I. Smorodinsky, D.B. Rubinstein, and D.H. Wreschner, *The MUC1 SEA module is a self-cleaving domain.* J Biol Chem, 2005. **280**(39): p. 33374-86.
44. Macao, B., D.G. Johansson, G.C. Hansson, and T. Hard, *Autoproteolysis coupled to protein folding in the SEA domain of the membrane-bound MUC1 mucin.* Nat Struct Mol Biol, 2006. **13**(1): p. 71-6.
45. Pemberton, L.F., A. Rughetti, J. Taylor-Papadimitriou, and S.J. Gendler, *The epithelial mucin MUC1 contains at least two discrete signals specifying membrane localization in cells.* J Biol Chem, 1996. **271**(4): p. 2332-40.
46. Parry, G., J.C. Beck, L. Moss, J. Bartley, and G.K. Ojakian, *Determination of apical membrane polarity in mammary epithelial cell cultures: the role of cell-cell, cell-substratum, and membrane-cytoskeleton interactions.* Exp Cell Res, 1990. **188**(2): p. 302-11.
47. Bennett, R., Jr., T. Jarvela, P. Engelhardt, L. Kostamovaara, P. Sparks, O. Carpen, O. Turunen, and A. Vaheri, *Mucin MUC1 is seen in cell surface protrusions together with ezrin in immunoelectron tomography and is concentrated at tips of filopodial protrusions in MCF-7 breast carcinoma cells.* J Histochem Cytochem, 2001. **49**(1): p. 67-77.
48. Wang, H., E.P. Lillehoj, and K.C. Kim, *Identification of four sites of stimulated tyrosine phosphorylation in the MUC1 cytoplasmic tail.* Biochem Biophys Res Commun, 2003. **310**(2): p. 341-6.

49. Li, Y., H. Kuwahara, J. Ren, G. Wen, and D. Kufe, *The c-Src tyrosine kinase regulates signaling of the human DF3/MUC1 carcinoma-associated antigen with GSK3 beta and beta-catenin.* J Biol Chem, 2001. **276**(9): p. 6061-4.
50. Schroeder, J.A., M.C. Thompson, M.M. Gardner, and S.J. Gendler, *Transgenic MUC1 interacts with epidermal growth factor receptor and correlates with mitogen-activated protein kinase activation in the mouse mammary gland.* J Biol Chem, 2001. **276**(16): p. 13057-64.
51. Li, Y., A. Bharti, D. Chen, J. Gong, and D. Kufe, *Interaction of glycogen synthase kinase 3beta with the DF3/MUC1 carcinoma-associated antigen and beta-catenin.* Mol Cell Biol, 1998. **18**(12): p. 7216-24.
52. Thathiah, A., C.P. Blobel, and D.D. Carson, *Tumor necrosis factor-alpha converting enzyme/ADAM 17 mediates MUC1 shedding.* J Biol Chem, 2003. **278**(5): p. 3386-94.
53. Thathiah, A. and D.D. Carson, *MT1-MMP mediates MUC1 shedding independent of TACE/ADAM17.* Biochem J, 2004. **382**(Pt 1): p. 363-73.
54. Kohlgraf, K.G., A.J. Gawron, M. Higashi, J.L. Meza, M.D. Burdick, S. Kitajima, D.L. Kelly, T.C. Caffrey, and M.A. Hollingsworth, *Contribution of the MUC1 tandem repeat and cytoplasmic tail to invasive and metastatic properties of a pancreatic cancer cell line.* Cancer Res, 2003. **63**(16): p. 5011-20.
55. Huang, L., D. Chen, D. Liu, L. Yin, S. Kharbanda, and D. Kufe, *MUC1 oncoprotein blocks glycogen synthase kinase 3beta-mediated phosphorylation and degradation of beta-catenin.* Cancer Res, 2005. **65**(22): p. 10413-22.
56. Yamamoto, M., A. Bharti, Y. Li, and D. Kufe, *Interaction of the DF3/MUC1 breast carcinoma-associated antigen and beta-catenin in cell adhesion.* J Biol Chem, 1997. **272**(19): p. 12492-4.
57. Li, Y., J. Ren, W. Yu, Q. Li, H. Kuwahara, L. Yin, K.L. Carraway, 3rd, and D. Kufe, *The epidermal growth factor receptor regulates interaction of the human DF3/MUC1 carcinoma antigen with c-Src and beta-catenin.* J Biol Chem, 2001. **276**(38): p. 35239-42.
58. Ren, J., Y. Li, and D. Kufe, *Protein kinase C delta regulates function of the DF3/MUC1 carcinoma antigen in beta-catenin signaling.* J Biol Chem, 2002. **277**(20): p. 17616-22.
59. Huang, L., J. Ren, D. Chen, Y. Li, S. Kharbanda, and D. Kufe, *MUC1 cytoplasmic domain coactivates Wnt target gene transcription and confers transformation.* Cancer Biol Ther, 2003. **2**(6): p. 702-6.
60. Wang, H., E.P. Lillehoj, and K.C. Kim, *MUC1 tyrosine phosphorylation activates the extracellular signal-regulated kinase.* Biochem Biophys Res Commun, 2004. **321**(2): p. 448-54.
61. Pandey, P., S. Kharbanda, and D. Kufe, *Association of the DF3/MUC1 breast cancer antigen with Grb2 and the Sos/Ras exchange protein.* Cancer Res, 1995. **55**(18): p. 4000-3.
62. Li, Y. and D. Kufe, *The Human DF3/MUC1 carcinoma-associated antigen signals nuclear localization of the catenin p120(ctn).* Biochem Biophys Res Commun, 2001. **281**(2): p. 440-3.

63. Wei, X., H. Xu, and D. Kufe, *MUC1 oncoprotein stabilizes and activates estrogen receptor alpha.* Mol Cell, 2006. **21**(2): p. 295-305.
64. Li, Y., W.H. Yu, J. Ren, W. Chen, L. Huang, S. Kharbanda, M. Loda, and D. Kufe, *Heregulin targets gamma-catenin to the nucleolus by a mechanism dependent on the DF3/MUC1 oncoprotein.* Mol Cancer Res, 2003. **1**(10): p. 765-75.
65. Ren, J., A. Bharti, D. Raina, W. Chen, R. Ahmad, and D. Kufe, *MUC1 oncoprotein is targeted to mitochondria by heregulin-induced activation of c-Src and the molecular chaperone HSP90.* Oncogene, 2006. **25**(1): p. 20-31.
66. Rahn, J.J., L. Dabbagh, M. Pasdar, and J.C. Hugh, *The importance of MUC1 cellular localization in patients with breast carcinoma: an immunohistologic study of 71 patients and review of the literature.* Cancer, 2001. **91**(11): p. 1973-82.
67. Ciborowski, P. and O.J. Finn, *Non-glycosylated tandem repeats of MUC1 facilitate attachment of breast tumor cells to normal human lung tissue and immobilized extracellular matrix proteins (ECM) in vitro: potential role in metastasis.* Clin Exp Metastasis, 2002. **19**(4): p. 339-45.
68. Bieche, I. and R. Lidereau, *A gene dosage effect is responsible for high overexpression of the MUC1 gene observed in human breast tumors.* Cancer Genet Cytogenet, 1997. **98**(1): p. 75-80.
69. Brockhausen, I., J.M. Yang, J. Burchell, C. Whitehouse, and J. Taylor-Papadimitriou, *Mechanisms underlying aberrant glycosylation of MUC1 mucin in breast cancer cells.* Eur J Biochem, 1995. **233**(2): p. 607-17.
70. Freire, T., S. Bay, S. von Mensdorff-Pouilly, and E. Osinaga, *Molecular basis of incomplete O-glycan synthesis in MCF-7 breast cancer cells: putative role of MUC6 in Tn antigen expression.* Cancer Res, 2005. **65**(17): p. 7880-7.
71. Regimbald, L.H., L.M. Pilarski, B.M. Longenecker, M.A. Reddish, G. Zimmermann, and J.C. Hugh, *The breast mucin MUC1 as a novel adhesion ligand for endothelial intercellular adhesion molecule 1 in breast cancer.* Cancer Res, 1996. **56**(18): p. 4244-9.
72. van de Stolpe, A. and P.T. van der Saag, *Intercellular adhesion molecule-1.* J Mol Med, 1996. **74**(1): p. 13-33.
73. Hubbard, A.K. and R. Rothlein, *Intercellular adhesion molecule-1 (ICAM-1) expression and cell signaling cascades.* Free Radic Biol Med, 2000. **28**(9): p. 1379-86.
74. Anderson, M.E. and T.J. Siahaan, *Targeting ICAM-1/LFA-1 interaction for controlling autoimmune diseases: designing peptide and small molecule inhibitors.* Peptides, 2003. **24**(3): p. 487-501.
75. Cook-Mills, J.M. and T.L. Deem, *Active participation of endothelial cells in inflammation.* J Leukoc Biol, 2005. **77**(4): p. 487-95.
76. van Buul, J.D. and P.L. Hordijk, *Signaling in leukocyte transendothelial migration.* Arterioscler Thromb Vasc Biol, 2004. **24**(5): p. 824-33.
77. Kannagi, R., *Carbohydrate-mediated cell adhesion involved in hematogenous metastasis of cancer.* Glycoconj J, 1997. **14**(5): p. 577-84.

78. Thurin, M. and T. Kieber-Emmons, *SA-Lea and tumor metastasis: the old prediction and recent findings.* Hybrid Hybridomics, 2002. **21**(2): p. 111-6.
79. Horne, G., *The Role of Breast Cancer Associated MUC1 in Tumor Cell Recruitment to Vascular Endothelium During Physiological Fluid Flow*, in *Labortatory Medicine and Pathology*. 1999, University of Alberta: Edmonton.
80. Rahn, J.J., J.W. Chow, G.J. Horne, B.K. Mah, J.T. Emerman, P. Hoffman, and J.C. Hugh, *MUC1 mediates transendothelial migration in vitro by ligating endothelial cell ICAM-1.* Clin Exp Metastasis, 2005. **22**(6): p. 475-83.
81. Kam, J.L., L.H. Regimbald, J.H. Hilgers, P. Hoffman, M.J. Krantz, B.M. Longenecker, and J.C. Hugh, *MUC1 synthetic peptide inhibition of intercellular adhesion molecule-1 and MUC1 binding requires six tandem repeats.* Cancer Res, 1998. **58**(23): p. 5577-81.
82. Hayashi, T., T. Takahashi, S. Motoya, T. Ishida, F. Itoh, M. Adachi, Y. Hinoda, and K. Imai, *MUC1 mucin core protein binds to the domain 1 of ICAM-1.* Digestion, 2001. **63 Suppl 1**: p. 87-92.
83. Rahn, J.J., Q. Shen, B.K. Mah, and J.C. Hugh, *MUC1 initiates a calcium signal after ligation by intercellular adhesion molecule-1.* J Biol Chem, 2004. **279**(28): p. 29386-90.
84. Chen, P., J.E. Murphy-Ullrich, and A. Wells, *A role for gelsolin in actuating epidermal growth factor receptor-mediated cell motility.* J Cell Biol, 1996. **134**(3): p. 689-98.
85. Perrin, B.J. and A. Huttenlocher, *Calpain.* Int J Biochem Cell Biol, 2002. **34**(7): p. 722-5.
86. Ranta-Knuuttila, T., T. Kiviluoto, H. Mustonen, P. Puolakkainen, S. Watanabe, N. Sato, and E. Kivilaakso, *Migration of primary cultured rabbit gastric epithelial cells requires intact protein kinase C and Ca2+/calmodulin activity.* Dig Dis Sci, 2002. **47**(5): p. 1008-14.
87. Rahn, J., *MUC1/ICAM-1 in Breast Cancer Migration*, in *Laboratory Medicine and Pathology*. 2004, University of Alberta: Edmonton.
88. Clontech, *Living Colors Fluorescent Protein Vectors.*
89. Inoue, H., H. Nojima, and H. Okayama, *High efficiency transformation of Escherichia coli with plasmids.* Gene, 1990. **96**(1): p. 23-8.
90. Jun, C.D., M. Shimaoka, C.V. Carman, J. Takagi, and T.A. Springer, *Dimerization and the effectiveness of ICAM-1 in mediating LFA-1-dependent adhesion.* Proc Natl Acad Sci U S A, 2001. **98**(12): p. 6830-5.
91. Sigurdson, W.J., F. Sachs, and S.L. Diamond, *Mechanical perturbation of cultured human endothelial cells causes rapid increases of intracellular calcium.* Am J Physiol, 1993. **264**(6 Pt 2): p. H1745-52.
92. Li, X., L. Wang, D.P. Nunes, R.F. Troxler, and G.D. Offner, *Pro-inflammatory cytokines up-regulate MUC1 gene expression in oral epithelial cells.* J Dent Res, 2003. **82**(11): p. 883-7.
93. Wen, Y., T.C. Caffrey, M.J. Wheelock, K.R. Johnson, and M.A. Hollingsworth, *Nuclear association of the cytoplasmic tail of MUC1 and beta-catenin.* J Biol Chem, 2003. **278**(39): p. 38029-39.

94. Constantinescu, S.N., T. Keren, M. Socolovsky, H. Nam, Y.I. Henis, and H.F. Lodish, *Ligand-independent oligomerization of cell-surface erythropoietin receptor is mediated by the transmembrane domain.* Proc Natl Acad Sci U S A, 2001. **98**(8): p. 4379-84.
95. Yu, X., K.D. Sharma, T. Takahashi, R. Iwamoto, and E. Mekada, *Ligand-independent dimer formation of epidermal growth factor receptor (EGFR) is a step separable from ligand-induced EGFR signaling.* Mol Biol Cell, 2002. **13**(7): p. 2547-57.
96. Au, D., *Effects of ICAM-1 on MUC1 Phosphorylation*, in *Laboratory Medicine and Pathology*. 2005, University of Alberta: Edmonton.
97. Miele, L., *Notch signaling.* Clin Cancer Res, 2006. **12**(4): p. 1074-9.
98. Brou, C., F. Logeat, N. Gupta, C. Bessia, O. LeBail, J.R. Doedens, A. Cumano, P. Roux, R.A. Black, and A. Israel, *A novel proteolytic cleavage involved in Notch signaling: the role of the disintegrin-metalloprotease TACE.* Mol Cell, 2000. **5**(2): p. 207-16.
99. Mumm, J.S., E.H. Schroeter, M.T. Saxena, A. Griesemer, X. Tian, D.J. Pan, W.J. Ray, and R. Kopan, *A ligand-induced extracellular cleavage regulates gamma-secretase-like proteolytic activation of Notch1.* Mol Cell, 2000. **5**(2): p. 197-206.
100. Qi, J., J. Wang, O. Romanyuk, and C.H. Siu, *Involvement of Src family kinases in N-cadherin phosphorylation and beta-catenin dissociation during transendothelial migration of melanoma cells.* Mol Biol Cell, 2006. **17**(3): p. 1261-72.
101. Katan, M., R. Rodriguez, M. Matsuda, Y.M. Newbatt, and G.W. Aherne, *Structural and mechanistic aspects of phospholipase Cgamma regulation.* Adv Enzyme Regul, 2003. **43**: p. 77-85.
102. Berridge, M.J., P. Lipp, and M.D. Bootman, *The versatility and universality of calcium signalling.* Nat Rev Mol Cell Biol, 2000. **1**(1): p. 11-21.
103. Lewalle, J.M., K. Bajou, J. Desreux, M. Mareel, E. Dejana, A. Noel, and J.M. Foidart, *Alteration of interendothelial adherens junctions following tumor cell-endothelial cell interaction in vitro.* Exp Cell Res, 1997. **237**(2): p. 347-56.
104. Heylen, N., R. Baurain, C. Remacle, and A. Trouet, *Effect of MRC-5 fibroblast conditioned medium on breast cancer cell motility and invasion in vitro.* Clin Exp Metastasis, 1998. **16**(2): p. 193-203.
105. Lee, T.H., H.K. Avraham, S. Jiang, and S. Avraham, *Vascular endothelial growth factor modulates the transendothelial migration of MDA-MB-231 breast cancer cells through regulation of brain microvascular endothelial cell permeability.* J Biol Chem, 2003. **278**(7): p. 5277-84.
106. Tozawa, K., S. Sakurada, K. Kohri, and T. Okamoto, *Effects of anti-nuclear factor kappa B reagents in blocking adhesion of human cancer cells to vascular endothelial cells.* Cancer Res, 1995. **55**(18): p. 4162-7.
107. Voisard, R., R. Fischer, M. Osswald, S. Voglic, R. Baur, M. Susa, W. Koenig, and V. Hombach, *Aspirin (5 mmol/L) inhibits leukocyte attack and triggered reactive cell proliferation in a 3D human coronary in vitro model.* Circulation, 2001. **103**(12): p. 1688-94.

108. Beauparlant, P. and J. Hiscott, *Biological and biochemical inhibitors of the NF-kappa B/Rel proteins and cytokine synthesis.* Cytokine Growth Factor Rev, 1996. **7**(2): p. 175-90.
109. Ruegg, C., J. Zaric, and R. Stupp, *Non steroidal anti-inflammatory drugs and COX-2 inhibitors as anti-cancer therapeutics: hypes, hopes and reality.* Ann Med, 2003. **35**(7): p. 476-87.
110. Vane, J.R. and R.M. Botting, *Anti-inflammatory drugs and their mechanism of action.* Inflamm Res, 1998. **47 Suppl 2**: p. S78-87.
111. Demierre, M.F., P.D. Higgins, S.B. Gruber, E. Hawk, and S.M. Lippman, *Statins and cancer prevention.* Nat Rev Cancer, 2005. **5**(12): p. 930-42.

Appendix I: DSS cross-linker optimization for 293T transfectants

Appendix I: DSS cross-linker optimization for 293T transfectants

To determine an appropriate cross-linker incubation period for 293T cells and 293T transfectants, SYM25 cells were incubated for 0, 5, 10, 15, 30, or 60 minutes with the DSS cross-linker in the cross-linking protocol. Subsequently, the cells were lysed, and cell lysates were run on a 4-20% polyacrylamide gel. Subsequently, the membrane was probed for the cytoplasmic fragment of MUC1 using the CT2 antibody (Figure AI.1). All of the tested incubation times displayed the presence of MUC1 monomer at approximately 25 kDa, and MUC1 dimer at approximately 50 kDa. In addition, there was an unidentified band just under 37 kDa that did not show up in untransfected 293T cells (Figure 3.2a, columns 4-6). Blotting for tubulin demonstrated that protein loading was fairly consistent. Interestingly, the amount of MUC1 varied between incubation times. This was most evident in the 0 minute incubation, where chemiluminescent detection of the monomer completely saturated the surrounding film. Furthermore, the ratio of MUC1 dimer to MUC1 monomer was not constant between conditions. In the end, a 10 minute incubation time was chosen for the following experiments, as the amount of MUC1 dimer in that condition was noticeably greater than the amount of MUC1 monomer.

Figure AI.1 Time course for DSS cross-linker incubation. Incubation of the DSS cross-linker with SYM25 cells was done for various amounts of time following stimulation with NIH ICAM cells. Lysates were separated on SDS-PAGE and blotted with CT2 antibody. From left to right, the incubation times were: 0, 5, 10, 15, 30, and 60 minutes. MUC1 monomer appeared at approximately 25 kDa, and MUC1 dimer appeared at approximately 50 kDa. Tubulin was used as a loading control. (n = 3)

Appendix II: Manipulation of the MUC1 transmembrane domain

Appendix II: Manipulation of the MUC1 transmembrane domain

AII.1 Introduction

The project in the core chapters presents data on the effects of MUC1 extracellular domain manipulation on ICAM-1-induced MUC1 signaling. The original thesis project, however, was to manipulate the MUC1 transmembrane domain and examine its role in ICAM-1-induced MUC1 signaling. The project was dropped because of problems in plasmid construction.

AII.1.1 Project Overview

Calcium-dependent signal transduction occurs on detergent-resistant cholesterol- and glycolipid-rich domains in cellular membranes (DRMs, or lipid rafts), and a portion of membrane MUC1 is located in these microdomains of the membrane (Figure 3.1b). We had recently demonstrated that disruption of these lipid raft domains, using methyl β-cyclodextran or nystatin, abolished calcium oscillations, implicating the involvement of these detergent-insoluble domains in ICAM-1-induced MUC1 signaling [1]. The role of MUC1/ICAM-1 binding and signaling outside of these regions, however, remains unclear. In order to examine the role of the non-raft population of MUC1, the proposed strategy was to inhibit MUC1 entry into detergent-resistant membranes (DRM) by swapping the MUC1 transmembrane domain with a transmembrane domain (TMD) from a molecule that does not partition into DRM. The TMD from the transferrin receptor was chosen, as Barman *et al* (2004) demonstrated that substitution of the neuraminidase TMD with the transferrin receptor TMD caused the neuraminidase chimera to localize to the non-raft regions of the plasma membrane [2]. It should also be noted that MUC1 contains a CQC motif adjacent to the cytoplasmic leaflet of the plasma membrane. Although the motif suggests a double palmitoylation site necessary for DRM localization, its role in MUC1 membrane distribution has not been examined. Consequently, constructs with and without the CQC sequence would be made to

determine if the localization of the protein would be affected. Following transfection and characterization, successful transfectants would be tested for their ability to induce calcium oscillations, stress fibre formation, and transendothelial migration following ICAM-1 stimulation. With a normal intact signaling pathway, ICAM-1-induced MUC1 signaling leads to repetitive calcium oscillations, lamellipodia formation, and increased transendothelial migration *in vitro* ([1, 3] and unpublished data). To verify these results, lipid rafts would be disrupted by treating MUC1-positive cells with statins, which inhibit cholesterol synthesis, followed by analysis of the cells's ability to induce calcium oscillations, stress fibre formation, and transendothelial migration after ICAM-1 stimulation.

AII.1.2 General Hypothesis and Objectives

It is proposed that if detergent-resistant membrane domains affect MUC1/ICAM-1 binding and/or signaling, then populations of MUC1 within or outside these regions will behave differently in the presence of ICAM-1. The specific objectives of this project were:

1. To determine the distribution of transmembrane-manipulated MUC1 between lipid rafts and the bulk plasma membrane;
2. To determine if MUC1 raft localization is necessary for ICAM-1-induced calcium oscillations;
3. To determine if MUC1 raft localization is required for ICAM-1-induced lamellipodia formation; and
4. To determine if MUC1 raft localization is necessary for ICAM-1-induced transendothelial migration.

AII.2 Materials and Methods

AII.2.1 Reagents

See sections 2.1.1 and 3.1.1. Primers for site-directed mutagenesis and sequencing were from Integrated DNA Technologies (Coralville, Iowa, USA). Oligomers for the transferrin receptor transmembrane domain were from Sigma Genosys (St. Louis, Missouri, USA).

AII.2.2 Site-directed mutagenesis

Site-directed mutagenesis was done with the Stratagene Quikchange II kit (PCR-based method). Unique restriction sites were generated 5' (Apa I) and 3' (Sac II) of the MUC1 transmembrane domain, and a second Apa I restriction site 3' of the MUC1 stop codon was removed. Primers were as follows, where bolded letters are either nucleotide insertions or changes: 5' Apa I sense - 5'-CT GGG GCT GGG **CCC** GTG CCA GGC TG-3', 5' Apa I anti-sense 5'-CA GCC TGG CAC **GGG** CCC AGC CCC AG-3', 3' Sac II sense (lacking CQC) - 5'-GCT GTC TGT CAG TGC **CCG CGG** CGC CGA AAG AAC TAC-3', 3' Sac II anti-sense (lacking CQC) 5'-GTA GTT CTT TCG GCG **CCG CGG** GCA CTG ACA GAC AGC-3', 3' Sac II sense (including CQC) - 5'-C TGT CAG TGC CGC **GGT** CGA AAG AAC TAC GGG-3', 3' Sac II anti-Sense (including CQC) - 5'-CCC GTA GTT CTT TCG **ACC** GCG GCA CTG ACA G-3', C1689A Apa I sense - 5'-AG CTC ATG TGG GC**A** CCT GAG GGCT CAT G-3', C1689A Apa I anti-Sense 5'-C ATG AGCC CTC AGG **T**GC CCA CAT GAG CT-3' (Figures AII.1A, AII.1B and AII.2B). PCR reaction mixtures were prepared using the manufacturer's guidelines, with 50 ng of template pCINeoMUC1TR+FLAG plasmid, and 50 mM dNTP mix (12.5 mM of each dNTP). PCR was done in an Applied Biosystems 2400 thermal cycler following the product instructions, with 16 segment 2 cycles for 10 minutes for the 5' Apa I and 3' Sac II (including CQC) mutagenesis, 12 segment 2 cycles for 10 minutes for the C1689A Apa I mutagenesis, and 18 segment 2 cycles for 10 minutes

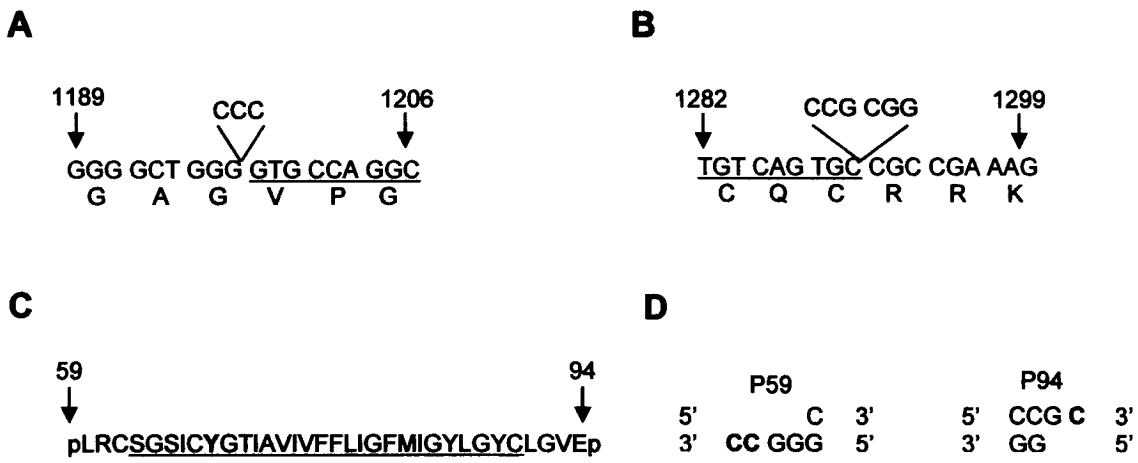

Figure AII.1 Proposed steps for MUC1 transmembrane domain (TMD) swapping (no CQC). **(A)** Insertion of three nucleotides (CCC) immediately 5' of the MUC1 TMD for generation of an Apa I restriction site. Underlined nucleotides are part of the MUC1 TMD sequence, and the remainder are proximal to the TMD sequence. **(B)** Insertion of six nucleotides immediately 3' of the MUC1 TMD for generation of a Sac II restriction site. **(C)** Amino acid sequence of the transferrin receptor (TR) TMD. The bolded tyrosine is a discrepancy between the original sequence from Knossow *et al* [4], and the sequence used in Barman *et al* [2]. Underlined letters indicate amino acids in the TMD, and lower case letters represent the prolines to be modified. The remainder are amino acids proximal to the TMD. **(D)** Modifications to the TR prolines to allow for insertion into the modified MUC1 plasmid. Bolded letters are additional nucleotides that must be included in the synthesized strand, and spaces above or below unbolded letters are nucleotides that must be excluded from synthesis.

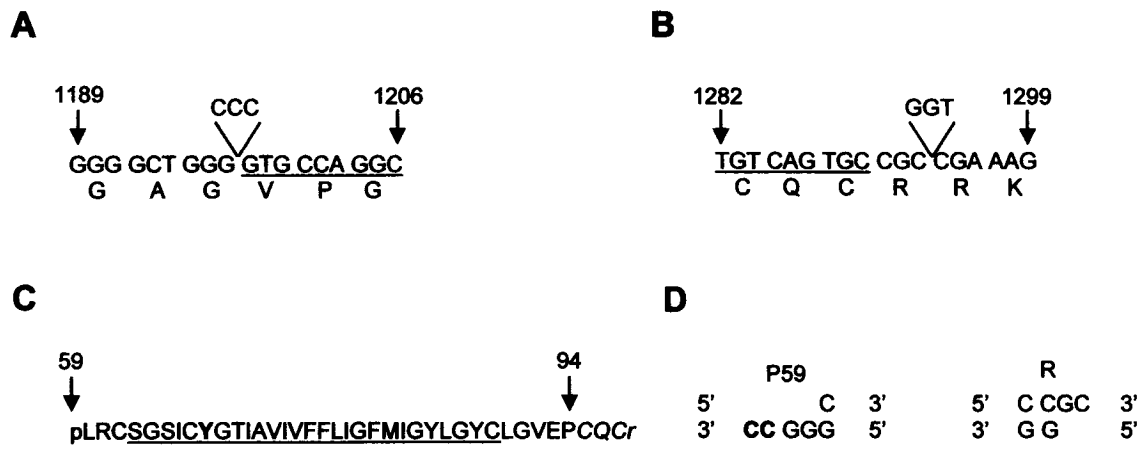

Figure AII.2 Proposed steps for MUC1 transmembrane domain (TMD) swapping (with CQC). **(A)** Insertion of three nucleotides (CCC) immediately 5' of the MUC1 TMD for generation of an Apa I restriction site. Underlined nucleotides are part of the MUC1 TMD sequence, and the remainder are proximal to the TMD sequence. **(B)** Insertion of three nucleotides immediately 3' of R406 for generation of a Sac II restriction site. **(C)** Amino acid sequence of the transferrin receptor (TR) TMD. The bolded tyrosine is a discrepancy between the original sequence from Knossow *et al* [4] and the sequence used in Barman *et al* [2]. Underlined letters indicate amino acids in the TMD, and lower case letters represent the residues to be modified. Italisized letters represent a fragment of MUC1 containing part of the TMD and CT domains. The remainder are amino acids proximal to the TR TMD. **(D)** Modifications to two residues in the synthesized insert to allow for insertion into the modified MUC1 plasmid. Bolded letters are additional nucleotides that must be included in the synthesized strand, and spaces above or below unbolded letters are nucleotides that must be excluded from synthesis.

for the 3' Sac II (lacking CQC) mutagenesis. To digest non-mutated parental plasmid after PCR, 1 μl of Dpn I was added to each reaction mixture, and the mixtures were subsequently incubated at 37 °C for 1.5 hours.

AII.2.3 Transformation, selection, amplification, and verification of plasmids

The mutated MUC1 plasmids were transformed in XL10-gold ultracompetent cells from Stratagene. For each Dpn I-digested reaction mixture, 45 μl of cells were thawed on ice and then transferred to 2 chilled tubes. 1 μl of the Dpn I-digested DNAwas added to each of the tubes, and the cells were incubated on ice for 30 minutes. Subsequently, cells were heat-shocked at 42 °C for 30 seconds. Cells were placed back on ice for 2 minutes, and then 500 μl of pre-heated 42 °C NZY+ broth was added to each tube. After a 1 hour incubation at 37 °C with shaking (~225 rpm), the entire transformation mixture volume was plated onto 4 LB agar plates containing 50 μg/ml ampicillin (250 μl per plate). Plates were incubated overnight at 37 °C.

Following this step, tubes containing 2 ml of LB broth with 50 μg/ml ampicillin were inoculated with individual colonies from the LB plates. The tubes were incubated at 37 °C with shaking (~225 rpm) overnight. The plasmids were isolated with the Qiagen QIAprep Spin miniprep kit (modified alkaline lysis) using the manufacturer's protocol, and DNA concentrations were determined by UV spectroscopy (1 Ab_{260} = 50 μg/ml double-stranded DNA).

To verify the mutations, plasmids were digested with *Apa I* or *Sac II*, and the sizes of the fragments were checked on a 1% agarose gel.

AII.2.4 Annealing the transferrin receptor TMD oligomers

The DNA sequences for the transferrin receptor transmembrane domain (TR TMD) were as follows: TR TMD sense (lacking CQC) - 5'-C AAA AGG TGT AGT GGA AGT ATC TGC TAT GGG ACT ATT GCT GTG ATC GTC TTT TTC TTG ATT GGA TTT ATG ATT GGC TAC TTG GGC TAT TGT AAA GGG GTA

GAA CCG C-3', TR TMD anti-sense (lacking CQC) - 5'-GG TTC TAC CCC TTT ACA ATA GCC CAA GTA GCC AAT CAT AAA TCC AAT CAA GAA AAA GAC GAT CAC AGC AAT AGT CCC ATA GCA GAT ACT TCC ACT ACA CCT TTT GGG CC-3', TR TMD (including CQC) sense - 5'-C AAA AGG TGT AGT GGA AGT ATC TGC TAT GGG ACT ATT GCT GTG ATC GTC TTT TTC TTG ATT GGA TTT ATG ATT GGC TAC TTG GGC TAT TGT AAA GGG GTA GAA CCA TGT CAG TGC CGC-3', TR TMD anti-Sense (including CQC) - 5'-G GCA CTG ACA TGG TTC TAC CCC TTT ACA ATA GCC CAA GTA GCC AAT CAT AAA TCC AAT CAA GAA AAA GAC GAT CAC AGC AAT AGT CCC ATA GCA GAT ACT TCC ACT ACA CCT TTT GGG CC-3'. Sequences were modified to form a sticky end for *Apa I* at the 5' end, and a sticky end for *Sac II* at the 3' end to allow for insertion into mutated MUC1 plasmids (Figures AII.1 and AII.2).

Complementary oligomers were mixed in equimolar concentrations, and 10x STE buffer (10 mM Tris base, 50 mM NaCl, 1 mM EDTA, final pH 8.0) was added to make a final mixture with a 1x STE buffer concentration. The mixtures were incubated at 95 °C for 5 minutes, and allowed to anneal overnight through gradual cooling in an insulated container filled with 95 °C water.

AII.2.5 Substitution of the MUC1 TMD for the transferrin receptor TMD

To prepare the mutated vectors for ligation, the two plasmids (including CQC, or lacking CQC) were digested with *Apa I* and *Sac II* and purified on a 1% (w/v) low melting point agarose gel. Following excision of the appropriate DNA band, the linearized plasmid was recovered by melting the gel slice at 70 °C, snap-freezing in a dry ice/acetone bath for 5 minutes, thawing the gel slice, centrifuging at 14k rpm for 5 minutes in an Eppendorf 5415C centrifuge, and removing the pelleted agarose. The concentration of the vector was determined by UV spectroscopy.

The concentration of the annealed TR TMD inserts were determined by UV spectroscopy, and then mixed with the purified vectors in a molar ratio between 5:1 and 10:1. Ligation was done with T4 ligase at 16 °C overnight. Ligated plasmids

were transformed, selected, amplified, and verified using the protocols from section AII.2.3.

AII.2.6 Sequencing of the MUC1 gene

A number of sequencing primers were designed for the MUC1 gene. The number in each name represents the approximate binding point of the 5' end of the primer (Figure AII.3), and F and R show the direction of sequencing (forward or reverse). Primers used were: 255R – 5'-GAG TAC GCT GCT GGT CAT AC-3', 285F – 5'-TCC ACC ACT CAG GGA CAG GAT G-3', 684F – 5'-CCA GCC AGC AAG AGC ACT CCA TTC-3', 834R – 5'-GGG AGA AGT GCT GTG ATT G-3', MUC1 5' TMD (1081F) – 5'-TGG AGA CAC AGT TCA ATC AG-3', 1446F – 5'-CAG CAG CCT CTC TTA CAC AAA C-3', and the T3 promoter and CMV forward primers from Integrated DNA Technologies.

Sequencing reaction mixtures consisted of 8 µl of ABI BigDye v3.1 reaction premix, 1 µl of 3.2 pmol/µl sequencing primer, 500 ng of the template to be sequenced, and ddH_2O for a total volume of 20 µl. Cycling was done on an Applied Biosystems PCR System 2400 with the following parameters:

1 cycle at 96 °C for 10 minutes (initial denaturation)
35 cycles of:
    96 °C for 10 seconds (denaturation)
    50 °C for 5 seconds (annealing)
    60 °C for 4 minutes (extension)
1 hold at 4 °C

The PCR products from these sequencing reactions were precipitated by adding 5 µl of 125 mM EDTA and 60 µl of 95 – 100% ethanol, inverted 4 times to mix, and incubated at 4 °C for 15 minutes. The mixtures were then centrifuged at 13.5k rpm at 4 °C for 30 minutes in an Eppendorf 5415C centrifuge to pellet the

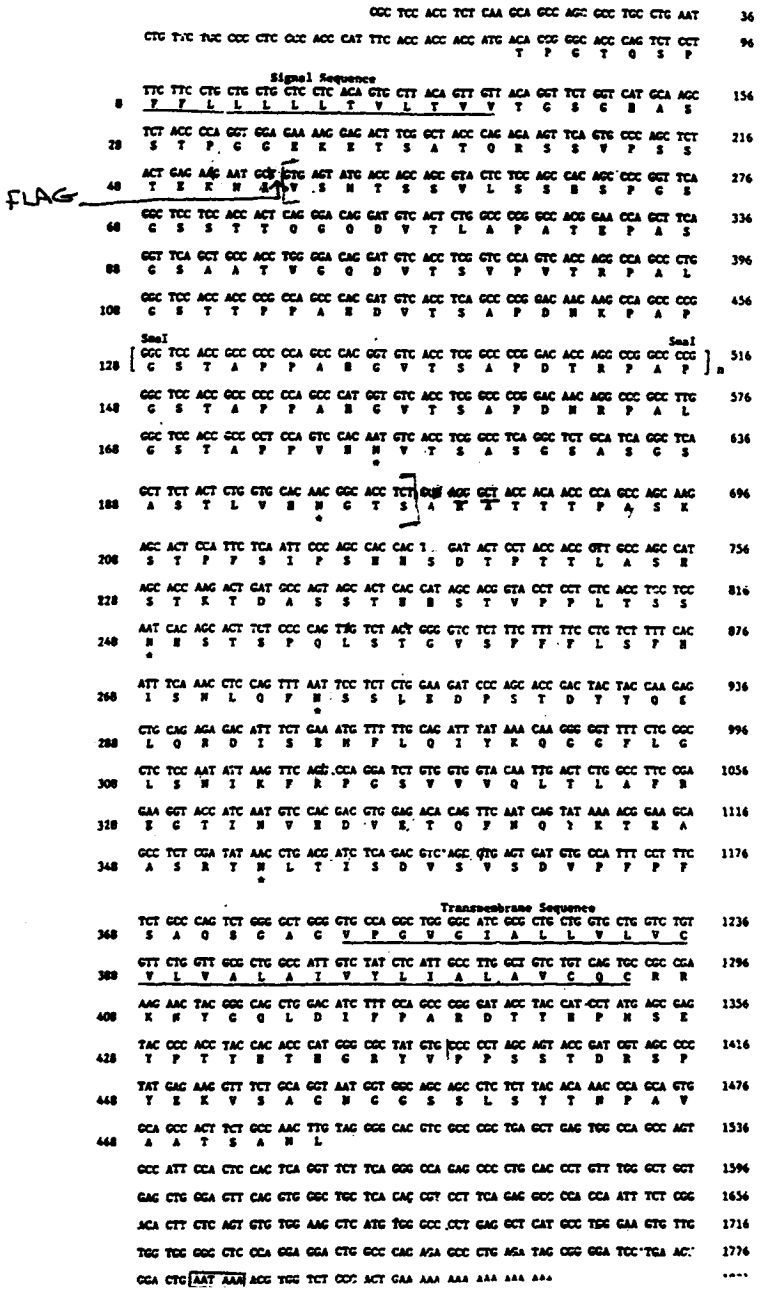

Figure AII.3 The MUC1 gene sequence. Sequence of the MUC1 gene and flanking regions in the pCINeoMUC1TR+FLAG plasmid. The numbering of the nucleotides is along the right side of the sequence, and the numbering of the amino acids is along the left side of the sequence. The 7 amino acid FLAG tag with a 7 amino acid polylinker inserted after residue 241 is not included in the numbering. The highlighted region between residues 457 and 516 represents one copy of the tandem repeats. The *Apa I* restriction site around residue 1689 is highlighted. The highlighted regions around residues 1080 and 1566 indicate *BmgB I* restriction sites.

DNA. The supernatant was aspirated, and the pellet was washed once with 60 µl of 70% ethanol. Following a spin at 13.5k rpm at 4 °C for 5 minutes in an Eppendorf 5415C centrifuge, the supernatant was once again aspirated, and the pellet was allowed to dry on the benchtop. If analysis of the sequencing products was not done on the same day, the DNA pellet was frozen at -20 °C.

On the day of analysis, the pellets were resuspended in 25 µl of ABI template suppression reagent (TSR), and vortexed well to resuspend the DNA. Following a 5 minute incubation at 95 °C, the samples were briefly cooled on ice, vortexed briefly, and incubated an additional 10 minutes on ice. Samples were transferred to separate septa tubes and analyzed on an ABI Prism 310 Genetic Analyzer.

AII.3 Results

AII.3.1 Swapping of the MUC1 transmembrane domain with the non-raft localized transferrin receptor transmembrane domain

To determine the role of the MUC1 population found in the bulk non-raft plasma membrane, a chimeric MUC1 protein in which the transmembrane domain (TMD) had been swapped with the DRM-excluded transferrin receptor TMD was to be generated. The strategy was to insert unique restriction sites on either side of the TMD in Dr. Sandra Gendler's pcINeoMUC1TR+FLAG plasmid, excise the MUC1 TMD using those sites, and ligate the transferrin receptor TMD into that space. Using site directed mutagenesis, 3 nucleotides (CCC) were inserted immediately 5' of the transmembrane sequence to generate an *Apa* I restriction site (Figure AII.1). Following amplification of the plasmid, the restriction site was verified by gel electrophoresis after digesting the plasmid with *Apa* I (Figure AII.4). Since the plasmid had an additional *Apa I* restriction site in the non-coding region 3' of the MUC1 stop codon, a cytosine in the restriction sequence at position 1689 was mutated to adenine (C1689A) (Figures AII.3 and AII.5A). The plasmid was then subjected to a third round of mutagenesis in which 6 nucleotides were inserted immediately 3' of the transmembrane sequence to generate a *Sac* II restriction site

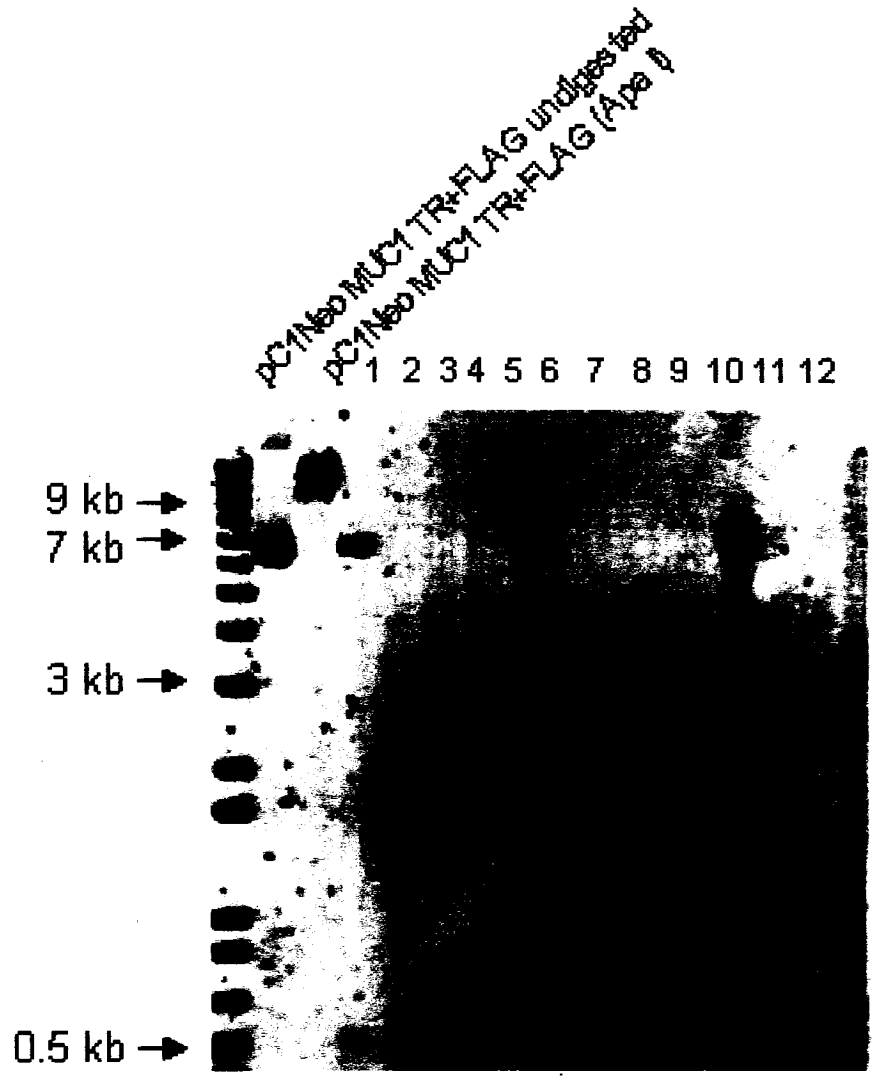

Figure AII.4 DNA gel electrophoresis of MUC1 plasmids after the first round of mutagenesis. Numbered lanes represent *Apa* I-digested plasmids isolated from *E. coli* colonies transformed with DNA from a site-directed mutagenesis reaction mixture that inserted nucleotides 5' of the MUC1 TMD to generate an *Apa I* cut site. Parental pC1NeoMUC1 plasmid stock has one *Apa* I restriction site that should be close to residue 1689. Plasmids isolated from bacterial colonies have one (plasmid 1, 5, and 10) or more (2-4, 7-9, 11-12) additional *Apa* I restriction sites, where a single additional restriction site indicates the presence of the *Apa I* site generated by mutagenesis, and multiple additional restriction sites may indicate false priming.

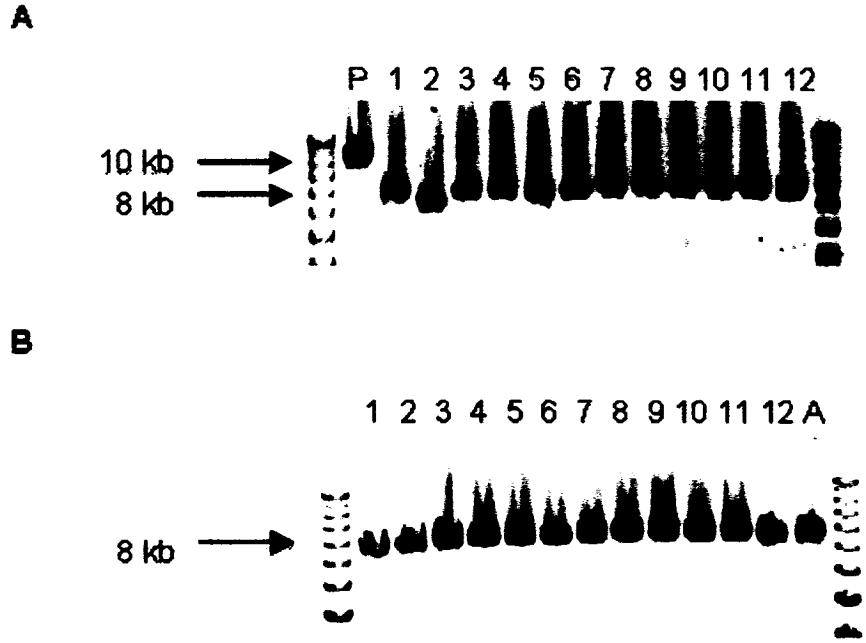

Figure AII.5 DNA gel electrophoresis of MUC1 plasmids after the second and third rounds of mutagenesis. (A) *Apa I* digestion of plasmids after the second round of mutagenesis, in which the cytosine at position 1689 was mutated to an adenine to remove the non-coding *Apa I* restriction site. As expected, all plasmids were singly-cut and ran as one fragment on an agarose gel. All clones isolated from the second round of mutagenesis (1 – 12), however, were truncated to approximately 8 kb compared to the parental MUC1 plasmid from the first round of mutagenesis used to generate them (P). (B) *Sac II* digestion of plasmids after the third round of mutagenesis, in which nucleotides were inserted 3' of the MUC1 TMD to introduce a unique *Sac II* cut site. All plasmids were singly-cut and ran as one fragment on an agarose gel. Clones 1 – 6 represent plasmids that include the MUC1 CQC motif, and clones 7 – 12 represent plasmids that lack the MUC1 CQC motif. All clones remained truncated at 8 kb, similar to the *Apa I*-digested plasmid from the second round of mutagenesis used to generate them (clone A).

(CCG CGG) (Figure AII.1B). This plasmid lacked the MUC1 CQC motif at the junction between the transmembrane and cytoplasmic domains, which may contribute to the membrane distribution of MUC1. Alternatively, to construct a chimera that retained the CQC motif, the third round of site directed mutagenesis inserted three nucleotides (GGT) immediately 3' of arginine 406 to generate a *Sac* II restriction site (CCG CGG) (Figure AII.2B). Verification of mutagenesis was done by restriction digest and gel electrophoresis (Figure AII.5B). After amplification of the plasmids with a miniprep, the TMDs were excised by digesting the plasmids with *Apa* I and *Sac* II. The plasmids, minus the TMD, were isolated by gel purification. The DNA for the TMD of the transferrin receptor was synthesized using a commercial service (Sigma Genosys). For the chimera without the CQC motif, the sequence extended from amino acid 59 (proline) to amino acid 94 (proline), and included the necessary alterations in the prolines for ligation into the modified pc1NeoTR+FLAG plasmid (ie. Proline 59: CCA to C, and proline 94: CCA to C) (Figures AII.1C and AII.1D). The complementary strand was similarly synthesized, and contained the appropriate overhangs for ligation. For the chimera with the CQC motif, the sequence extended from amino acid 59 (proline) to amino acid 94 (proline), and included a small fragment of the MUC1 TMD and CT domains (i.e. CQCR, for both inclusion of the CQC sequence into the plasmid, and generation of a Sac II restriction site) (Figures AII.2C and AII.2D). In addition, the synthesized DNA included the necessary alterations for ligation into the modified pc1NeoTR+FLAG plasmid (ie. Proline 59: CCA to C, and overhang modifications).

The synthesized TMDs were ligated into the modified pc1NeoTR+FLAG plasmids, and initial verification was done by checking the size of the fragments run on an agarose gel following digestion with *Apa* I and/or *Sac* II (Figure AII.6). The TMD of several plasmids passing the initial verification were sequenced using the 1081F primer. Two clones were selected for each of the TR TMD-swapped plasmids (lacking or including the CQC motif). One of the 2 clones that had the CQC motif was successfully ligated to the transferrin receptor TMD (Figure AII.7A). Although the second clone contained the engineered restriction sites, the TMD in between them was the MUC1 TMD, suggesting incomplete digestion of the

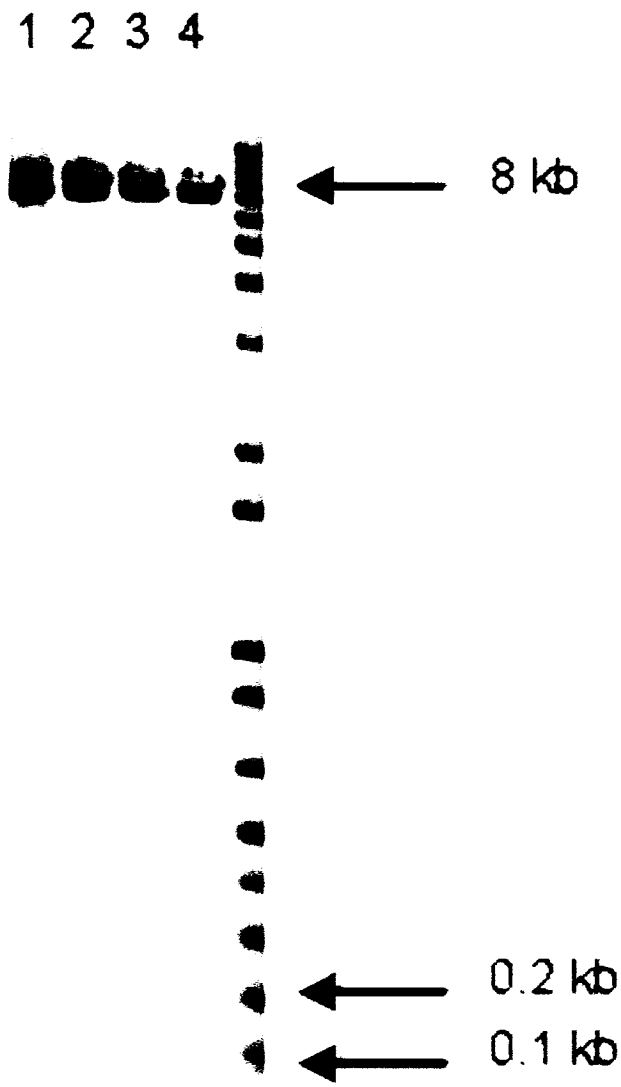

Figure AII.6 DNA gel electrophoresis of plasmids after substitution of the MUC1 TMD with the transferrin receptor TMD. Plasmids passing through the third round of mutagenesis were digested with *Apa I* and *Sac II* to excise the MUC1 TMD, and ligated to the transferrin receptor TMD. Ligated plasmids were digested with *Apa I* and *Sac II* and run on a 1% agarose gel to verify the sizes of the fragments. Lanes 1 – 2 represent two plasmids that include the CQC motif, and lanes 3 – 4 represent two plasmids that lack the CQC motif. All 4 plasmids ran as two fragments, with one fragment around 8 kb, and the other between 0.1 kb and 0.2 kb. The size of the first fragment is consistent with the overall size of the mutated MUC1 plasmids, and the size of the second fragment is consistent with the size of the TMD. The second fragment was extremely faint, most likely due to a combination of incomplete digestion and small fragment size, since the intensity of ethidium bromide staining correlates with the degree of ethidium bromide intercalation with DNA, which is proportional to DNA length.

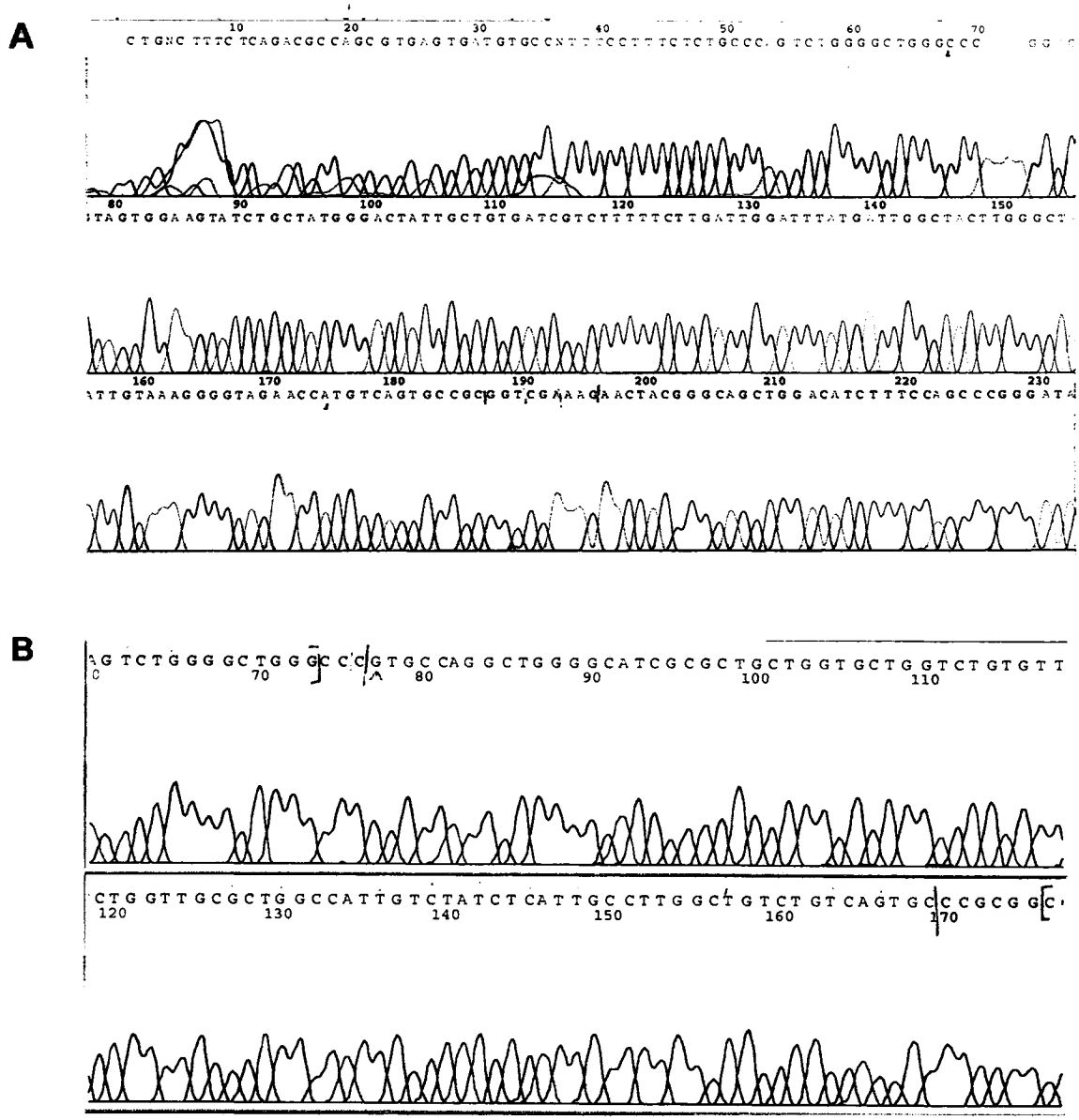

Figure AII.7 Sequencing the MUC1 +CQC plasmids. The region surrounding and including the transmembrane domain of the MUC1 plasmids retaining the MUC1 CQC motif from figure AII.6 was sequenced. Highlighted regions represent the transmembrane domain. Clone 1 **(A)** contained the transferrin receptor TMD, but clone 2 **(B)** retained the MUC1 TMD.

plasmid prior to TR TMD ligation (Figure AII.7B). Conversely, both clones lacking the CQC motif were successfully ligated to the transferrin receptor TMD (Figure AII.8). Every plasmid was truncated from an original size of approximately 10 kb to between 7 – 8 kb following the second round of the site directed mutagenesis (Figure AII.5A). Since the MUC1 gene was originally inserted into the pCINeo plasmid with *Not I*, the mutated plasmids were cut with *Not I* and run on an agarose gel to determine if the missing nucleotides were from the plasmid backbone or from the MUC1 gene. The backbone from the original unmutated parental plasmid was approximately 5.5 kb, and the MUC1 gene was approximately 3.8 kb (Figure AII.9). Fragments from the mutated plasmids ran at approximately 5.5 kb and 1.8 kb, demonstrating that the missing nucleotides were from the MUC1 gene. To determine which nucleotides were missing, the entire mutated MUC1 gene and flanking regions between the *Not I* restriction sites was sequenced. The data indicated that the majority of the MUC1 gene was intact, but a large section of the tandem repeats was missing (data not shown).

Since the modified transmembrane domain and the flanking regions were intact, the strategy chosen to repair the gene was to excise the modified transmembrane domain using restriction sites in the regions proximal to the TMD, and ligate this fragment into the same location in the parental pCINeoMUC1TR+FLAG plasmid. This was first attempted with *BmgB I* (Figures AII.3 and AII.10). Initial verification through *Not I* digestion and gel electrophoresis demonstrated that the fragment sizes were correct, with the plasmid backbone running at approximately 5.5 kb, and the mutated MUC1 gene running at approximately 3.9 kb, as the transferrin TMD is slightly longer than the MUC1 TMD. Sequencing of the MUC1 gene, however, demonstrated that all plasmids isolated had a backwards insertion of the excised MUC1 fragment, which was unsuitable for our purposes. Future attempts at plasmid repair may need an approach that guarantees directionality, such as excising the transmembrane fragment with 2 restriction enzymes that cut in unique sites in the regions flanking the mutated MUC1 transmembrane domain. The difficulty with the approach is that the pCINeoMUC1TR+FLAG plasmid has few unique restriction sites close to the

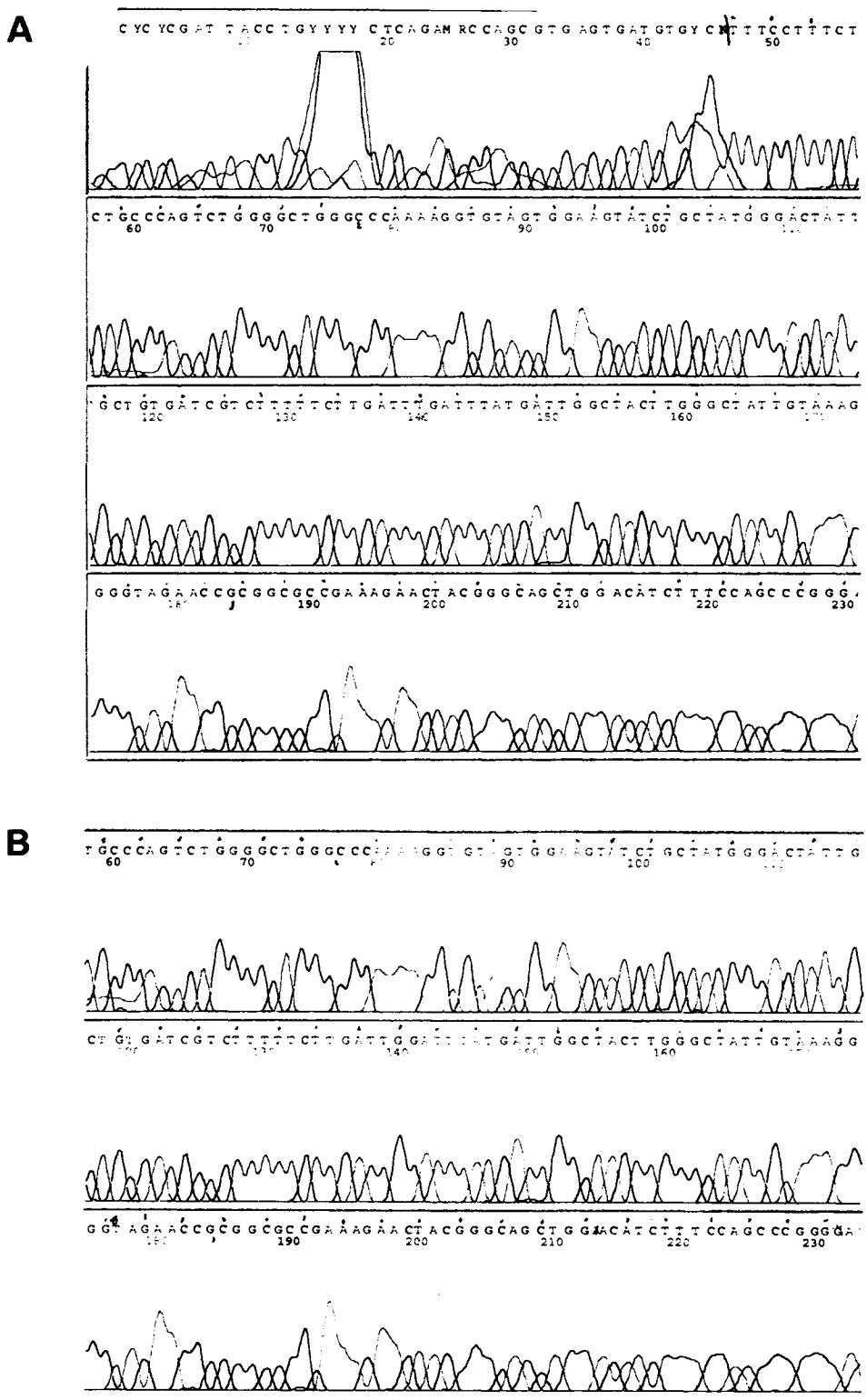

Figure AII.8 Sequencing the MUC1 -CQC plasmids. The region surrounding and including the transmembrane domain of the MUC1 plasmids lacking the MUC1 CQC motif from figure AII.6 was sequenced. Highlighted regions represent the

Figure AII.8 (continued): transmembrane domain. Both clones (**A** and **B**) contained the transferrin receptor TMD.

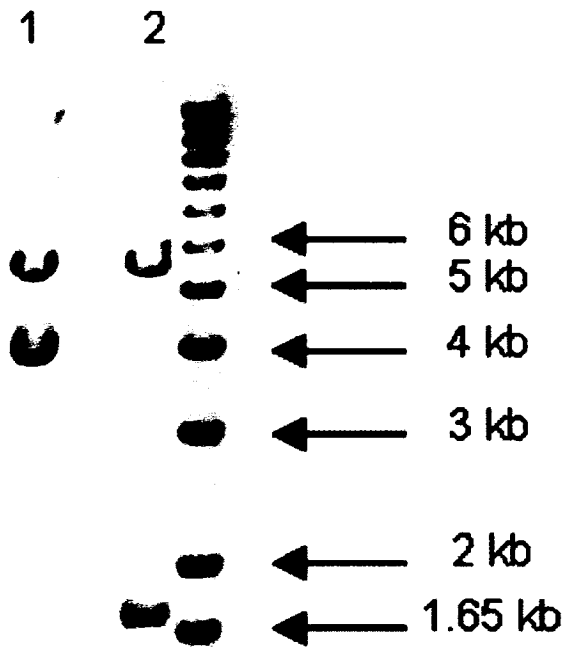

Figure AII.9 Representative DNA electrophoresis of MUC1 plasmids after Not I digestion. The parental unmutated pCINeoMUC1TR+FLAG plasmid (lane 1) and MUC1 +CQC clone 1 (lane 2) plasmid were digested with Not I to excise the MUC1 gene, and run on a 1% (w/v) agarose gel to determine the fragment sizes. The parental MUC1 plasmid showed the vector backbone running between 5 and 6 kb and the MUC1 gene at just under 4 kb, resulting in a total of approximately 10 kb. Similarly, the MUC1 +CQC plasmid backbone ran between 5 and 6 kb, but the MUC1 gene ran at just over 1.65 kb, demonstrating that the missing nucleotides were in the MUC1 gene. All of the other mutated plasmids displayed a similar pattern (data not shown). Total plasmid sizes were consistent with previous digestions.

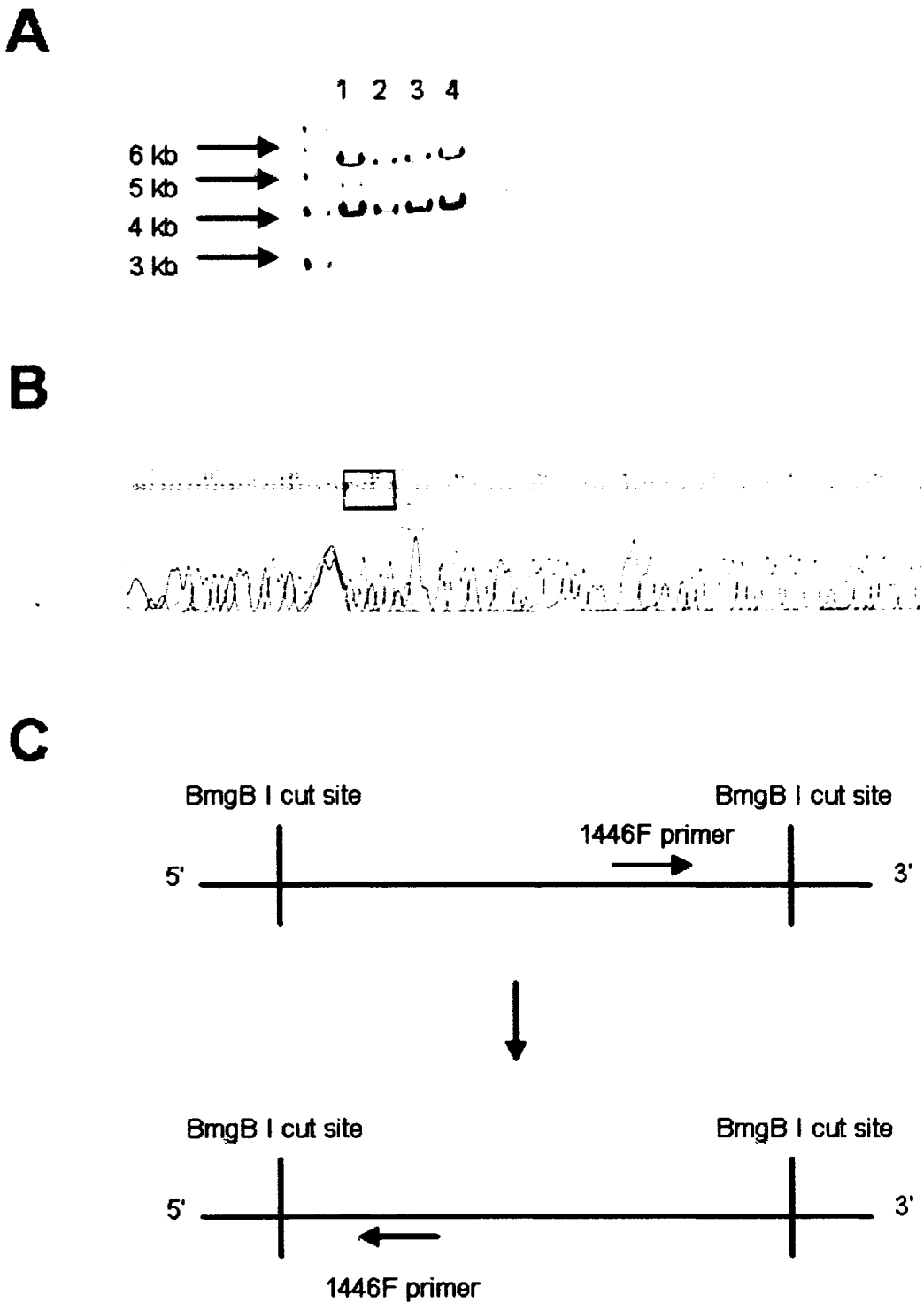

Figure AII.10 Attempt at repairing the TR TMD-swapped MUC1 plasmids with BmgB I. The mutated transmembrane domain from the truncated mutated plasmids was excised with *BmgB I* and inserted into the identical location in the parental unmutated MUC1 plasmid in an attempt to recover the lost trandem repeats.

Figure AII.10 continued: Plasmids were subsequently digested with *BmgB I* and run on a 1% agarose gel. The results for 4 of the isolated clones are shown (**A**). All clones displayed the proper size fragments, with the plasmid backbone running between 5 – 6 kb, and the MUC1 gene running at just under 4 kb. However, sequencing of the swapped region with the 1446F primer showed that all inserts were ligated backwards (**B**). The boxed nucleotides represent the *BmgB I* restriction site at bases 1078 – 1083 from figure AII.3, and the highlighted region represents the reverse complement of bases upstream of the cut site, demonstrating backwards insertion. (**C**) A schematic showing the reasoning behind this conclusion. If the insert was in the forward direction, sequencing with the 1446F primer would display the sense strand sequence 3' of the *BmgB I* site at bases 1504 – 1509. Instead, the primer displayed the anti-sense sequence before the *Bmg B I* site at bases 1078 – 1083.

MUC1 transmembrane sequence, and most of them are recognized by unusual enzymes that do not digest DNA effectively.

References:

1. Rahn, J.J., Q. Shen, B.K. Mah, and J.C. Hugh, *MUC1 initiates a calcium signal after ligation by intercellular adhesion molecule-1.* J Biol Chem, 2004. **279**(28): p. 29386-90.
2. Barman, S., L. Adhikary, A.K. Chakrabarti, C. Bernas, Y. Kawaoka, and D.P. Nayak, *Role of transmembrane domain and cytoplasmic tail amino acid sequences of influenza a virus neuraminidase in raft association and virus budding.* J Virol, 2004. **78**(10): p. 5258-69.
3. Rahn, J.J., J.W. Chow, G.J. Horne, B.K. Mah, J.T. Emerman, P. Hoffman, and J.C. Hugh, *MUC1 mediates transendothelial migration in vitro by ligating endothelial cell ICAM-1.* Clin Exp Metastasis, 2005. **22**(6): p. 475-83.
4. Knossow, M., R.S. Daniels, A.R. Douglas, J.J. Skehel, and D.C. Wiley, *Three-dimensional structure of an antigenic mutant of the influenza virus haemagglutinin.* Nature, 1984. **311**(5987): p. 678-80.